

Freie Universität Berlin



Master Thesis

**Influence of local donor/acceptor geometry
on charge separation in organic solar cells**

First supervisor: Prof. Dr. Jan Behrends

Second supervisor: PD Dr. A. Lindinger

Daria Dymnikova

06.12.2017

Contents

1	Introduction	7
2	Theoretical aspects	9
2.1	Physical properties of organic materials	9
2.2	Electrons in the magnetic field	12
2.3	Interactions	12
2.4	Quantum-mechanical calculations	15
2.5	CT states observed in EPR	18
2.6	CT state simulations	19
2.7	System orientations	19
2.8	Electron paramagnetic resonance (EPR)	21
3	Simulations and Visualization Toolbox	22
3.1	Simulations	22
3.2	Fixed relative orientation in the powder model	22
3.3	Random relative orientations in the powder model	23
3.4	Visualization Toolbox	23
3.5	Comparison between two models in a powder	25
3.6	Influence of J- and D-coupling on CT spectra	28
3.7	Influence of g-tensor and line widths uncertainty on CT state spectra	32
4	Experimental aspects	34
4.1	Experimental Setup	34
4.2	Sample preparation	35
5	Results and Discussion	38
5.1	P3HT:PCBM vs. P3HT:C60	38
5.2	Stronger coupled CT states	45
5.3	PBT ₃ :PCBM and BT ₃ (2,3):PCBM	47
5.4	C-PCPDTBT:PCBM and F-PCPDTBT:PCBM	53
5.5	Inter-spin distances	59
6	Summary and Outlook	63
	Bibliography	69
A	Visualization tool manual	70
A.0.1	Running the tool	70
A.0.2	Background corrections and initial parameters	71

CONTENTS

A.0.3 Simulations	72
A.1 Acknowledgments	76
A.2 Declaration of Authorship	77

List of Abbreviations

C ₆₀	(C ₆₀ -Ih)[5,6]fullerene
C-PCPDTBT	poly[2,6-(4,4-bis(2-ethylhexyl)-4H-cyclopenta[2,1-b;3,4-b']-dithiophene)-alt-4,7-(2,1,3-benzothiadiazole)]
CS	charge separated
CT	charge transfer
cwEPR	continuous wave EPR
D	z-component of magnetic dipole-dipole interaction
EPR	electron paramagnetic resonance
F-PCPDTBT	poly[4,4'-bis(2-ethylhexyl)dithieno[3,2-b:2',3'-d]silole)-2,6-diylalt-(4,7-bis(2-thienyl)-2,1,3-benzothiadiazole)5,5'-diyl]
FP	full powder, random relative orientation
FRO	fixed relative orientation
HFI	hyperfine interaction
HOMO	highest occupied molecular orbital
J	electron-exchange interaction
light-induced signal	light with subtracted dark signal
LUMO	lowest unoccupied molecular orbital
lw	line width
mw	microwave
P3HT	Poly(3-hexylthiophene-2,5-diyl)
PBT _T T	Poly(2,5-bis(3-alkylthiophene-2-yl)thieno[3,2-b]thiophene)
PCBM	Phenyl-C ₆₁ -butyric acid methyl ester
pEPR	pulsed EPR
rpm	rounds per minute
RRO	random relative orientation, full powder
trEPR	transient EPR

Chapter 1

Introduction

Silicon solar cells are already commercial. They can be bought and used as an alternative source of energy.

For a long time Si and GaAs were investigated as absorber materials for inorganic solar cells and high efficiencies of such cells were achieved: 20-28%. These are pretty close to the Shockley-Quassier limit – 30% [1]. For multi-junction solar cells even higher values were obtained: up to 38.8% (up to 46.0% with concentration of light). [2].

An alternative for solar cell absorbers are organic semiconductors. Several advantages make them promising: flexibility, lightness, abundance and an easily tunable band gap which allows for creation of multicolored solar cells. They open a new perspective of usage, for example they can be implemented into facades of houses, or into colorful stained glass windows, that produce electricity. The big problem though is the poor efficiency of organic solar cells, that slightly exceeds 11% at the present time[2].

There is a lot of open questions about working principles of organic solar cells which limit their efficiency. One of the most important processes that is not fully understood, is the charge separation. In this work, the separation of charges is considered at the interface between two blended organic semiconductors [3]. A blend is a typical structure of the organic solar cell absorber (Fig. 1.2). It was found that there is an intermediate state of charge separation between the bound state of two charges and the separated state of two charges [4]. This intermediate state is referred to as the Charge Transfer (CT) state. There an electron and a hole are already situated on different molecules but they still interact with each other. The local morphology of a donor and an acceptor may influence the CT states, which, in turns, influences the charge separation. In this thesis, we studied the influence of the local morphology on the CT states.

The polymer Poly(3-hexylthiophene-2,5-diyl) or P3HT (Fig. 1.1) and the fullerene Phenyl-C61-butrylic acid methyl ester or PCBM (Fig. 1.2) were chosen as the blend compounds because this blend is well studied and its parameters are well known. The CT states in P3HT:PCBM were observed in previous studies [5, 4]. The attempts to understand the influence of morphology were already made in [6, 7]. The disordered nature of blends suggests random relative orientations between the donor and the acceptor molecules, while in the above-mentioned studies, the relative orientation between the molecules is considered to be fixed. It is not clear, why some particular orientations yield a good agreement with the experiment and the other orientations do not. Here we try to understand this.

Transient Electron Paramagnetic Resonance (trEPR) spectroscopy can be used to

probe the CT states. By comparing experimental spectra with the simulations, one can extract the exchange and dipolar couplings between the spins and some information about the local morphology. From that, energy levels, inter-spin distances and relative orientations can be extracted.

The work was divided in several parts. In the first part, the code for simulating a trEPR spectrum of a CT state was improved, so the simulations became faster. A visualization tool was created to ease the finding of the fitting parameters. In the second part, the created tool was applied to determine the influence of the coupling parameters on the CT spectra. In the third part, the tool was used to simulate the real spectra of different semiconducting blends.

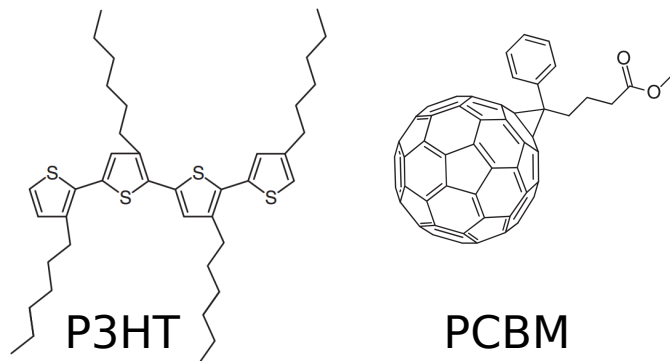


Figure 1.1: Structures of P3HT and PCBM [3]

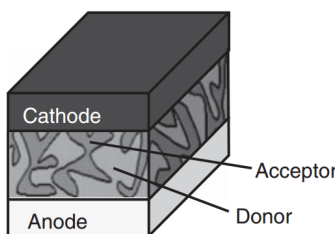


Figure 1.2: Donor and acceptor blend (bulk heterojunction) between anode (covered substrate) and cathode, taken from [3]

Chapter 2

Theoretical aspects

A solar cell is a device that converts solar energy into electrical energy. The simplest solar cell consists of an absorber layer and two selective contacts. An absorbed photon excites an electron that goes to one of the contacts, and a created vacancy goes to the other contact – an electrical current flows. That is how a solar cell works (Fig 2.1).

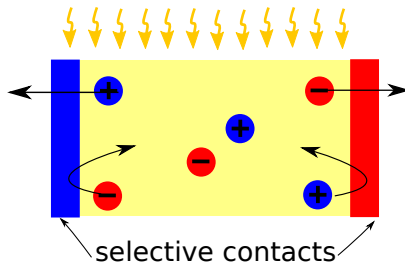


Figure 2.1: A working principle of a primitive solar cell

The efficiency of a solar cell is governed by two entities. First one is the absorber material, that influences the efficiency of photon absorption, electron-hole separation and charge transfer to the electrodes. And the second one is the relative energy structure between the contact metals and the absorber, that influences the efficiency of charge extraction. For a highly efficient solar cell, a good absorber is therefore very important. Organic semiconductors are very promising for efficient solar cells with a new field of application. Let us consider them in more detail.

Physical properties of organic materials

We start with a small organic molecule - ethylene (Fig. 2.2). It consists of two carbon atoms and four hydrogens. The carbon atom has a '2s'- and three '2p'-orbitals. The '2s'-orbital interacts with '2p_x' and '2p_y' that creates three sp²-hybrid orbitals. They lie in a plane and have an angle of 120° in between. The C-H σ-bond is created by the interaction of the 'sp²'-hybrid orbital of a C atom and a '1s'-orbital of an H atom. The C-C σ-bond is created by the interaction of the C atoms 'sp²'-hybrid orbital. Each C has an additional 'p_z'-orbital. They interact to form the C-C π-bond that can be either bonding (symmetric) or anti-bonding (antisymmetric).[8]

The bonding molecular orbital is lower in energy and is called HOMO (Highest Occupied Molecular Orbital) and an anti-bonding state is called LUMO (Lowest Unoccupied

2.1. PHYSICAL PROPERTIES OF ORGANIC MATERIALS

Molecular Orbital). In the ground state there are two electrons in the HOMO. By photon absorption, one of the electrons can be excited to the LUMO.

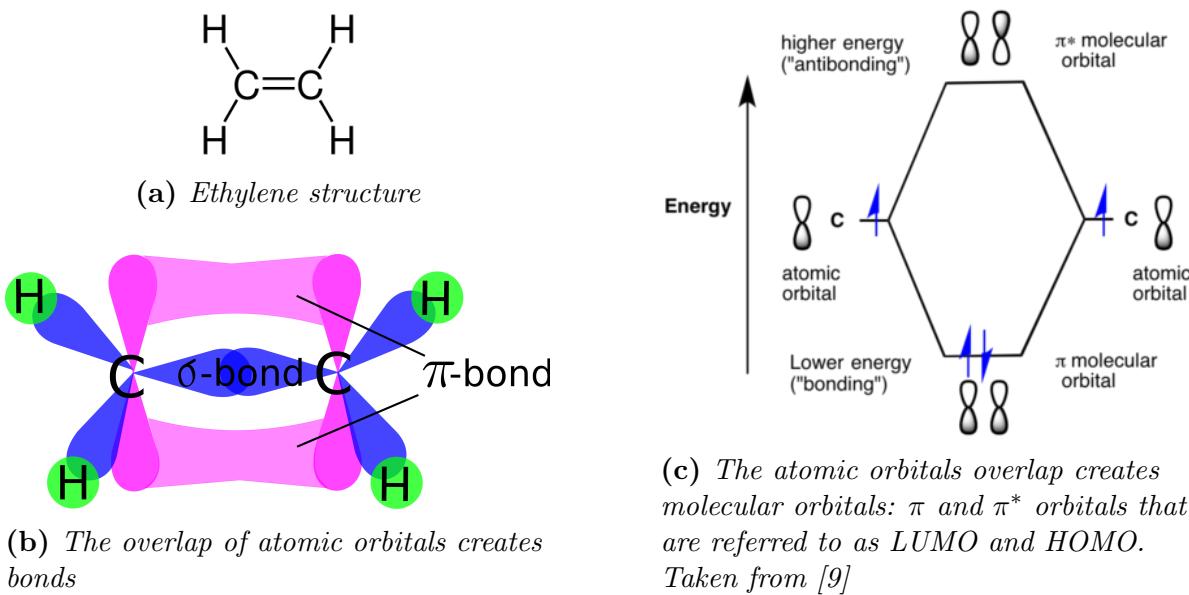


Figure 2.2: Molecular orbitals creation by atomic orbitals overlap in ethylene

Consider now a longer chain, which is a sequence of double and single bonds. Such a chain is called a conjugated polymer. One can easily see that there are more occupied and unoccupied states available (Fig. 2.3). The energetic structure can be considered then as energy bands. This is an analogy to inorganic semiconductors. The difference between LUMO and HOMO is an analogy to the band gap. It is important to keep in mind that in organic materials, 'bands' are represented by separated levels of individual molecules. A molecule is much bigger than an atom. The interactions inside a molecule are stronger than between neighboring molecules. An overlap of the molecule wave functions is small and therefore, an excited electron is localized within one molecule. In inorganic materials, a strong overlap of wave functions makes an excited electron common for several atoms, therefore electrons are delocalized over the whole crystal. One can consider an inorganic material as a big organic molecule.

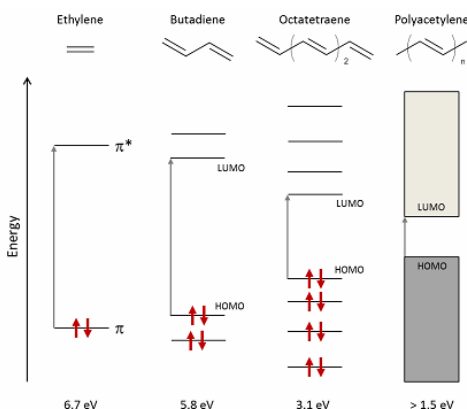


Figure 2.3: Schematic energy-level splitting with different conjugation lengths. The band-gap depends on the chain length in the polymer. Taken from [10]

There is one more difference between organic and inorganic materials. It is characterized by the dielectric constant. It gives a measure of ease with which charges are displaced in response to an electric field. In inorganic materials, the dielectric constant is high $\epsilon \approx 12$. [3] This means that screening by other electrons (holes) is strong. In addition, charge carriers are relatively delocalized (the states are extended in space). Thus, an electron and a hole can easily be separated even by thermal energy $kT = 25$ meV at 300 K.

In contrast, for organic semiconductors, the low value of the dielectric constant of $\epsilon \approx 3.5$ means that the Coulomb interaction between electrons is substantial and cannot be neglected. Therefore a bound state between an excited electron and a hole is created. It is called an exciton. Its binding energy is high - larger than 0.5 eV. [3] But it is very much depends on the material and can be smaller in some cases.

An exciton can go through the conjugated polymer. It may hop to another polymer nearby, but the probability of this process is low.

If one now mixes a conjugated polymer with a fullerene, then the excited electron can hop very fast towards the neighboring fullerene. This process happens within femtoseconds with almost a 100% probability. This can be explained by the Marcus theory [11, 12]. The resulting state is called the Charge Transfer (CT) state (Fig. 2.4). In this state, an electron and a hole still interact with each other, but they are weakly coupled because of the longer distances. If the charge separation happens afterwards, an electron travels to a selective contact trough the acceptor-fullerene and a hole travels to another contact trough the donor-polymer. A recombination can happen as well, then the charges will be 'lost' and a total extracted current and therefore the efficiency of a solar cell will be lower.

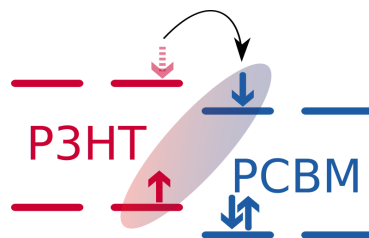


Figure 2.4: Charge Transfer (CT) state

So far we have not considered the spin of electron. To understand the spin role in charge separation, let us consider this process from the beginning. There are two electrons in the ground state, which are on the polymer's π -molecular orbital. Due to the Pauli principle, they are having opposite spins. When one electron is excited, because of the low dielectric constant, it strongly interacts with the hole that is a vacancy near the second electron. The probability of an excited electron to return back to its vacancy depends on the second spin, as Pauli principle should be satisfied. With some small external influences and/or the local magnetic fields (due to spin-orbit coupling) the spins can be flipped. If the electrons are on the same molecule, then their spins are changed simultaneously, so they still have opposite spins. However, if the excited electron hops onto the fullerene, then the two spins have various environments and a larger distance. It is then easy to change them separately. They are not opposite anymore and the probability of the electron-hole recombination is low, as Pauli principle is no longer satisfied. This affects the life time of the CT state. A distinct energy level and a finite life time make the CT

state important in charge separation.

There are lots of discussions about the CT state origins and about their influence on the charge separation and recombination probabilities [13, 14, 15, 16]. We want to make more research in this direction and try to solve the uncertainty about the impact of relative orientations between the donor and the acceptor on the CT states. And we want to show that in some studies, the obtained inter-spin distances may contain an error, as several factors are usually not taken into account.

In the field of organic semiconductors, an electron is often referred to as a negative polaron. When a charge is placed on a molecule, not only the geometry of the molecule changes, but also the mean distance to the neighboring molecules. This is caused by the different polarization of the charged molecule. As the charge moves through the material by transferring from molecule to molecule, it carries the lattice distortion with it. The combination of the charge and the accompanying lattice distortion is correctly termed a polaron. [3]

The same is true for the hole: it is referred to as a positive polaron.

Electrons in the magnetic field

Each electron has an intrinsic angular momentum. In a magnetic field the projection of it along the direction of the magnetic field B can be $m_S=+1/2$ ("spin up") or $m_S=-1/2$ ("spin down"). These two states have different energies in a magnetic field. The energetic splitting between them is referred to as the "Zeeman splitting". The Zeeman interaction between a spin and the magnetic field can be described by the following Hamiltonian:

$$\mathcal{H}_{\text{Zeeman}} = \beta_e \mathbf{B}_0 \mathbf{g}_A \mathbf{S}_A \quad (2.2.1)$$

where β_e is Bohr magneton, \mathbf{B}_0 is the magnetic field vector pointing along the z-axis in the laboratory frame, \mathbf{g}_A is the g tensor of spin A and \mathbf{S}_A is the spin operator for spin A.

Using microwave (mw) frequency radiation, a spin can be flipped. In other words, by the absorption of mw radiation, an electron can be excited from a lower energy state ("spin down") to a higher energy state ("spin up"), or it can return from the higher energy state to the lower one by the stimulated emission. The mw absorption and emission intensities can be measured as a function of the magnetic field. The obtained values are Electron Paramagnetic Resonance (EPR) spectrum.

We are interested in a system, that consists of two spins that slightly interact with each other. We refer to it as to a weakly coupled polaron pair or a CT state. The spin interactions are considered in the next section.

Interactions

There are two different mechanisms of interaction between electrons, referred to as J- and D-coupling. The electron-exchange interaction (J) is described by the wave function overlap. It is responsible for the energy splitting between a singlet and a triplet, represented by the spin Hamiltonian

$$\hat{\mathcal{H}}_{\text{exch}} = \frac{1}{2} (\hat{\mathbf{S}}_A^T \cdot \mathbf{J} \cdot \hat{\mathbf{S}}_B + \hat{\mathbf{S}}_B^T \cdot \mathbf{J} \cdot \hat{\mathbf{S}}_A) \quad (2.3.1)$$

where $\hat{\mathbf{S}}_A$ and $\hat{\mathbf{S}}_B$ are the electron-spin operators for electrons A and B. \mathbf{J} is a tensor that describes the Coulomb interaction between two unpaired electrons, but not the magnetic interaction. The most important part is the isotropic electron-exchange coupling constant $J_0 = Tr(\mathbf{J})/3$, which, to the first approximation, is given by the exchange integral. [17]

Whether the singlet or the triplet state lies lower depends on the sign of J_0 . See an example of energy splitting for a negative J_0 in the Fig. 2.5. The magnitude of J_0 depends on the distance r between electrons. For relatively localized wave functions, $J_0 \propto \exp(-r)$. This is probably not the case for the considered systems, but should work in the first approximation.

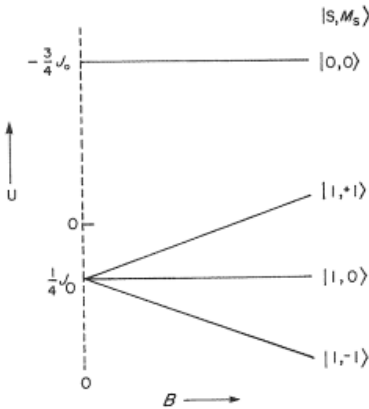


Figure 2.5: Energy levels of a system that consist of two strongly interacting electrons ($J_0 \gg \Delta g$). Only exchange interaction $J_0 < 0$ is considered. For a positive J_0 , the singlet state lies lower in energy. Taken from [17]

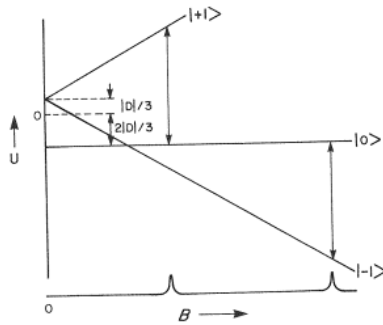


Figure 2.6: Energy levels of a system with spin $S = 1$. $\mathbf{B}||\mathbf{z}$, $D > 0$, $E=0$. Two possible transitions are indicated with arrows. If $E \neq 0$, then the degeneracy at $B=0$ is shifted and the energies vary non-linearly with B . Taken from [17]

In addition to the electron exchange coupling, a second anisotropic coupling exists. This is the magnetic dipole-dipole interaction. It removes the three-fold degeneracy of the triplet state even in the absence of a magnetic field (Fig. 2.6).

Classical electrodynamics allows one to write a part of the Hamiltonian corresponding to the interaction between two magnetic moments at a distance \mathbf{r} as follows

$$\hat{\mathcal{H}}_{Dip} = \mu_0 \pi \left(\frac{\hat{\mu}_1^T \cdot \hat{\mu}_2}{r^3} - \frac{3(\hat{\mu}_1^T \cdot \mathbf{r})(\hat{\mu}_2^T \cdot \mathbf{r})}{r^5} \right) \quad (2.3.2)$$

Here, the magnetic moment of the electron is $\hat{\mu}_i = -\beta_e g_i \hat{\mathbf{S}}_i$. If one plugs this into the Hamiltonian and does transformations, one gets $\hat{\mathcal{H}}_{Dip} = 2\mathbf{S}_{\mathbf{A}}^T \mathbf{D} \mathbf{S}_{\mathbf{B}} = \mathbf{S}^T \mathbf{D} \mathbf{S}$ (for more details see [17]). \mathbf{D} can be diagonalized. The diagonal elements are D_{xx}, D_{yy}, D_{zz} . Because $Tr(\mathbf{D}) = 0$ (this is clear why, if abovementioned transformations are done), there are only two independent variables:

$$D := \frac{3}{2} D_{zz} \quad E := \frac{1}{2} (D_{xx} - D_{yy}) \quad (2.3.3)$$

For big distances ($>10 \text{ \AA}$) the point dipole approximation will work, thus $D_{xx} = D_{yy}$, and hence one can neglect E. D_{zz} is usually referred to as D , which we will do here as well. The distances between polarons in CT states are smaller and, hence, this approximation is very rough and will probably be removed in future studies.

$$\mathbf{D} = \begin{pmatrix} -\frac{1}{3}D & 0 & 0 \\ 0 & -\frac{1}{3}D & 0 \\ 0 & 0 & \frac{2}{3}D \end{pmatrix}, \quad \text{where} \quad D = -\frac{3\mu_0 h}{8\pi} \frac{g_A g_B}{r^3} \beta^2 \quad (2.3.4)$$

Here, D is actually D_{zz} . Later this will be meant without any additional comments. Also D is a frequency and it is calculated here as an angular frequency. One should pay attention to it, as at some literature different values by D could be meant: $D = \frac{3}{2}D_{zz}$ and $D = 2\pi\tilde{D}$.

When a direction of the magnetic field $\mathbf{e}_{\mathbf{B}}$ is determined, the effective dipolar coupling is defined:

$$d = \mathbf{e}_B^T \mathbf{D} \mathbf{e}_B = D(\cos^2 \theta - \frac{1}{3}) \quad (2.3.5)$$

Here θ is the angle between the magnetic field and the principle z axis of the system.

D-coupling is usually used for finding the distances between two spins. If one puts numbers in the equation 2.3.4 above, one gets that for $g_A = g_B = 2$

$$D(\text{MHz}) = \frac{3}{2} D_{zz}(\text{MHz}) = \frac{78}{(r[\text{nm}])^3} \quad (2.3.6)$$

In the Table 2.1 some D values and inter-spin distances are shown to get a better impression of the values for CT states.

r (nm)	D (G)	D (MHz)	D _{zz} (G)	D _{zz} (MHz)
0.5	222	622	148	414
1.0	28	78	19	52
1.5	8.2	23	5.5	15
2.0	3.5	9.8	2.3	6.5
4.0	0.43	1.2	0.29	0.80
6.0	0.13	0.36	0.09	0.24

Table 2.1: Magnitude of D and D_{zz} as a function of the inter-spin distance [18]

There is additional interaction of electron with nuclei. In the considered systems, charges are delocalized on the molecules. This means that the interaction with nuclei (hyperfine coupling) is averaged out, therefore it can be included as a broadening mechanism and hence will not be considered as a part of the Hamiltonian.

Quantum-mechanical calculations

The derivations and equations here were taken from [19, 20, 17, 21].

Summarizing previous sections, the total Hamiltonian for two polaron system inside the magnetic field can be written as

$$\mathcal{H}_0 = \beta_e \mathbf{B}_0 \mathbf{g}_A \mathbf{S}_A + \beta_e \mathbf{B}_0 \mathbf{g}_B \mathbf{S}_B + \frac{1}{2} (\hat{\mathbf{S}}_A^T \cdot \mathbf{J} \cdot \hat{\mathbf{S}}_B + \hat{\mathbf{S}}_B^T \cdot \mathbf{J} \cdot \hat{\mathbf{S}}_A) + 2 \mathbf{S}_A^T \mathbf{D} \mathbf{S}_B \quad (2.4.1)$$

where β_e is Bohr magneton, \mathbf{B}_0 is the magnetic field vector pointing along the z-axis in the laboratory frame, \mathbf{g}_A and \mathbf{g}_B are the g tensors of spins A and B, \mathbf{S}_A and \mathbf{S}_B are the spin operators for spins A and B, \mathbf{J} is the exchange coupling tensor and \mathbf{D} is the dipole-dipole coupling tensor. The first two terms in the Hamiltonian correspond to the Zeeman interaction of the spins with the magnetic field. The last two terms correspond to the interaction of two electrons with each other.

If each molecule of the system has a defined fixed orientation in the magnetic field then it is enough to consider effective g values g_A and g_B . The Hamiltonian for a fixed system orientation in the magnetic field becomes

$$\mathcal{H}_0 = \beta_e B_0 g_A S_{A_z} + \beta_e B_0 g_B S_{B_z} - J(S^2 - 1) + \frac{1}{2} d(3S_z^2 - S^2) \quad (2.4.2)$$

where B_0 is the magnetic field strength; S_{A_z} and S_{B_z} are the components of the electron spin operators along the magnetic field direction; $\mathbf{S} = \mathbf{S}_A + \mathbf{S}_B$ is the operator for the total spin and S_z is its z component. J and d are exchange and dipolar interactions between the electron spins respectively.

The Hamiltonian operator can be represented as a matrix. It can be diagonalized in the eigenfunction basis.

Depending on the interaction strength between two charge carriers, the Hamiltonian (eq. 2.4.2) has different eigenfunctions. In case of strong coupling, there are four eigenfunctions that are referred to as singlet (total spin is zero) $|S\rangle$ and three triplets (total spin is one) $|T_+\rangle$, $|T_-\rangle$, $|T_0\rangle$, see Fig. 2.8. Weakly coupled electron pairs can be described by four eigenstates – two triplets - $|T_+\rangle$ and $|T_-\rangle$ and states $|2\rangle$ and $|3\rangle$ that are mixtures of triplet and singlet.

In a basis $|S\rangle$, $|T_+\rangle$, $|T_-\rangle$, $|T_0\rangle$, the Hamiltonian may be written in the following form:

$$\hat{\mathcal{H}}_0 = \begin{pmatrix} |T_+\rangle & |S\rangle & |T_0\rangle & |T_-\rangle \\ \omega - J + \frac{1}{2}d & 0 & 0 & 0 \\ 0 & J & Q & 0 \\ 0 & Q & -J - d & 0 \\ 0 & 0 & 0 & -\omega - J + \frac{1}{2}d \end{pmatrix} \quad (2.4.3)$$

with ω and Q that are half sum and half difference of the Larmor frequencies

$$\omega = \frac{1}{2}(\omega_A + \omega_B) = \frac{1}{2}(g_A + g_B)\beta_e B_0 \quad (2.4.4)$$

$$Q = \frac{1}{2}(\omega_A - \omega_B) = \frac{1}{2}(g_A - g_B)\beta_e B_0. \quad (2.4.5)$$

Diagonalization of this matrix allows one to find corresponding eigenvalues and eigenstates for a weakly coupled case:

$$\begin{aligned} |1\rangle &= |T_+\rangle & w_1 &= \omega - J + \frac{1}{2}d \\ |2\rangle &= \cos\phi|S\rangle + \sin\phi|T_0\rangle & w_2 &= \Omega - \frac{1}{2}d \\ |3\rangle &= -\sin\phi|S\rangle + \cos\phi|T_0\rangle & w_3 &= -\Omega - \frac{1}{2}d \\ |4\rangle &= |T_-\rangle & w_4 &= -\omega - J + \frac{1}{2}d \end{aligned} \quad (2.4.6)$$

With Ω and ϕ defined as:

$$\Omega = [(J + \frac{1}{2}d)^2 + Q^2]^{1/2} \quad (2.4.7)$$

$$\tan 2\phi = \frac{Q}{J + \frac{1}{2}d} \quad (2.4.8)$$

ϕ is the angle that shows contribution of triplet and singlet states (with $m_s = 0$) in a particular state. If $\phi = 0$, then $|2\rangle = |S\rangle$, $|3\rangle = |T_0\rangle$. If $\phi = \pi$, then $|2\rangle = |T_0\rangle$, $|3\rangle = |S\rangle$. The mixing ratios depend on interaction strength and on $\Delta g = g_A - g_B$.

The found eigenstates describe states in which our system (a weakly coupled polaron pair) can be situated. The eigenvalues describe energies of these states.

Using an appropriate frequency of radiation, it is possible to induce transitions between the four eigenstates. These frequencies can be easily calculated: a frequency of transition from state i to j $w_{ji} = w_j - w_i$.

The intensity of the transitions is proportional to the probability of the transitions and to the population of the states (n):

$$I_{ji} \propto \langle j|\hat{\mathcal{H}}_1|i\rangle (n_i - n_j) \quad (2.4.9)$$

Hamiltonian $\hat{\mathcal{H}}_1$ describes an interaction between a CT state (a weakly coupled polaron pair) and an oscillatory magnetic field: $\hat{\mathcal{H}}_1 = g\beta_e B_1 \hat{S}_x$. The latter should always be perpendicular to the static B_0 field that is parallel to z axis. Here we considered that B_1 is along the x axes.

The probabilities of transitions $\langle 1|\hat{\mathcal{H}}_1|2\rangle^2$ and $\langle 4|\hat{\mathcal{H}}_1|2\rangle^2$ are proportional to $\sin^2\phi$; $\langle 1|\hat{\mathcal{H}}_1|3\rangle^2$ and $\langle 4|\hat{\mathcal{H}}_1|3\rangle^2$ are proportional to $\cos^2\phi$.

To calculate the intensities, we need to know the populations of the eigenstates. We know that the ground state is a singlet state, as two electrons on the HOMO of the polymer should have opposite spins due to the Pauli principle, hence the total spin is zero. Singlet-triplet transitions are forbidden, thus an excited state should be a singlet as well - a singlet exciton. With the same reasoning, only the singlet part of the CT state can be occupied. Then it is easy to determine the populations: $n_1 = 0$, $n_4 = 0$, $n_2 = \cos^2\phi$, $n_3 = \sin^2\phi$.

It is now clear from eq.2.4.9 that

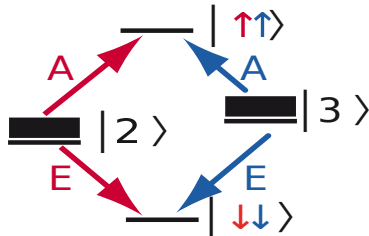
$$\begin{aligned} |2\rangle \rightarrow |1\rangle & \quad w_{12} = \omega - \Omega - (J - d) & I_{12} &= \cos^2\phi \sin^2\phi \\ |2\rangle \rightarrow |4\rangle & \quad w_{24} = \omega + \Omega + (J - d) & I_{24} &= -\cos^2\phi \sin^2\phi \\ |3\rangle \rightarrow |1\rangle & \quad w_{13} = \omega + \Omega - (J - d) & I_{13} &= \sin^2\phi \cos^2\phi \\ |3\rangle \rightarrow |4\rangle & \quad w_{34} = \omega - \Omega + (J - d) & I_{34} &= -\sin^2\phi \cos^2\phi \end{aligned} \quad (2.4.10)$$

It is interesting, that all four transitions will have the same intensities.

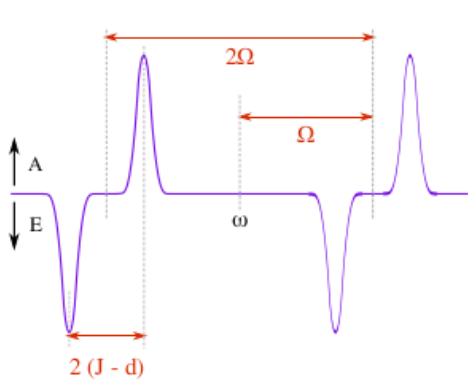
These transitions can be observed in the experiment, but first, let us understand how the spectra should look like. For this we can visualize the obtained equations.

We know that a CT state is described by four eigenstates and in the beginning only states $|2\rangle$ and $|3\rangle$ are populated. Afterwards, the mw radiation initiates four transitions (Fig. 2.7a) - two absorptive and two emissive. In the simplest case, they will look like Fig. 2.7b. The transition probabilities (the intensity of the peaks) depend on the energy splitting and on the state populations. The energy splitting (the peak positions) depends on the electron-electron and the electron magnetic field interactions, that is indicated on the figure. There, the simplest case is shown: the isotropic g-values are used and the lines are not overlapping.

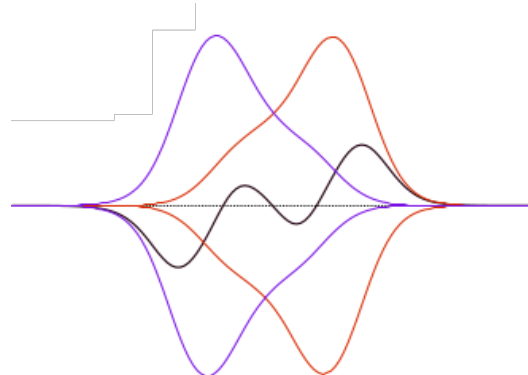
In a more complex case (anisotropic g-values) the spectra look like in Fig. 2.7c. The red and the blue peaks each correspond to one of the transitions. It is not possible to measure them separately in the experiment, so one observes the sum spectrum (black curve).



(a) *Mw induced transitions between eigenstates of a CT state. Taken from [4]*



(b) *The easiest case (isotropic g-values, energies of transitions do not overlap). Taken from [21]*



(c) *Usual case (anisotropic g-values, energies of transitions overlap). That leads to the case that in an experiment one sees the sum of the four transitions (black line). Taken from [21]*

Figure 2.7: *Transitions between the eigenstates lead to four peaks (two absorptive and two emissive) in trEPR spectra*

The experimental technique that corresponds to the described calculations is called time resolved or transient EPR (trEPR).

CT states observed in EPR

Paramagnetic states can be detected with paramagnetic resonance. We want to study CT states that exist after photon absorption for some time and then disappear through relaxation or through charge separation. Thus, we want to see induced transitions at a certain time after light excitation. Therefore, the most convenient detection technique in this case is trEPR.

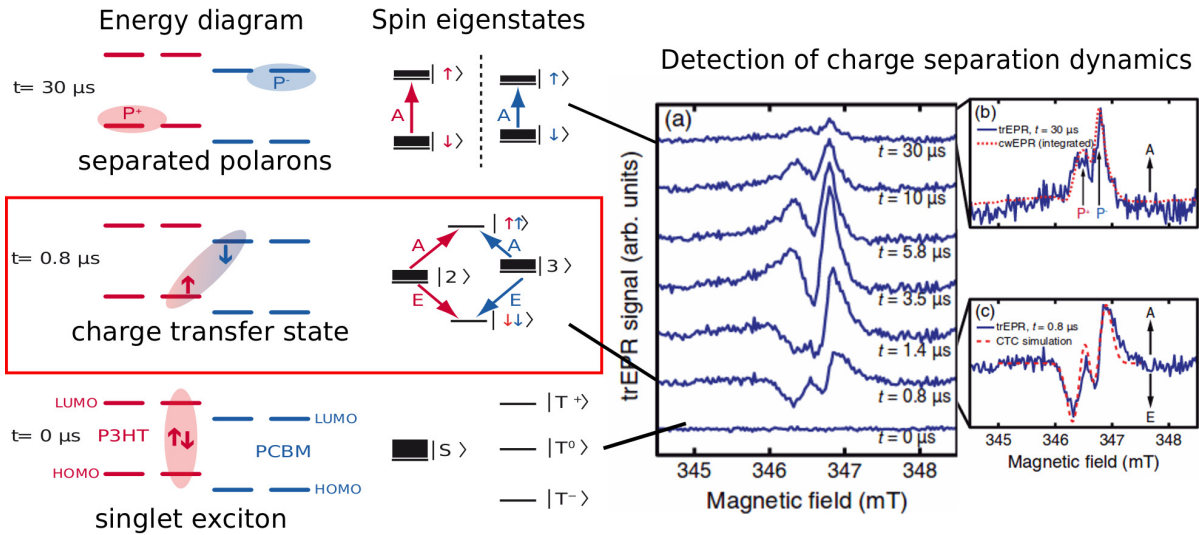


Figure 2.8: *On the left:* a schematic energy diagram of the HOMO and LUMO levels and corresponding spin-pair eigenstates. The arrows indicate the EPR-active transitions that give rise to absorptive (A) and emissive (E) signals in the trEPR spectrum.

On the right: Series of trEPR spectra of a P3HT:PCBM blend obtained at $T = 100$ K. (a) Spectra recorded for several delay times after the laser flash. (b) Zoom into the spectrum at $t = 30 \mu\text{s}$ along with the integrated cwEPR spectrum measured under continuous illumination with white light (c) Zoom into the spectrum at $t = 0.8 \mu\text{s}$ together with the simulation results for a coupled polaron pair. Taken from [4]

An example of a trEPR spectrum and an explanation of the observed transitions as well as their origin are given in Fig. 2.8. Here, one can see some spectra measured at different times after the laser flash. On the left, the corresponding energy diagrams and the spin eigenstates are shown.

There is no signal right after the flash ($0 \mu\text{s}$). This is because the singlet excitons are not visible in trEPR.

After a very long time ($30 \mu\text{s}$ in this case), one sees two mw absorption peaks that correspond to a flip of the electron on a fullerene and a flip of the hole that remains on a polymer. This corresponds to the separated charges – free polarons. Behrends *et al.* [4] measured the cwEPR spectra and it gave the same shape and peak positions as the trEPR spectra at later times (in red in Fig. 2.8 b).

The most interesting part are the spectra from 0.8 to $10 \mu\text{s}$ after the laser flash. This is an intermediate state between a singlet exciton on the polymer and separated polarons - the CT state. In this state, the electron has already been transferred to the fullerene but it still interacts with a hole. The distance between them is bigger than when they

were sitting on the same molecule (polymer) and therefore the interaction between them is weaker, but still not zero.

We consider only the earliest CT states because the initial population is known and we want to neglect the relaxation processes. A CT state is coming from a singlet exciton and, because of momentum conservation, the initial population can occur only in the singlet state, i.e. in states $|2\rangle$ and $|3\rangle$.

CT state simulations

We want to simulate a trEPR spectrum of a CT state which are absorption and emission peaks of mw radiation.

From the equations above, it is clear that in order to simulate trEPR spectra for such a CT state, one needs to determine the following parameters:

1. g-value, g-strain, line width
2. couplings J and D

The first three parameters can be extracted from cwEPR spectra. The simulations of trEPR spectra are made by adding the two coupling parameters.

In cwEPR one observes free (uncoupled) polarons. The signal of the CT state obtained in trEPR is a signature coming from the coupled polarons. The following assumption should be made: polarons in both cases - as they are free or coupled - are in the same environment. Hence, the same g-values are considered. If we consider a hole sitting on the polymer, then in the CT state, it will sit on the polymer near the donor/acceptor interface. If the CT state dissociates and the hole hops further, it will then sit on a different molecule, but that is still the identical polymer. So one can state that the environment of the hole (electron) does not change.

Other important factors taken into account are the relative orientation of both radicals as well as the orientation of the whole system in the magnetic field. This is discussed in the next section.

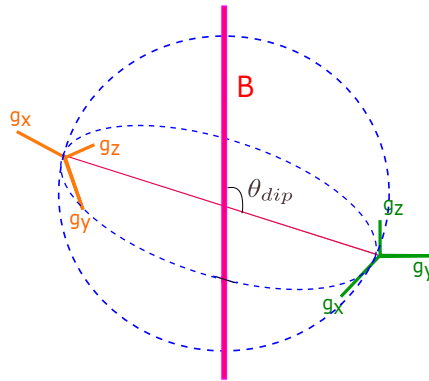


Figure 2.9: System model: two interacting spins sit on two different molecules (two different anisotropic g-tensors) in the magnetic field B

System orientations

As it is shown in the previous sections, the simulated spectra depend on $Q \propto g_A - g_B$ and $w \propto g_A + g_B$. Both polarons can have anisotropic g-matrices, due to the anisotropic

molecular structure. It is clear that a trEPR spectrum depends on the relative orientation of the molecules, as a g-tensor is associated with the molecule. Also the position of the peaks depends on the couplings between electrons. The D-coupling depends on the system orientation in the magnetic field. Also this should be taken into account. Let us consider this in more detail.

In this thesis, charge separation at the polymer-fullerene interface is considered. More precisely, two interacting spins are studied: one sits on a polymer, another one - on a fullerene. This means that the system consists of two interacting charge carriers in two different environments. Each of them in general has an anisotropic g-tensor, the orientation of which is given by the molecule orientation, see Fig 2.9. There are several possibilities for the relative orientation of two molecules:

1. Relative orientation of two radicals is fixed and described by the Euler angles. This approach is widely used in biology, where two radicals are usually two parts of one protein that has a fixed structure. For example, it is used in [22].

The same approach of a fixed relative orientation between two polarons was implemented for the polymer:fullerene blends by Kobori [6, 7]. He considered two radicals that are two different molecules, P3HT⁺ and PCBM⁻, and he found a relative orientation between them that gave a good result for a trEPR CT state spectra simulation.

In general, two different molecules can have random orientations and it is not clear if a fixed orientation is the right approach.

2. All relative orientations are equally probable - this statement should be applicable for disordered blends.
3. Intermediate approach – there are some preferential relative orientations. This means that different relative orientations of two molecules have different probabilities.

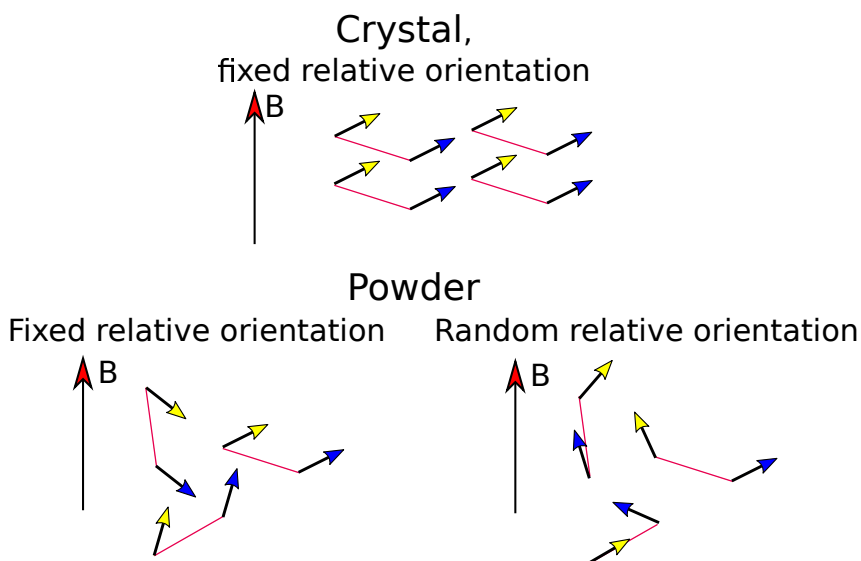


Figure 2.10: Different possible orientations of the system in a magnetic field. Arrows indicate the g_{zz} directions. Yellow corresponds to one molecule and blue to another one. Red lines indicate, which two spins are coupled.

Another consideration regarding the orientation is that two molecules are situated in the magnetic field B . In a crystal, the orientation of every system would be fixed with respect to the magnetic field. It is easy to simulate such a case. In this work only amorphous materials are considered. So the system (that consists of two radicals) can have all possible orientations in the magnetic field and these orientations are all equally probable. We refer to it as to a powder.

Possible models are indicated in the Fig. 2.10.

The main goal of the first part of the thesis is to compare two models under assumption of a powder:

- the relative orientation between radicals is fixed
- all orientations are possible and equally probable

For this, one should be able to simulate both cases.

Electron paramagnetic resonance (EPR)

Several types of EPR have already been mentioned. Here the difference between them is clarified.

Three different kinds of paramagnetic resonance detection techniques exist: continuous wave (cw), transient (tr) and pulsed (p).

In cwEPR, a light excitation (if it is used), a mw radiation and a magnetic field are switched on all the time. This technique is used to extract the system parameters such as g-factor, g-strain, line width (lw), strong hyperfine interaction (HFI) constants and weights of spectral components.

In trEPR, mw absorption is measured as a function of time delay after the light flash. It can be used to determine electron-electron couplings.

In pEPR, light is always on and the change of the magnetization is measured after a mw pulse. It can give information about electron-nuclei interactions.

All these techniques provide an insight into the electron environment and give valuable information about the structure and properties of materials.

In this thesis only cw and trEPR are used. Using trEPR, coupled polarons are studied. And in cwEPR, the spectra from separated polarons are observed. A lock-in amplifier is usually used for detection in cwEPR spectroscopy, that increases the signal-to-noise ratio and results in the first derivative of the spectra. This makes cwEPR spectra look similar to trEPR spectra. It is important to remember that they represent completely different situations! An integrated cwEPR spectrum should correspond to a late-time trEPR signature, that is two absorptive peaks.

Different mw frequency ranges together with different strengths of the magnetic field can be used to resolve different properties. For example, X- (around 10 GHz, 0.3 T) and Q-band (around 35 GHz and 1.2 T) can be used to distinguish between the line width and the g-strain. The line width characterizes a field independent broadening that includes hyperfine interaction. The g-strain characterizes a field dependent broadening, mostly a distribution over g-values.

Chapter 3

Simulations and Visualization Toolbox

Simulations

Easyspin[23] is the most common toolbox for EPR simulations. It is an extension module for Matlab (The MathWorks, Natick, MA). It has a lot of functions for EPR simulations for different cases. One of the functions is suitable for trEPR simulations of the CT states. It works for both crystals and powders. It takes the electron couplings into account, but works only for the relatively fixed orientation between two radicals.

The problem occurs when the orientation between two radicals is not fixed. In general it is possible to use the Easyspin function for different relative orientations. But this leads to long calculation times. The solution for this was found by Felix Kraffert [19] and it is discussed later.

In this thesis, only blends and therefore powders are considered: the system can have equally probable orientations in the magnetic field, described by the angles θ and ϕ . In simulations, it is impossible to consider a continuous distribution of angles, so that a set of θ and ϕ should be selected. For this, an Easyspin function "sphgrid" can be used [23]. It allows one to choose such a set in an effective way. It exploits the symmetry of the system and the fact that, for example, pairs $[\theta, \phi] = [0, 0], [0, \pi/100], [0, \pi/10], [0, \pi/2], \dots$ correspond to the same point - the pole. This function is also aware of the fact that it is not an effective approach to take the same amount of points for different θ , because the distribution of points near the pole is more dense than on the equator.

As discussed, there are two parameters, which depend on the orientation in the magnetic field: the D-coupling and the effective g-values. It does not matter, by which angle ϕ the system is being rotated around the magnetic field axis. Hence, it is enough to consider only θ values.

There are two possibilities for relative orientations: a fixed relative orientation and random relative orientations that are equally probable. These are discussed in the following sections.

Fixed relative orientation in the powder model

In this case, the system consists of two electrons, their g-tensors have the relatively fixed orientation described by the Euler angles, see Fig. 2.9

The trEPR spectrum is the mw absorption intensity as a function of the magnetic field B_0 . It is measured at a fixed mw frequency w_{mw} . This means that in eq. 2.4.10 $w_{12} = w_{24} = w_{13} = w_{34} = w_{mw}$. And that equation can be written as

$$w_{mw} = \frac{1}{2}(g_A + g_B)\beta_e B_0 \pm [(J + \frac{1}{2}d)^2 + Q^2]^{1/2} \pm (J - d), \quad \text{where } d = D(\cos^2 \theta - \frac{1}{3}) \quad (3.2.1)$$

Every magnetic field position from the experiment should be checked. If one of the four equalities for frequencies from eq. 3.2.1 is satisfied then the intensity for the current B_0 field position is not zero and it could be calculated by using expressions for intensities (eq. 2.4.10). For the equation 3.2.1, all parameters are known: from the X- and Q-band cwEPR spectra, anisotropic g-values, g-strains and line widths were extracted (using the Easyspin functions). Different J, D parameters and Euler angles should be tried to find a proper fitting.

This procedure (calculating intensities for each B_0 field position) should be repeated for each θ angle.

If the obtained spectrum does not fit the experimental data, another set of J, D and six Euler angles should be tried.

Random relative orientations in the powder model

In comparison to the previous case, all possible relative orientations should be considered. For each rotation of the first radical, every possible rotation of the second radical should be considered as well as every orientation of the whole system in the magnetic field. All three rotations are described by the sets of θ and ϕ that are obtained with Easyspin function "sphgrid".

This is a long procedure with long calculation times. The solution was found by Kraffert [19]. Analytical solutions of equations 3.2.1 give resonance magnetic fields. So not all magnetic field positions should be considered but only the resonant ones. That decreases the calculating time dramatically (in some cases to less than 1 second). The four real solutions are following:

$$\begin{aligned} B_{12} &= \frac{a(w+(J-d))}{a^2-b^2} + \sqrt{\frac{a^2(w+(J-d))^2}{(a^2-b^2)^2} - \frac{(w+(J-d))^2-c^2}{a^2-b^2}} \\ B_{13} &= \frac{a(w+(J-d))}{a^2-b^2} - \sqrt{\frac{a^2(w+(J-d))^2}{(a^2-b^2)^2} - \frac{(w+(J-d))^2-c^2}{a^2-b^2}} \\ B_{24} &= \frac{a(w-(J-d))}{a^2-b^2} - \sqrt{\frac{a^2(w-(J-d))^2}{(a^2-b^2)^2} - \frac{(w-(J-d))^2-c^2}{a^2-b^2}} \\ B_{34} &= \frac{a(w-(J-d))}{a^2-b^2} + \sqrt{\frac{a^2(w-(J-d))^2}{(a^2-b^2)^2} - \frac{(w-(J-d))^2-c^2}{a^2-b^2}} \end{aligned} \quad (3.3.1)$$

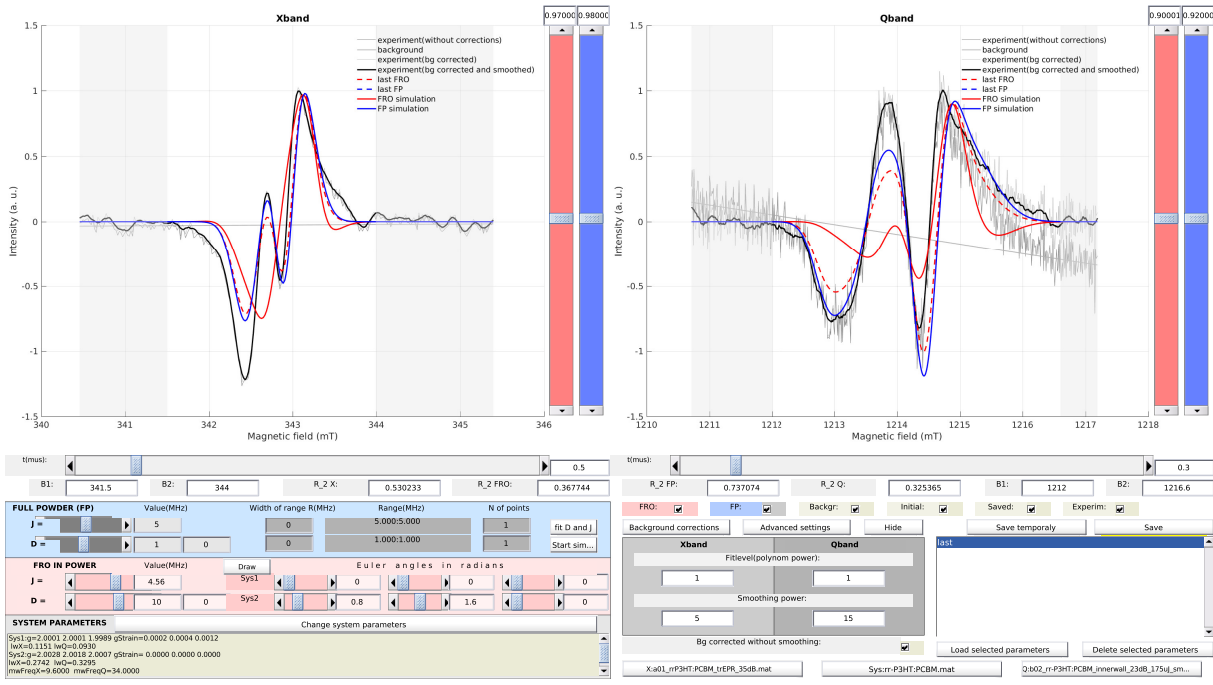
where $a = \frac{1}{2}(g_A + g_B)\beta_e$, $b = \frac{1}{2}(g_A - g_B)\beta_e$, $c = (J + \frac{1}{2}d)^2$ and $w = w_{mw}$

Visualization Toolbox

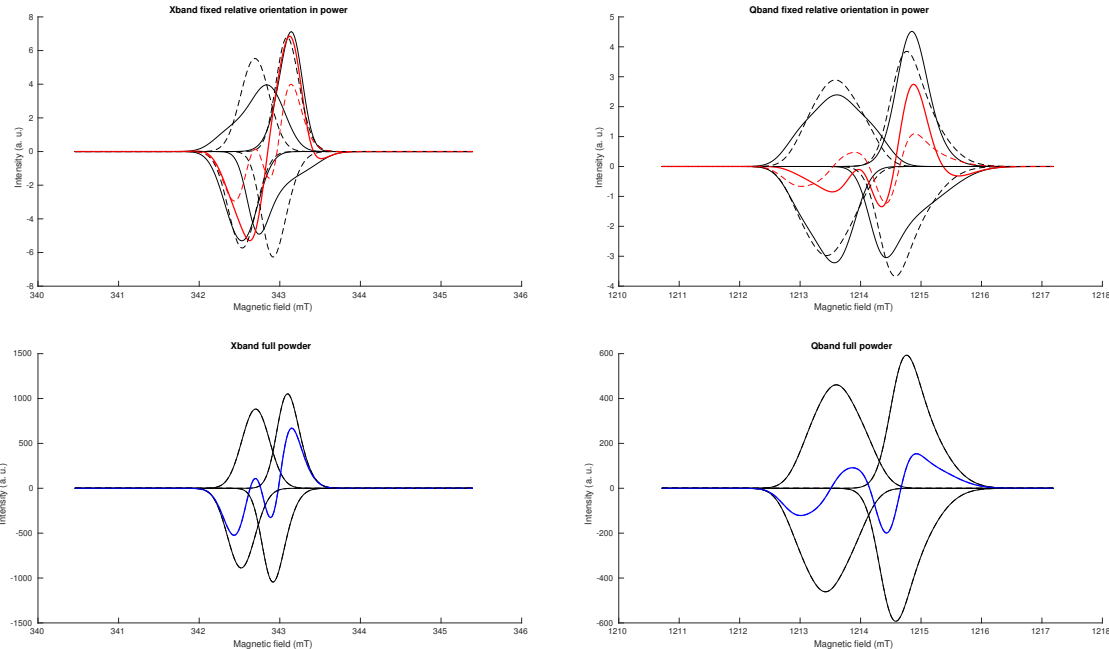
From the previous sections it is clear that there are many different parameters and even two different models for the simulations of trEPR spectra of a CT state.

In order to find the parameters that give the best correspondence between simulation and experimental spectra, one should try different sets of variables. For this, one needs to search in a code for a parameter one wants to change, then to run the program with the changed parameter, save the result, then to find another parameter, change it, run

3.4. VISUALIZATION TOOLBOX



(a) Different parameters can be changed. In black - background corrected and smoothed experimental spectrum, red - fixed relative orientation simulations, blue - arandom relative orientations simulations. Dashed line shows temporary saved simulations for easier comparison of a different parameter set. In dark-gray - initial spectrum, in light-gray - background corrected spectrum.



(b) Here, four simulated transitions are shown separately in black. The sum of them is shown in blue or in red, depending on the relative orientations (random or fixed). Dashed lines show spectra for temporary saved simulations for another parameter set.

Figure 3.1: Screen shot of the visualization tool. It consist of two windows. In one window parameters can be changed and all spectra and simulations can be observed. In the other one, four separate transitions are simulated.

the program once more and so on. These steps are very inconvenient including search for saved result through the plenty of them. Also it is hard to see, how different parameters influence the spectrum. This is why the idea of a visualization toolbox came out. The main idea is to have a tool for changing all required parameters easily in order to simulate trEPR spectra of a CT state (simultaneously for the X- and Q-band) and to be able to compare two different models (fixed and random relative orientations in the powder).

Fig. 3.1a and 3.1b show images of the tool. The description of variable parameters and the additional information can be found in Appendix A.

Comparison between two models in a powder

In this section, the comparison between two models is made. The first model describes two radicals in a powder with a fixed relative orientation (FRO), in the second model - random relative orientations (RRO) between two radicals or all relative orientations are possible and equally probable that will be referred here to as a full powder (FP). The trEPR spectra of P3HT:PCBM is used as a reference. Extracted from the Q-band cwEPR P3HT:PCBM spectrum parameters are used. To show the difference between two models clearly, smaller line widths are considered, see Table 3.1:

	P3HT	PCBM
\mathbf{g}_x	2.0028(0)	2.0001(2)
\mathbf{g}_y	2.0018(0)	2.0001(4)
\mathbf{g}_z	2.0007(0)	1.9989(12)
lw X-band (mT)	0.10	0.12
lw Q-band (mT)	0.30	0.12

Table 3.1: Parameters that were used for simulations. In brackets *g*-strain values are indicated. For the X- and Q-band, different line widths (lw) are used. To show the difference between the two models (fixed and random relative orientation in a powder) arbitrary line widths are taken. Other parameters are extracted from the Q-band cwEPR P3HT:PCBM spectrum.

The results of different simulations are given in Fig. 3.2, where simultaneous simulations of X- and Q-band trEPR spectra of CT states are shown using the two models. First one is FRO of two radicals in a powder (red curve). And the second one is RRO of radicals in a powder (blue curve). For both models, only different electron-electron couplings and relative orientations are used. All other parameters, such as g-factors, g-strains, line widths are the same. Experimental spectra are black lines. Two mw bands (X and Q) are used for better comparison and in order to distinguish between different parameters.

At the top figure of Fig. 3.2 the best found simulations for both models are plotted. They give the same line shape but different coupling parameters. Are they different? Are the small J and D couplings influence the system in the same way? For FRO model, a very small D-coupling is used. For such small values relative orientation and orientations in the magnetic field influence the simulation curve very slightly (it will be discussed and shown in the next section). Thus in this case, J and D parameters influence the FRO spectrum in the same way, because there is no angular dependence for both parameters. But if we exchange them (make J = -0.1 MHz and D = 1.7 MHz), then we get a different spectrum. Because then the D coupling is already big enough to give different results for

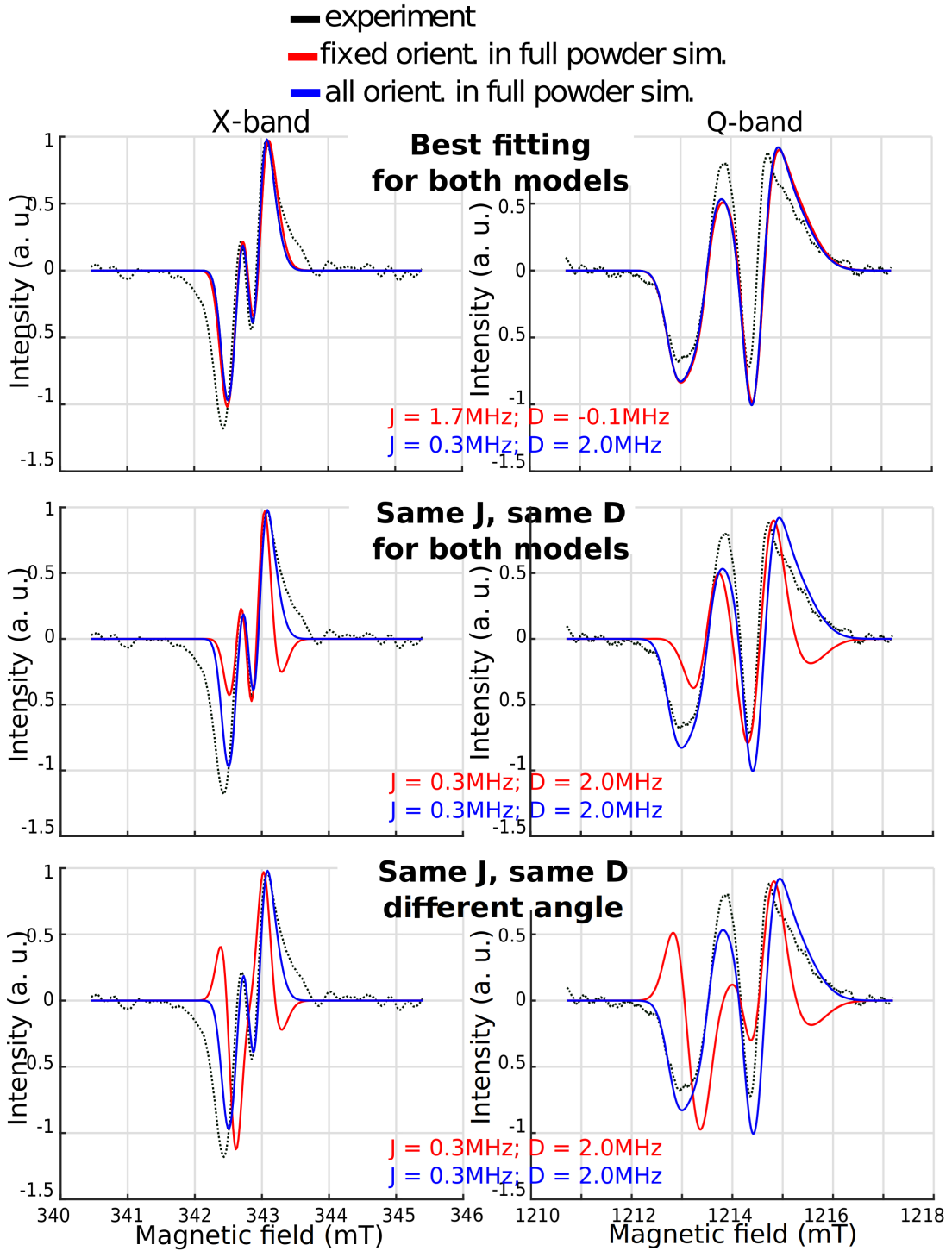


Figure 3.2: The results of simultaneous simulations of trEPR spectra of CT states in a sample like P3HT:PCBM (considered parameters are not from experimental spectra, but close to them) in X- and Q-band using two models are shown. First model is a fixed relative orientation (FRO) of two radicals in a powder (red curve). And the second one is random relative orientations (RRO) of radicals in a powder (blue curve). Experimental spectra are black lines. Two bands are used for better comparison and in order to distinguish between different parameters. For both models same parameters are used, except the electron-electron couplings and the relative orientations. From the top: the best found simulations; the best found simulations for the same couplings; the worst found simulations for the same couplings. Euler angles only of the second system (polymer) are changed: top picture [0 0 0], in the middle [0 0.7 0], in the bottom [0 1.7 0]

different orientations. Therefore, the found parameters for both models are quite different.

Another interesting observation is, that line widths of the simulations are the same. First glance says that the FRO model should give narrower peaks than the RRO model, which, in general, is the sum of different FRO spectra.

But a closer look at the equations shows that the line widths should be similar. For the simplicity let us assume no natural line width. As it was shown in the Fig. 2.7b, in the simplest case with isotropic g-values the spectra look like four peaks. Their positions are determined by eq. 3.3.1. So $B_{ij} \propto \frac{1}{(g_A+g_B)^2 - (g_A-g_B)^2}$. This is a very rough estimation. But it should work as a first approximation.

Using g-tensors for P3HT:PCBM (see caption for Fig. 3.2), following numbers are obtained: for RRO $g_A + g_B = 3.9996 \dots 4.0029$ and $g_A - g_B = 0.0017 \dots 0.0018$; for FRO (when two molecules have same orientation: g_z is parallel to B_0) $g_A + g_B = 3.9996 \dots 4.0029$ and $g_A - g_B = 0.0006 \dots 0.0039$. For both cases $(g_A+g_B)^2 \gg (g_A-g_B)^2$, hence $B_{ij} \propto \frac{1}{(g_A+g_B)^2}$. $(g_A+g_B)^2$ is the same for both models, hence the line widths should be the same. If we add a natural line width, it will have the same effect in both models.

For the RRO, only two parameters additional to the parameters indicated in the Table 3.1 were changed: J and D. For the FRO, eight parameters were used: J, D, three Euler angles for one radical and three angles for another radical. Not all of the angles influence the spectra (for a PCBM like molecule, the g-tensor has axial symmetry) and it does not matter if the first radical is rotated on the angle ϕ or another one on the angle $-\phi$. The last argument is always true, thus five angles are enough. That lead to seven additional parameters, in general, for FRO model. Still more parameters are needed for the FRO model, than for the RRO. So the simulation for the RRO is more trusted, because only two parameters were added.

For the FRO model, more parameters are considered, therefore, it is more probable that other solutions exist. Therefore, it is interesting, whether it is possible to find a good fitting by using the same couplings as for the RRO simulations. The best found result for FRO model, using the couplings from RRO model, is shown in the middle of Fig.3.2. However, the simulation is still acceptable, the result is worse than the one with different couplings.

To see the influence of the Euler angles on the simulation, the worst found fitting for the same couplings is shown on the bottom of Fig.3.2. In comparison with the previous simulations, only angles were changed. The differences are clearly visible.

The outcomes so far are:

1. If it is known that all relative orientations are possible in the system, then the RRO model should be used. J and D couplings can be found if the simulations give a good agreement with the experimental spectrum.
2. Simulations for the fixed relative orientation in the powder model are possible. Some sets of angles give a good result for some fixed J and D. Other angles give worse approximations. This means that more knowledge about the system is needed. If the relative orientation or the couplings are known, then the unknown parameters can be defined. Without any additional information, several sets of parameters can be found and it is not possible to say which parameters are correct.
3. It was shown that the two models can yield in the same result. The random relative orientations in the powder model give a spectrum that is the average of all possible orientations. It should be possible to find parameters for a fixed relative orientation that

corresponds to the average result. This means that in general, just from different simulations, it is not possible to extract the information neither about the couplings, nor about the relative orientations.

How does the gained information contribute towards optimizing the organic solar cells? Well, from the simulations, it is clear that different morphologies of donor and acceptor materials can give the same spectra with different couplings, hence the different distances between electrons can be extracted. So without any knowledge about the local geometry, a wrong D-coupling and therefore wrong inter-spin distances can be extracted. The rate of charge separation and hence the efficiency of a solar cell should depend on the inter-spin distances and probably directly on the relative orientations. The wrong parameters can lead to wrong outcomes. Thus the right parameters are needed for understanding, which inter-spin distances and which relative orientations lead to a higher charge separation rate. Then it will be possible to create a more efficient solar cell.

The next step is to understand, which local geometries correspond to which various materials and try to extract the right D-values to find the right inter-spin distances. For this purpose, the demonstrated visualization toolbox is extremely helpful.

Influence of J- and D-coupling on CT spectra

From the equations for the magnetic fields 3.3.1, it is not possible to see how the exchange and dipolar couplings influence the CT spectra. So the calculated spectra for the different parameters were plotted, see Fig 3.3 and 3.4. For a better understanding, X- and Q-band frequencies were used, as different bands help to resolve different properties. A P3HT:PCBM blend was considered, but smaller line widths were taken to see the features better. The bigger the line width is, the more features are smoothed. The used parameters are shown in the Table 3.2.

	P3HT	PCBM
\mathbf{g}_x	2.0028(0)	2.0001(2)
\mathbf{g}_y	2.0018(0)	2.0001(4)
\mathbf{g}_z	2.0007(0)	1.9989(12)
lw X-band (mT)	0.14	0.06
lw Q-band (mT)	0.17	0.05

Table 3.2: Parameters that were used for simulations. In brackets g-strain values are indicated. For X- and Q-band, different line widths (lw) were used. To see the features better, the line widths smaller than extracted from cwEPR values, were used.

In the figure 3.3 the CT spectra for different fixed relative orientations are shown. When there is no dipolar coupling, then there is just a small angular dependency that is coming from the g-anisotropies, as it is expected. When there is a non zero dipolar coupling, then there is a bigger angular dependency. It is important to see the difference. We are talking here about the different relative orientations. But the D-coupling depends on the orientation of the system in the magnetic field. How is the D-coupling and the relative orientations are related?

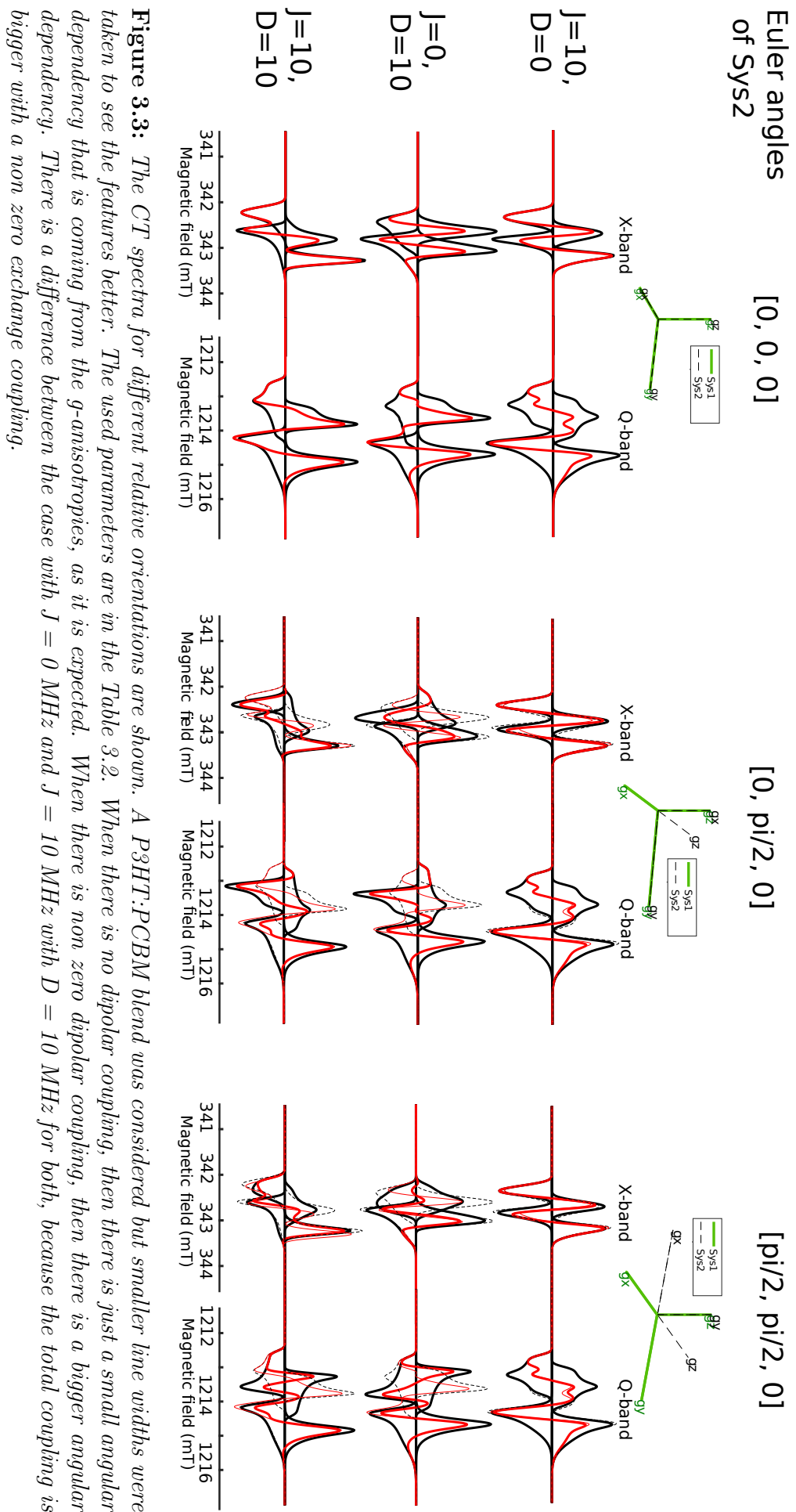


Figure 3.3: The CT spectra for different relative orientations are shown. A P3HT:PCBM blend was considered but smaller line widths were taken to see the features better. The used parameters are in the Table 3.2. When there is no dipolar coupling, then there is just a small angular dependency that is coming from the g-anisotropies, as it is expected. When there is non zero dipolar coupling, then there is a bigger angular dependency. There is a difference between the case with $J = 0$ MHz and $J = 10$ MHz with $D = 10$ MHz for both, because the total coupling is bigger with a non zero exchange coupling.

For the simplicity, no J coupling is assumed for a moment. Then the equation 3.2.1 can be written as

$$w_{mw} = w \pm [\frac{1}{4}d^2 + Q^2]^{1/2} \pm d \quad (3.6.1)$$

where $w = \frac{1}{2}(g_A + g_B)\beta_e B_0$ and $Q = \frac{1}{2}(g_A - g_B)\beta_e B_0$.

We can neglect the D-coupling if $\beta_e B \Delta g$ is much greater than d for the most orientations in the magnetic field, as both values are responsible for the splitting (see eq. 3.6.1).

For very big d values, one can neglect the g-anisotropies and use g_e instead of g-factors, thus the relative orientation does not play any role. This is done in the simulations for triplets, where $D \propto 1$ GHz. Be careful. In triplets, only three states (not four) are important, as allowed transitions are only between the triplets. So the equations 3.2.1 are not valid for this case.

Consider a weakly coupled polaron pair. For each orientation in the magnetic field, d and Δg will have different correlations. The spectrum shape is influenced by these correlations that depend on the relative orientations, as Δg depends on them. The study of the local morphology makes sense in the case when D and Δg have similar values.

$\Delta g = \frac{2h}{\beta_e B} \Delta \nu$. Let us consider $\Delta \nu$ as a dipolar coupling. The minimum possible Δg in P3HT:PCBM is equal to 0.0006. This gives a value of $d = 10.9$ MHz for the Q-band and $d = 2.9$ MHz for the X-band. This means that if $D \ll 2.2$ MHz, then it can be neglected in case of P3HT:PCBM in the X-band (for the Q-band this value is higher). This is enough to be true for the most of the orientations in the magnetic field, so D and $J < 0.5 - 1.5$ MHz can already be neglected. Important is, that the considered equations were obtained using the fact, that spins interact with each other. If it is not the case, separated polarons should be considered and different equations should be used.

If the couplings are very small, D and $J < 0.5 - 1.5$ MHz, then it is better to measure at smaller frequencies than the X-band to determine J and D .

For the cases with $D = 10$ MHz (Fig. 3.3), there is a difference between spectra with $J = 0$ MHz and $J = 10$ MHz, because the total coupling is bigger with a non zero exchange coupling.

Figure 3.4 shows the CT spectra for the full powder model simulations. Both J and D parameters influence the spectra in a different way. The exchange coupling mainly changes the positions of the peaks, this corresponds to the figure 2.7b as well.

The dipole-dipole interaction mainly changes the shape of the peaks due to $d = D(\cos^2 \theta - \frac{1}{3})$. d depends on θ , therefore there is a resonance at different magnetic fields for the polaron pairs with the same D , but with the different orientations in the magnetic field. d can have values from $-\frac{4}{3}D$ to $\frac{2}{3}D$, including 0, assuming a powder orientation in the magnetic field. It gives that the bigger D is, the bigger range of resonant magnetic field is and hence, the broader the spectrum is. This is clearly visible on the figure.

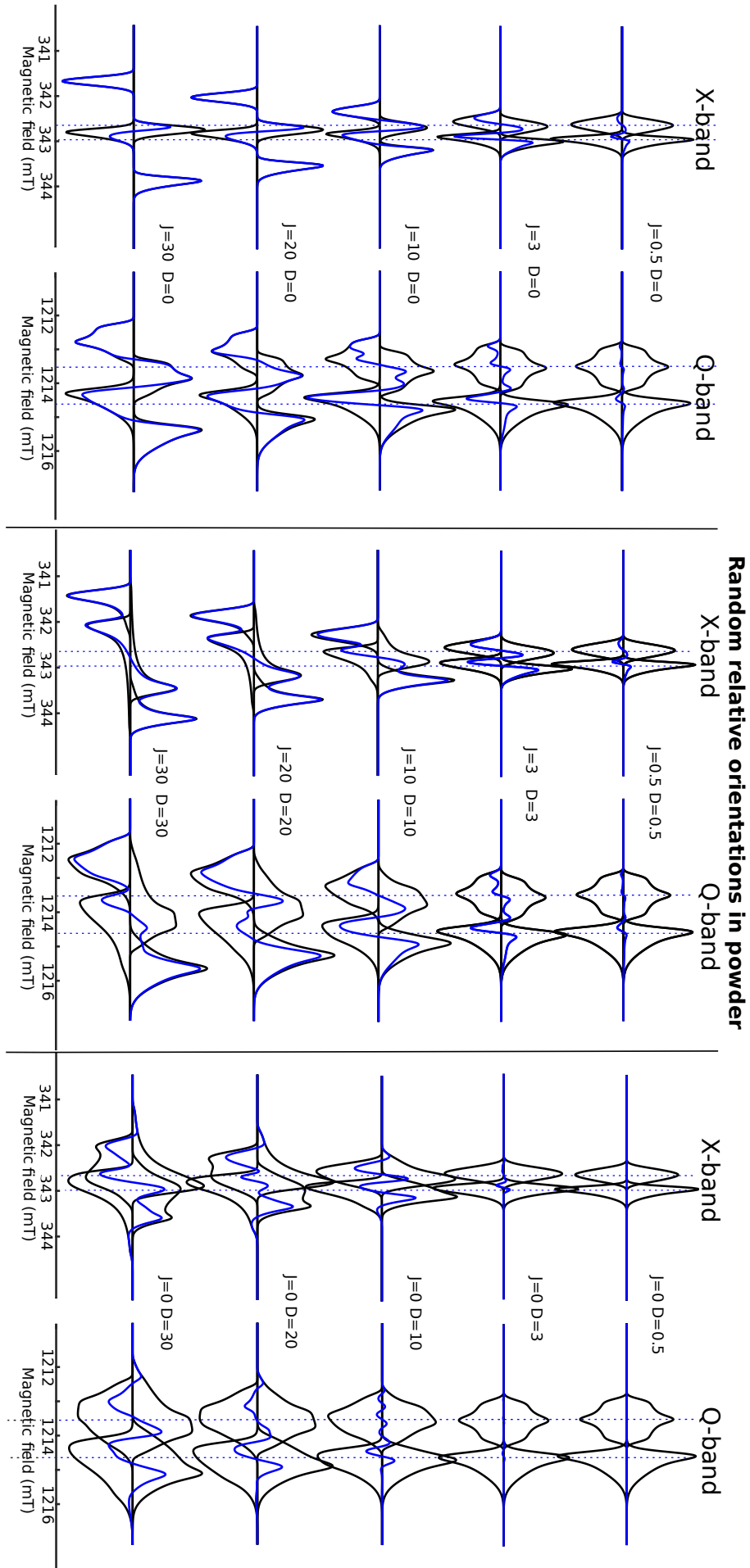


Figure 3.4: The CPMAS NMR spectra for the full powder model simulations. A P3HT:PCBM blend is considered but the smaller line widths are taken to see the features better. The used parameters are shown in the Table 3.2. Both J and D parameters influence the spectra in a different way. The exchange coupling mainly changes the positions of the peaks. The dipole-dipole interaction mainly changes the shape of the peaks due to $d = D(\cos^2 \theta - \frac{1}{3})$. d depends on θ , therefore there is a resonance at different magnetic fields for the polaron pairs with the same D , but with the different orientations in the magnetic field.

Influence of g-tensor and line widths uncertainty on CT state spectra

The g-tensor, g-strain and line widths are extracted from cwEPR experiment for each system. Sometimes several sets of these parameters give a good agreement between a real cwEPR spectrum and its simulation. How do these uncertainties influence the parameters used for trEPR simulations?

In Fig. 3.5 the influence of the line width is shown. All the parameters are the same as in Table 5.1 except for the line width for PCBM, that was set to 0.2 mT, instead of 0.1 mT. The original spectra simulations are shown as a dotted line, while the simulations with a changed line width are shown as a solid line.

One example of a wrong extracted line width is the saturated cwEPR spectrum.

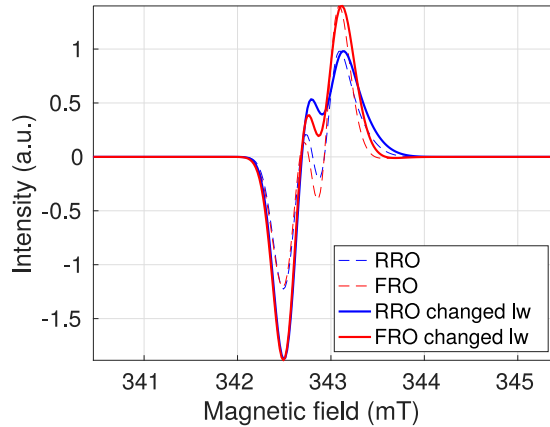
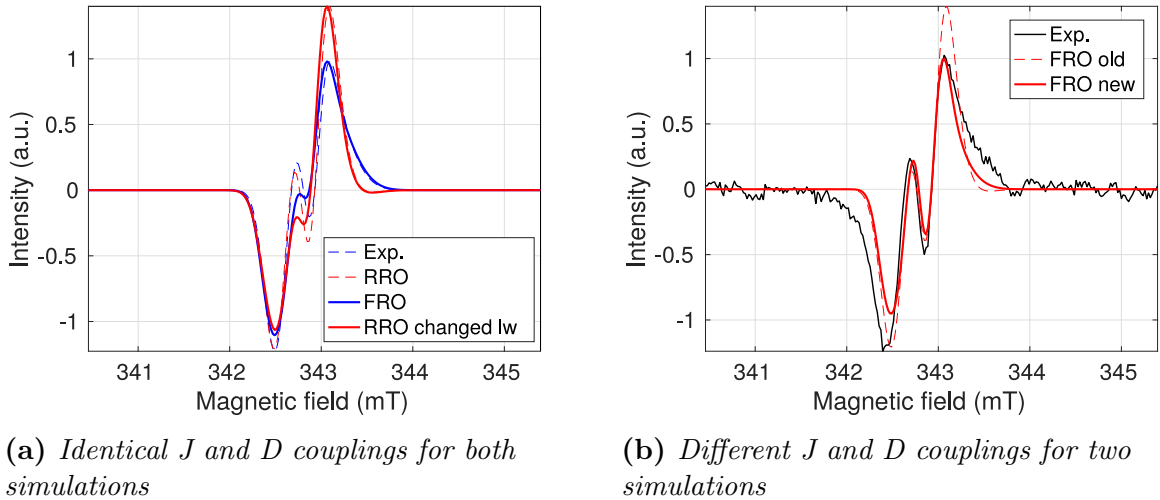


Figure 3.5: Influence of the line width on the trEPR spectrum simulation of the CT state. All the parameters are the same as in Table 5.1 except the line width for PCBM, that was set to 0.2 mT, instead of 0.1 mT. The original spectra simulations are shown as a dotted line, while the simulations with a changed line width are shown as a solid line.

In Fig. 3.6a the influence of shifted g-factors is shown. The simulation, indicated with a dashed line, is the same as in the previous case (with the parameters from Table 5.1). As a solid line, the simulations with new g-factors are indicated. A comparison between the used g-factors is in Table 3.3. Since the two used g-factor sets have quite similar values, that indicates a possible error and it is interesting to see, which J and D will give a good fitting with an experimental spectrum, using the changed g-factors. The result is shown in Fig. 3.6b.

One can conclude, that one should extract parameters from cwEPR very precisely, otherwise a big error is introduced in the extracted coupling parameters. This can lead to some uncertain inter-spin distances. It is hard to estimate the order of uncertainty, but from the considered examples, it should not change the distance in more than two times. But it pretty much depends on the system and on the introduced uncertainties in the parameters.



(a) *Identical J and D couplings for both simulations*

(b) *Different J and D couplings for two simulations*

Figure 3.6: *Influence of the g-tensor uncertainties on the trEPR spectrum simulation of a CT state. The simulation indicated with a dashed line is made with parameters from the Table 5.1. The solid line is the simulations with the changed g-factors. The comparison of the used parameters is shown in Table 3.3*

	arbitrary g-values		extracted from cwEPR g-values	
	P3HT	PCBM	P3HT	PCBM
\mathbf{g}_x	2.0030(0)	2.0003(2)	2.0028(0)	2.0001(2)
\mathbf{g}_y	2.0016(0)	2.0001(4)	2.0018(0)	2.0000(3)
\mathbf{g}_z	2.0007(0)	1.9985(12)	2.0007(0)	1.9987(22)
lw (mT)	0.17	0.1	0.17	0.1
AddBr. (mT)	0.1		0.2	
FRO J (MHz)	3		1	
FRO D (MHz)	1		1	

Table 3.3: *Parameters that were used for simulations in Fig. 3.6a and 3.6b. One set of g-values and *lw* was extracted from cwEPR. Together with the *J*, *D* couplings and an additional broadening (AddBr.), they were used for simulations of trEPR spectra. The other set of g-factors is arbitrary, it was used in order to see, how the g-tensor uncertainties influence the CT spectrum simulations*

Chapter 4

Experimental aspects

Experimental Setup

In this thesis we do not want to elaborate on experimental setup (for trEPR and cwEPR), because it is already described in several thesis and papers, so, please, see it for example here: [24, 25, 26].

All spectra were measured on the mentioned setup in X- or Q-band frequencies and magnetic field ranges, afterwards all spectra were frequency corrected (shifted) so that the magnetic fields correspond to 9.6 GHz and 34.0 GHz respectively. This makes the comparison between different spectra easier. Later the frequencies are not mentioned, only a band is indicated.

All the measurements were made at 80 K.

When there is no excitation, there is no paramagnetic states in polymer that could be seen in EPR (all electrons are in pairs). This is usually not the case, due to the impurities, defects and non zero temperatures. Thus there is some dark (without light excitation) signal, that can be measured in cwEPR. We are interested in the light induced signal only, so dark signal should be subtracted from the light one. The schematic is shown on the figure 4.1. For some of the samples, dark signals were not recorded, but it is not critical, because for the most considered samples the dark signal was very weak.

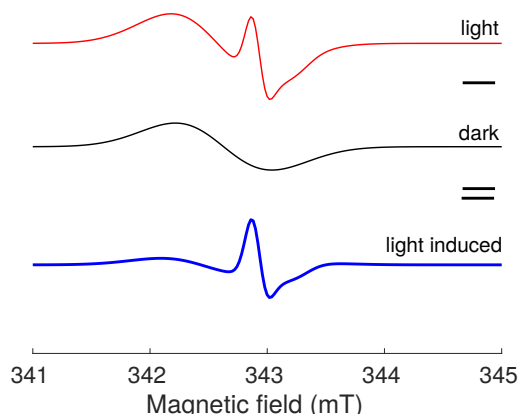


Figure 4.1: Difference between light and dark signal gives light induced signal. Light - dark = ligh induced. Schematic illustration.

Before fitting, the background subtraction was made.

Sometimes, the spectrum can be very noisy, thus the data was averaged (smoothed) with the Matlab function 'smooth'.

If in trEPR relatively high powers are used, then the saturation of some signatures can happen, as the spin can be flipped completely. It can be the reason of some deviations between the experimental and simulated curve.

Sample preparation

Different samples were used during this Master project. They can be divided in two groups: inner-wall samples and substrate samples. Inner-wall samples were made in 3 mm outer-diameter tubes for Q-band measurements and in 4 mm tubes for X-band measurements. Substrate samples were spin-coated on a quartz glass, which was put into 5 mm outer-diameter tube afterwards. The tubes were annealed at 750°C before usage to remove all the defects, so that the tubes will not be visible in EPR.

Sample examples are shown in Fig. 4.2. All the samples were prepared from solutions in a glove-box in a nitrogen atmosphere, where almost no oxygen and no water are present. Their amount is less than 0.1 ppm. After the preparation tubes were taken out in a closed transportation device, inner-wall samples were dried by evaporation of the solvent under vacuum (so that no water or oxygen would get inside) and all tubes were sealed in the end.



Figure 4.2: Samples. From left to right: 5 mm tube with substrate, 4 mm tube for X-band, 3 mm tube for Q-band.

Q-band measurements are only possible on a tubes with a maximum of outer diameter 3 mm. 4 mm and 5 mm tubes can be measured in X-band. In order to have better signal to noise ratio, it is better to have more material in the cavity of the spectrometer. This is why inner-wall samples are preferential to substrates and it explains why different tubes are used for X- and Q-band measurements (4 mm tube contains more material than 3 mm one).

Substrate samples were needed for P3HT doped with (C₆₀-Ih)[5,6]fullerene (C₆₀) preparation via evaporation.

Here, the preparation of each sample is described in more detail.

1. P3HT:PCBM

The sample that was used in the very beginning of the thesis was a P3HT:PCBM blend (for structure see Fig. 1.1). It was prepared and measured by Felix Kraffert. It was prepared in a 1:1 ratio in chloroform solution and inner-wall X- and Q-band samples were made. The spectra obtained from this sample were used for adjusting the program and on that spectra were checked how the visualization tool is working, see Fig. 5.2 and 3.2.

2. P3HT:PCBM and P3HT:C₆₀

For comparison between P3HT:PCBM and P3HT:C₆₀ new samples were prepared. Chlorbenzin was used as a solvent. First, P3HT and PCBM solutions (30 mg/ml) were prepared. P3HT:PCBM 1:1 solution was made by mixing first two. The sample was spin-coated at 2000 rounds per minute (rpm) for 40 s.

Additionaly, several other substrates were spin-coated with pure P3HT at 1200 rpm for 40 s.

All substrates (including P3HT:PCBM) were annealed for 10 minutes on a hot plate at a temperature of 120°C. Then, C₆₀ was evaporated onto P3HT substrates: first, 5.5 nm were evaporated at T = 390°C with a rate of 0.1-0.2 Å/s; the rest was evaporated at T = 450°C with a rate of 0.4-0.5 Å/s. In the beginning, a slower rate is needed to create more homogeneous layers. The total thickness of C₆₀ is 808 nm. Then one of P3HT:C₆₀ substrates was annealed at 120°C for 10 minutes and another one was left as prepared.

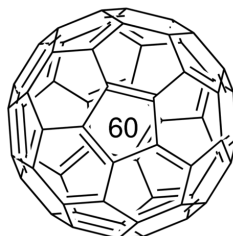


Figure 4.3: C₆₀ structure [27]

3. PBTTT:PCBM, BT3:PCBM, BT2:PCBM

These samples were prepared by Robert Steyrleuthner. The preparation is described in the article [28].

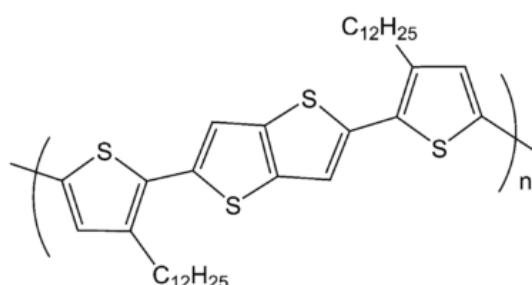


Figure 4.4: PBTTT structure [28]. Olygomers consist of this unit taken 2 times in case of BT2 and three times in case of BT3, polymer consists of a very large number of this unit.

4. PBTTT:PCBM

Because of crystallinity of PBTTT and intercalation of PCBM, that give known local morphology, it was decided to perform a series of measurements using this polymer and different fullerene derivatives. A good polymer from Potsdam was available, that gave nice efficiencies and well defined structures.

It was decided to make probe preparation and measurements on the material that was available in the lab first to try all the parameters. Therefore, PBTTT:PCBM samples were prepared, using the same polymer as it was used in [28]. The polymer was purchased from Sigma Aldrich ($M_n = 15\text{ kDa}$, PDI 2.9).

1,2-Dichlorobenzene was used to solve the polymer at a concentration 15 mg/ml PBTTT-C12:PCBM 1:1 solution was prepared (first polymer and fullerene were mixed together and then solvent was added). The solution was left at 85^0 C overnight. A substrate sample was made from the hot solution. 1500 rpm, acceleration rate 255, 60 seconds. Inner-wall 3 mm tube was also made from the same solution, it was drying over night under vacuum. Afterwards it was annealed at $T = 140^0$ for 15 minutes and then sealed. This tube gave a clear additional signature that can correspond to a stronger coupled CT state. This is discussed later.

5. C-PCPDTBT:PCBM and F-PCPDTBT:PCBM

poly[2,6-(4,4-bis(2-ethylhexyl)-4H-cyclopenta[2,1-b;3,4-b']-dithiophene)-alt-4,7-(2,1,3-benzothiadiazole)] or C-PCPDTBT and poly[4,4'-bis(2-ethylhexyl)dithieno[3,2-b:2',3'-d]silole]-2,6-diylalt-(4,7-bis(2-thienyl)-2,1,3-benzothiadiazole)5,5'-diyl] or F-PCPDTBT were used in a blend with PCBM. These samples were prepared by Robert Steyrleuthner. C-PCPDTBT was purchased from 1. Material and F-PCPDTBT from Fritz-Haber-Institute. First, polymers were mixed with PCBM in 1:1 ratio, afterwards mixtures were dissolved in chloroform till 20 mg/ml solution concentrations. Inner-wall Q-band samples were made.

These samples were measured together with Felix Kraffert.

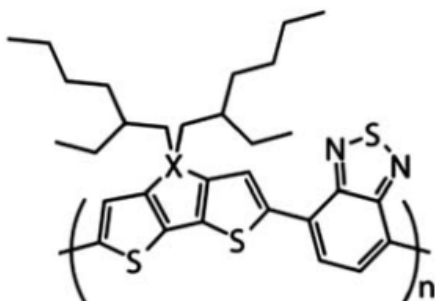


Figure 4.5: *X-PCPDTBT structure [29]. In this work C-PCPDTBT and F-PCPDTBT are used*

The PCBM was always used from the same batch obtained from Solenne BV.

Chapter 5

Results and Discussion

In previous chapters it was shown that when only experimental spectra are available and the relative orientations are unknown, the extracted couplings are inaccurate. That leads to a big error in the inter-spin distances. In this chapter, the measured spectra and their simulations are shown. The simulations were based on two different models (FRO and RRO). As the main goal of this thesis suggests, the information about local morphology between a donor and an acceptor as well as the inter-spin distances are extracted from the comparison between the simulated and the measured spectra.

P3HT:PCBM vs. P3HT:C60

Let us consider a P3HT:PCBM blend. Their cw and trEPR spectra in the X- and Q-bands measured by Felix Kraffert were available. They were used to check the created visualization tool. The cwEPR simulations are shown in Fig. 5.1 and the values which were used in the simulations are shown in Table 5.1. Using the found values, trEPR spectra were simulated: Fig. 5.2. It is important that in the simulation, we obtain D that is actually the D_{zz} . One should keep that in mind, when distances are calculated (see equation 2.3.6).

	P3HT	PCBM
\mathbf{g}_x	2.0028(0)	2.0001(2)
\mathbf{g}_y	2.0018(0)	2.0000(3)
\mathbf{g}_z	2.0007(0)	1.9987(22)
lw X-band (mT)	0.17	0.10
lw Q-band (mT)	0.33	0.07
weight X-band (mT)	0.6	1.0
weight Q-band(mT)	0.9	1.0

Table 5.1: Parameters that were used for the simulations of the cwEPR P3HT:PCBM blend spectra. In brackets, g-strain values are indicated. For the X- and Q-band, different line widths (lw) are used.

Two models result in different parameters. The best FRO simulation gives $J = 2$ MHz and $D = 2$ MHz (red line), while the best RRO simulation gives $J = 1$ MHz and $D = 1$ MHz (blue line). It is not clear, which result should be used in oder to extract the distances between the radicals: the simulations are equally good for both models.

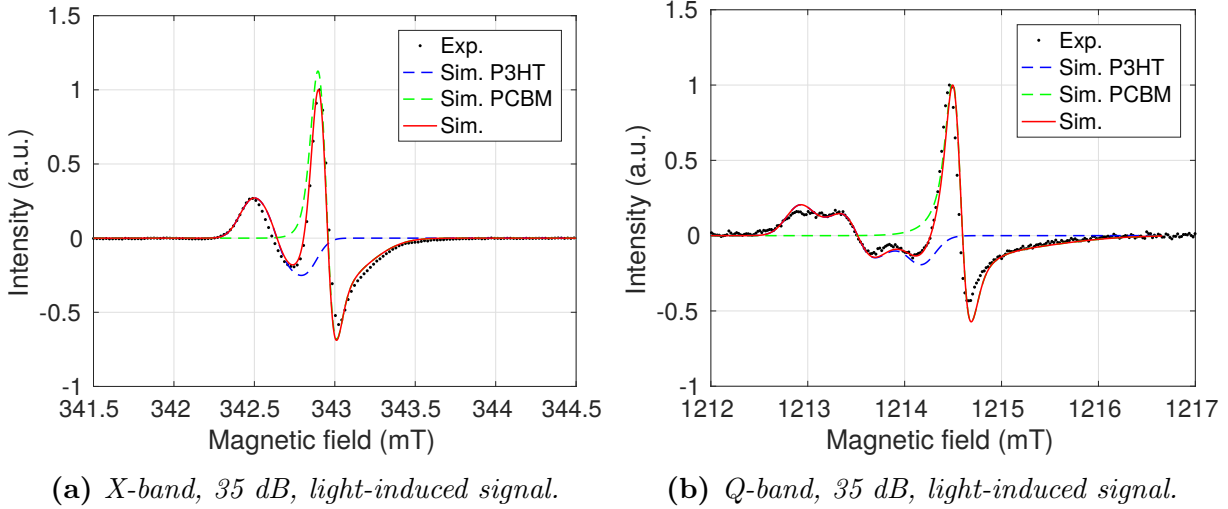


Figure 5.1: Simultaneous simulations of X- and Q-band cwEPR spectra of the P3HT:PCBM blend. The extracted values are summarized in Table 5.1. The dotted black line is the experimental data, the green and blue lines show P3HT and PCBM simulation components, while the red line is the sum of them.

On one hand, a blend structure suggests that the relative orientation between PCBM and P3HT should be random. On the other hand, PCBM is a C_{60} derivative that has an anisotropic g-tensor because of the Jahn-Teller effect. [30] One has to analyze, if this is the case for PCBM as well. It can happen that the side chain of PCBM does not play any role in the g-tensor anisotropy. It could be possible that, when an electron jumps from a polymer to a fullerene, it introduces a distortion (Fig. 5.3), that leads to the g-tensor anisotropy. As an electron always comes from the polymer, the distortion should have a fixed relative orientation to the polymer. Therefore one can say that the polymer and the distorted fullerene have a fixed relative orientation with respect to each other.

To elucidate the problem of Jahn-Teller effect in PCBM, we fabricated some thin films of a P3HT:PCBM blend and also some bilayers of P3HT: C_{60} . If the resulting g-tensors of PCBM and C_{60} are the same, then Jahn-Teller effect will be present in PCBM.

The detailed preparation procedure is described in the corresponding section. For g-values determination, cwEPR spectra of the films and bilayers were measured and simulated. The not annealed (as prepared) P3HT: C_{60} bilayer sample has a very strong dark signal due to the predominant defects. The light-induced signal that is the difference between the signal under illumination and the dark signal, is small. This is due to the small interface area between the donor and the acceptor where the charge separation is happening (Fig. 5.5). With the annealing of another sample, C_{60} has penetrated into the polymer. Thus the interface area has increased and the defects have partially disappeared (Fig. 5.4). That has led to a smaller dark signal and a higher light-induced signal.

The dark signal of the as-prepared sample contains an additional low field component. It was already observed earlier in as-prepared samples and it usually corresponds to the presence of oxygen. Probably, the oxygen is being released during annealing.

Via the measurements, an interesting fact was observed. The saturation of the polymer and the fullerene was happening at different powers (Tables 5.2). The dependency of peak intensities of the annealed sample as a function of the mw power is shown in Fig. 5.6. For the as-prepared sample, the intensities of the dark and light signals are indicated. This corresponds to the dark and light signals of the polymer, because from the figure 5.5a it is clear, that a C_{60} component is shifted from the maximum and the minimum of the total

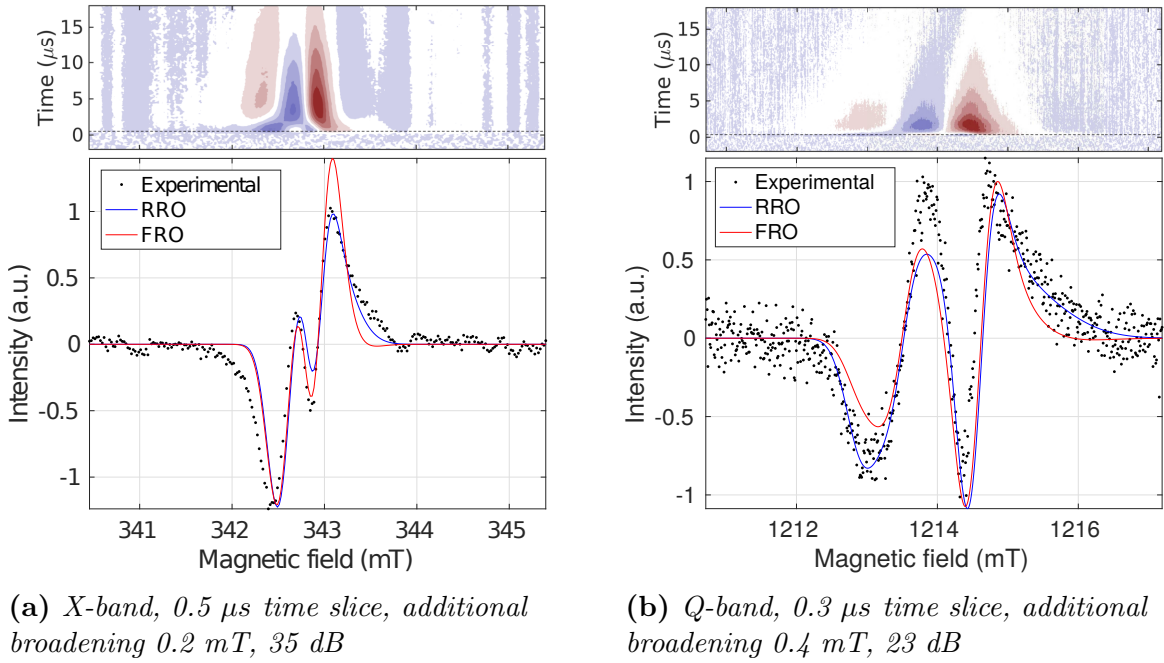


Figure 5.2: TrEPR spectra of CT states at the P3HT:PCBM interface. The top figures contain the complete trEPR spectra for the X- and Q-bands, while the bottom figures show the time slices and their simultaneous simulations. For the simulations, two models are used. First one is the FRO of two radicals in a powder (red curve). And the second one is the RRO of radicals in a powder (blue curve). For the both models, only different electron-electron couplings and the relative orientations are used. All the other parameters are the same and they are extracted from cwEPR. The background-corrected experimental spectra is a black line. The two bands (X and Q) are used for a better comparison. The best FRO fitting gives $J = 2$ MHz, $D = 2$ MHz and the Euler angles for PCBM = [0.0 0.0 0.0], for P3HT = [0.0 0.6 0.0], while the best RRO simulation gives $J = 1$ MHz and $D = 1$ MHz.

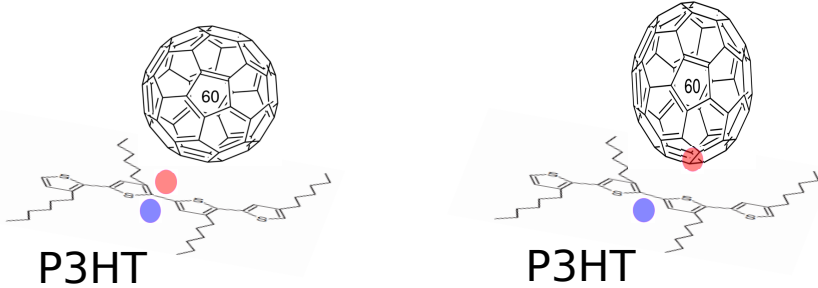


Figure 5.3: The Jahn-Teller distortion is shown schematically. By light excitation, an exciton is created on the polymer (P3HT). Afterwards an electron can hop on the fullerene (C_60). By this, the symmetry of the fullerene ball is broken, therefore an energetically favorable anisotropy is created. An electron is always coming from the polymer, thus the relative orientation of the polymer and the distorted fullerene should always be the same.

signal.

If the signal is not saturated, a 6 dB decrease in the attenuation should half the intensity. In the not saturated case, the intensity should be $\propto \sqrt{mw\text{power}}$ [31]. This is

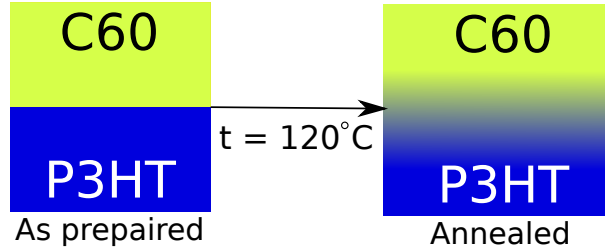


Figure 5.4: Penetration of C_60 into polymer while annealing

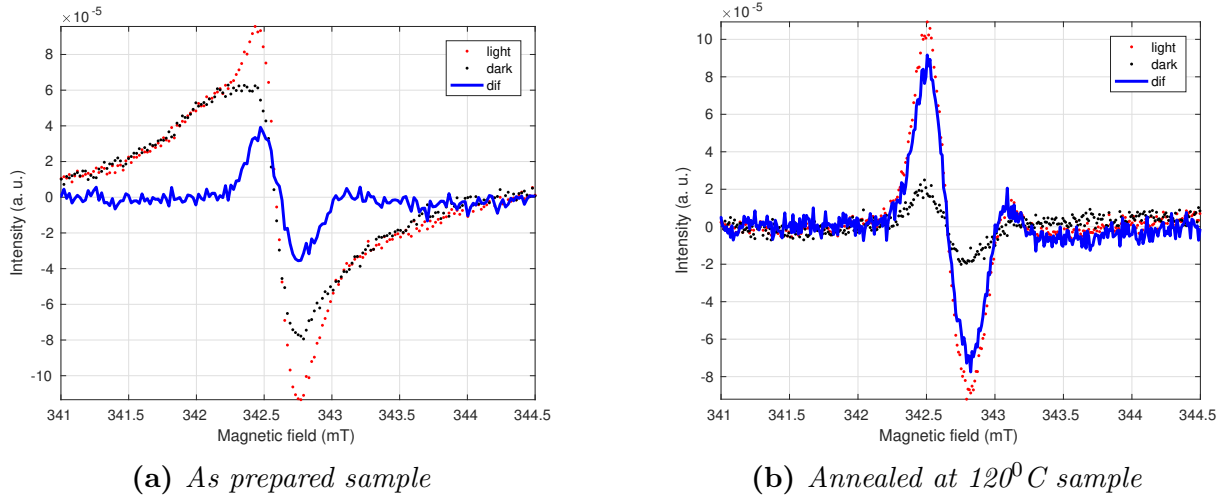


Figure 5.5: $CwEPR$ spectra of $P3HT:C_60$ measured at $80K$ at 41 dB attenuation. The black dotted line is the dark signal, the red dotted line is the light signal, the blue solid line is the light-induced signal, that is the difference between the light and dark signals

more or less true for all the signals, except for the P3HT signal from the annealed sample that is clearly saturated (Fig. 5.6).

Atten.(dB)	Power(mW)	Annealed sample peak intensities		As-prepared sample peak intensities	
		P3HT(a.u.)	C_60 (a.u.)	dark(a.u.)	light(a.u.)
23	1.002	190	200	898	913
29	0.252	200	115		
35	0.063	231	52	254	298
41	0.016	237	21	142	209
47	0.004	167	14		141
53	0.001				79

Table 5.2: Intensities of the $cwEPR$ peaks of the annealed and the as-prepared $P3HT:C_60$ samples vs. different powers. Total power is 200 mW. Other powers were achieved by attenuation (atten.). In the non-saturated case, the attenuation decrease on 6 dB halves the peak intensities. The dependency of peak intensities of the annealed sample is shown on the Fig. 5.6. For the as-prepared sample, the intensity of the dark and light signals are indicated, that more likely corresponds to the dark and light signals of the polymer.

Interesting is, that in the as-prepared sample, the P3HT signal is not saturated. During the evaporation of C_60 , a lot of defects may be produced. There the recombination is

happening which leads to a smaller life time, therefore no saturation is happening. These defects are probably removed with annealing.

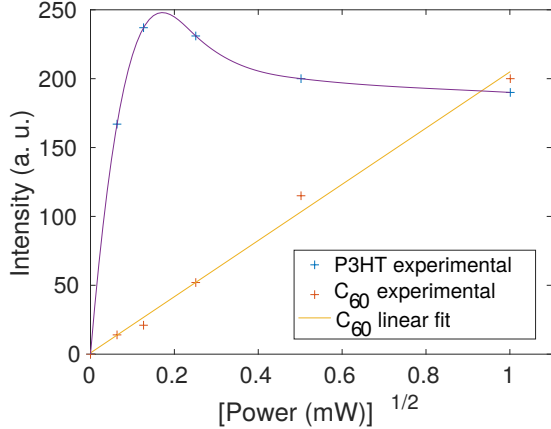


Figure 5.6: Intensities of the cwEPR peaks of the annealed P3HT:C₆₀ sample as a function of the microwave power. Total power is 200 mW. Smaller powers were achieved by attenuations. If the signal is not saturated, then the intensity should be $\propto \sqrt{\text{Power}}$ [31]

C₆₀ saturates at higher powers as compared to P3HT, hence the relaxation of C₆₀ could be faster. From [32] the relaxation time for C₆₀ is 8 ns at 80 K and for PCBM it is 1.9 μ s at 10K [33], that will be even longer at 80 K. The relaxation of PCBM is approximately 1000 times slower than that for C₆₀. Such a small life time means also a small T₂ time. So the coherence is lost very fast and the spins compensate each other. This leads to a smaller absorber intensity, as some spins absorb the radiation, while the other spins relax under stimulated emission, that gives no change in mw photon number. This would mean that at the same conditions P3HT will have higher intensity compared to C₆₀. This is clearly visible in Fig. 5.6.

	P3HT	PCBM	C ₆₀
g_x	2.0028(0)	2.0001(2)	1.9991(0)
g_y	2.0018(0)	2.0001(4)	1.9977(18)
g_z	2.0007(0)	1.9989(12)	1.9955(50)
lw for P3HT:PCBM(mT)	0.223	0.133	
lw for P3HT:C60 at 41dB(mT)	0.223		0.168
lw for P3HT:C60 ar 23dB(mT)	0.223		0.216
weight for P3HT:PCBM	1.00	1.05	
weight for P3HT:C60 at 41dB	1.00		0.28
weight P3HT:C60 ar 23dB	1.00		3.90

Table 5.3: Parameters extracted from cwEPR for annealed PCBM:C₆₀ measured at 41 and 23 dB and for P3HT:PCBM measured at 41 dB. The last two spectra are light signals, the first one is the light-induced signal. For more details see the text and Fig. 5.7. In brackets g-strain values are indicated

Because P3HT saturates at low powers, there is no power at which both components would have good intensities for fitting. Therefore, the spectrum was recorded at two

different powers in order to be able to simulate both components. At one of the spectra P3HT is saturated but C₆₀ has a high intensity. At another spectrum the polymer is not saturated. This allows to find a natural line width of the polymer component.

Two cwEPR spectra at different powers for annealed P3HT:C₆₀ were simulated. For both cases the same parameters are used except the line widths and weights. The line widths are affected by saturation. Different weights are used because one of the spectra is light-induced and the other one is a light signal. The light signal includes the dark signal from the polymer that gives a bigger weight to the polymer.

It was better to measure the dark signal for both spectra for completeness, but it was not the main focus of this study and it was not done. The P3HT:PCBM spectrum was simulated as well. The extracted values are summarized in Table 5.3, the simulations are shown in Fig. 5.7.

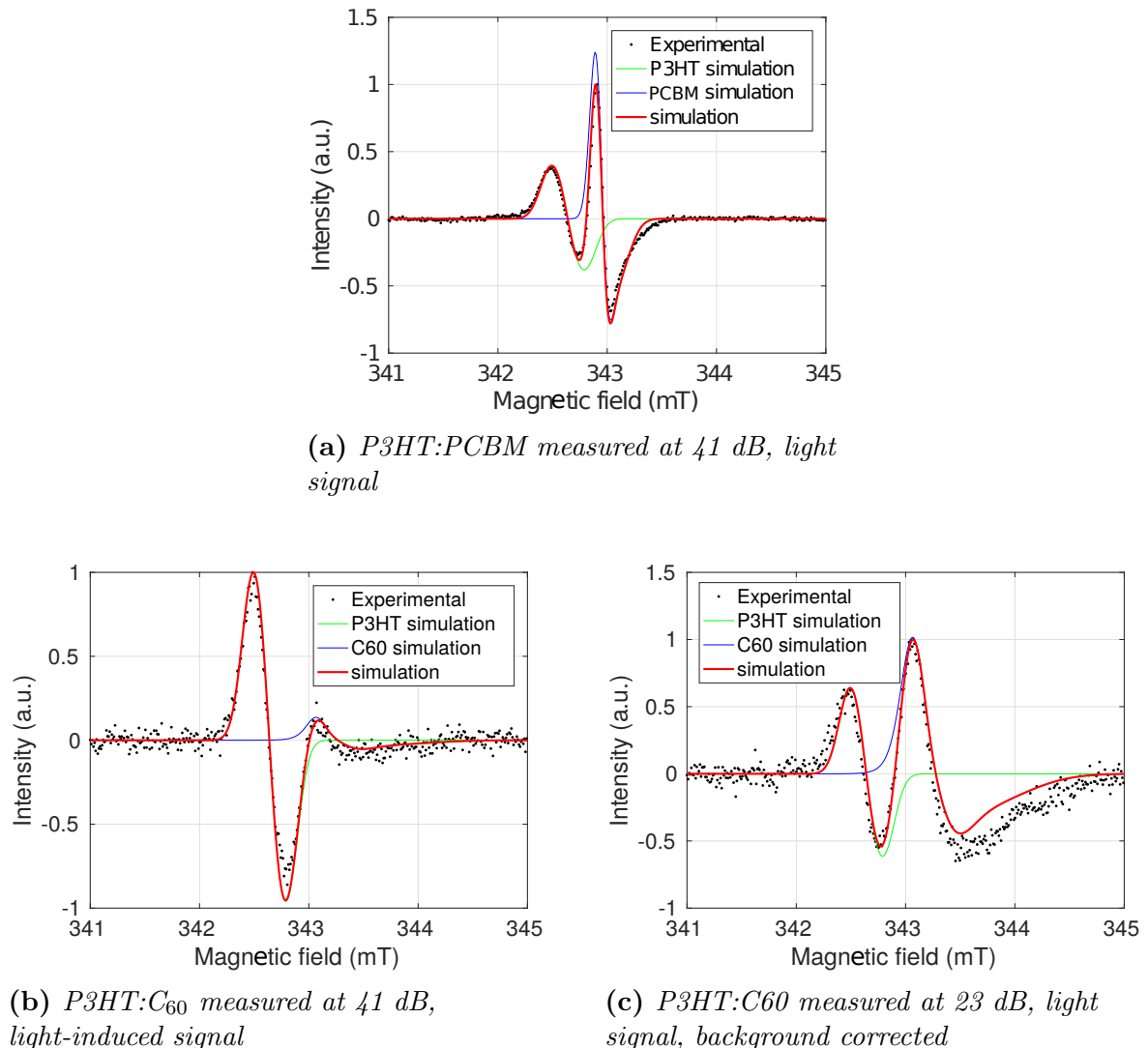
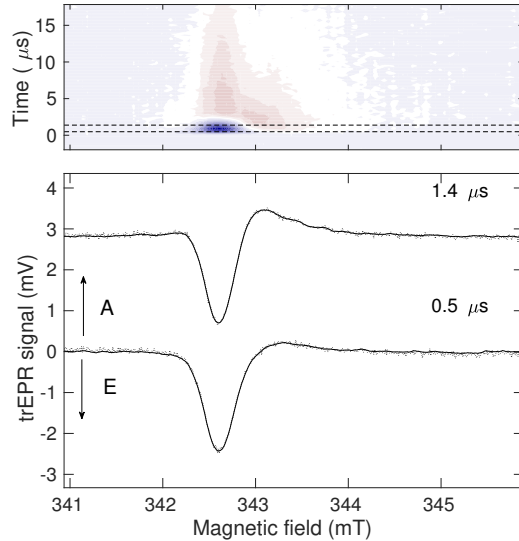


Figure 5.7: CwEPR spectra simulations for annealed P3HT:C₆₀ and for P3HT:PCBM. The extracted values are summarized in Table 5.3. The dotted black line is the experimental data, the green and the blue lines show P3HT and PCBM or C₆₀ components, while the red line is the sum of them.

It was forgotten to switch on the gauss-meter to measure the precise field position

and the measurements were performed only in the X-band, it resulted in an error in the g-values. Also the g_z component of C_{60} can differ by approximately 0.0025 and the large g-strain also indicates this. For a better g-factor resolution, Q- or/and V- or/and W-band measurements should be performed. It was not done, because the sample size was too big to measure it in the Q-band, as it is a substrate sample in a 5 mm tube. From the available spectra it is already clear that g-tensors for PCBM and C_{60} differ dramatically. This means that more likely, PCBM is not influenced by Jahn-Teller effect and the g-matrix anisotropy of PCBM must come from the side chain. Thus the relative orientations between P3HT and PCBM are random and equally probable.



(a) Total recorded spectrum with two selected time slices, that are simulated below

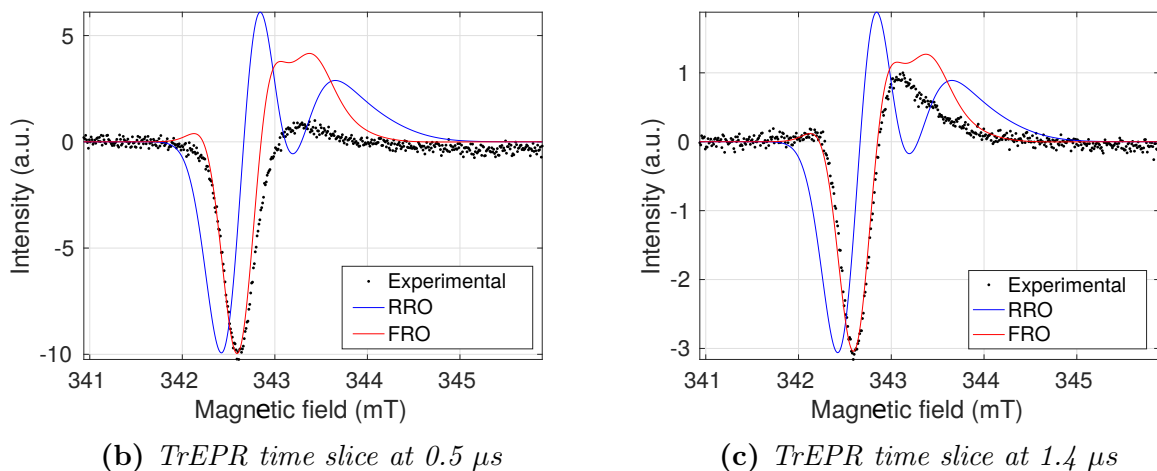


Figure 5.8: X-band trEPR spectrum of P3HT: C_{60} . Two time slices are simulated using two different models - random and fixed relative orientations (RRO and FRO). For the RRO (blue line) $J = 3.0$ MHz and $D = -3.0$ MHz are used. For the FRO (red line) $J = 2.0$ MHz, $D = -4.8$ MHz and Euler angles for the fullerene = $[0.00 \ 1.95 \ 0.00]$ and for the polymer = $[0.00 \ 0.00 \ 0.00]$ in radians. Additional broadening is 0.4 mT. the black dots are the experimental data

A P3HT:PCBM trEPR spectrum was simulated before, but it was not clear which simulation should have been used. Now we can assume that the RRO model is the right approach. For this model we obtained $D = 1$ MHz which gives the distance $r = 3.7$ nm between the radicals (if we assume the point dipole approximation). This is the same value (4 nm) as Uvarov *et al.* got using pEPR [34] by making the same approximation.

Jahn-Teller distortions in C_{60} are created by the electron hopping from the polymer. We believe that therefore the distortion and thus the C_{60} g-tensor orientation have a fixed relative orientation to the polymer. This means that P3HT and C_{60} should have a fixed relative orientation.

To proof this hypothesis, trEPR on the P3HT: C_{60} annealed bilayer was performed. The spectra are shown in Fig. 5.8.

Two time slices were considered. Both were simulated (Fig. 5.8) using the parameters extracted from the cwEPR (Table 5.3) and by adding some interaction parameters. It is obvious that the fixed relative orientation model gives a much better agreement with the experimental spectra than the random relative orientation model. This is with an agreement with the hypothesis about Jahn-Teller distortion described above, that is coming from the hopped electron and therefore that is giving the FRO between a polymer and a deformed fullerene.

The simulations look good but do not give a total agreement. This can be due to the relaxation effects that were not taken into account. They should play a role, as the relaxation time for C_{60} is very fast (ns scale).

To check if the random relative orientation model does not work for the P3HT: C_{60} completely, some simulations using J- and D-strains were tried out. But this was not successful. The results did not change much.

The main outcome so far is, that in some cases, it is possible to determine the couplings and the relative orientations between the polarons directly from the trEPR spectra. The second outcome is that P3HT and C_{60} are more likely having a fixed relative orientation, when P3HT and PCBM have a random relative orientation.

The distance between the polarons on a P3HT: C_{60} interface can be calculated from $D = 4.8$ MHz and is equal to $r = 2.2$ nm.

Here, it will be interesting to compare the external quantum efficiency (EQE) of P3HT:PCBM and of P3HT: C_{60} . This would give an insight about which relative orientations (random or fixed) and which inter-system distances give a better charge separation. This can be done in a future research.

Stronger coupled CT states

In several spectra discussed later, some broader signatures will appear. They are wider than the signatures from usual CT states and more narrow than the signatures coming from triplet excitons. Probably, these broader signatures correspond to some other states. What states are possible in organic materials during charge separation? In several papers [25, 16, 36, 35] charge separation paths are shown (see Fig. 5.9).

There are some broad signatures which were found, for example, in PBTTT:PCBM. The corresponding spectra and simulations are shown in Fig. 5.10. It was simulated using the model of a CT state, but stronger couplings were considered. The used parameters are following: additional broadening 0.9 mT, for both models (FRO and RRO) same couplings are used $J = 20$ MHz, $D = 100$ MHz. The change of Euler angles was not giving a different result. The calculated inter-spin distance is $r = 0.8$ nm (using eq. 2.3.6). Also interesting

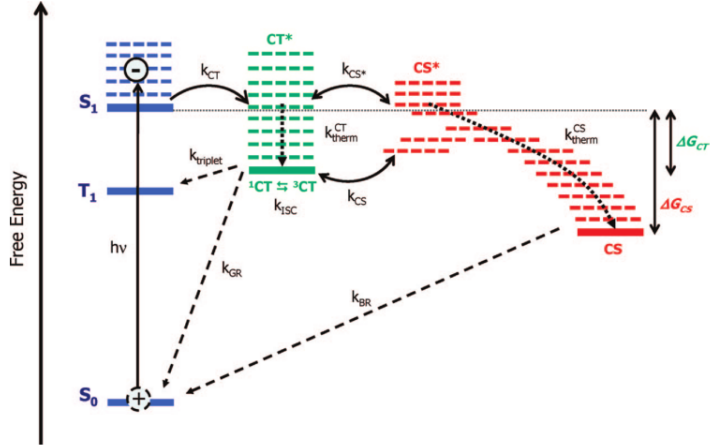


Figure 5.9: Energy level diagram summarizing the main processes involved in charge photogeneration. $h\nu$: Photoexcitation to singlet exciton (S_1). k_{CT} : Exciton dissociation to form the hot CT state. k_{therm}^{CT} : Thermal relaxation of the CT state. k_{ISC} : Spin mixing of the ${}^1\text{CT}$ and ${}^3\text{CT}$ states. $k_{triplet}$: coupled polaron pair (geminate) recombination of the ${}^3\text{CT}$ to the triplet exciton, T_1 . k_{GR} : Geminate recombination of the ${}^1\text{CT}$ state back to the ground state, S_0 . k_{CS*} : Dissociation of the hot CT state into a fully charge-separated (CS) state. k_{CS} : Dissociation of the thermally relaxed CT state into the CS state. k_{therm}^{CS} : Thermal relaxation of the CS state and migration away from the donor/acceptor interface. k_{BR} : Bimolecular recombination of the CS state. This diffusion-limited bimolecular process may result from either direct recombination or, more probably, reformation of interfacial charge-transfer states (shown as reversible arrows in processes k_{CS*} and k_{CS} and subsequent geminate recombination (k_{GR})). [35]

is, that this CT signature is inverted (negative scaling is used). The line width is broader. For singlet CT states, the line width is around 0.2-0.7 mT and $D < 10 \text{ MHz}$ ($r > 1.7 \text{ nm}$). A bigger line width for stronger coupled CT states can indicate a higher localization and therefore a higher hyperfine coupling. These CT states are stronger coupled than usually the observed ones, that corresponds to the shorter distances between the spins. The fact, that simulation spectrum should be inverted, suggests, on one hand, that these CT states can be populated from triplets and therefore can have inverted populations. On the other hand, the inversion can be obtained from the negative sign of J .

It is not clear, where these states can be on the diagram (Fig. 5.9). They can lie lower in energy compared to the triplet state T_1 , and can be populated from it. But this is a hypothesis. It should be checked.

The two models for the relative orientations give similar simulations. During the fitting procedure it was noticed that Euler angles influence the simulations only a little bit. This can be easily explained.

The D couplings are big enough, so that the relative orientations do not play any role, since Δg is very small as compared to D . This means that it does not matter, which model is used for simulations of the stronger coupled CT states. And these states can not help with determination of the relative orientation between the donor and the acceptor. However, they should play a role in the charge separation and should be studied to create a highly efficient solar cell.

A stronger coupled CT state has an interesting dynamics. It is not visible until $0.3 \mu\text{s}$,

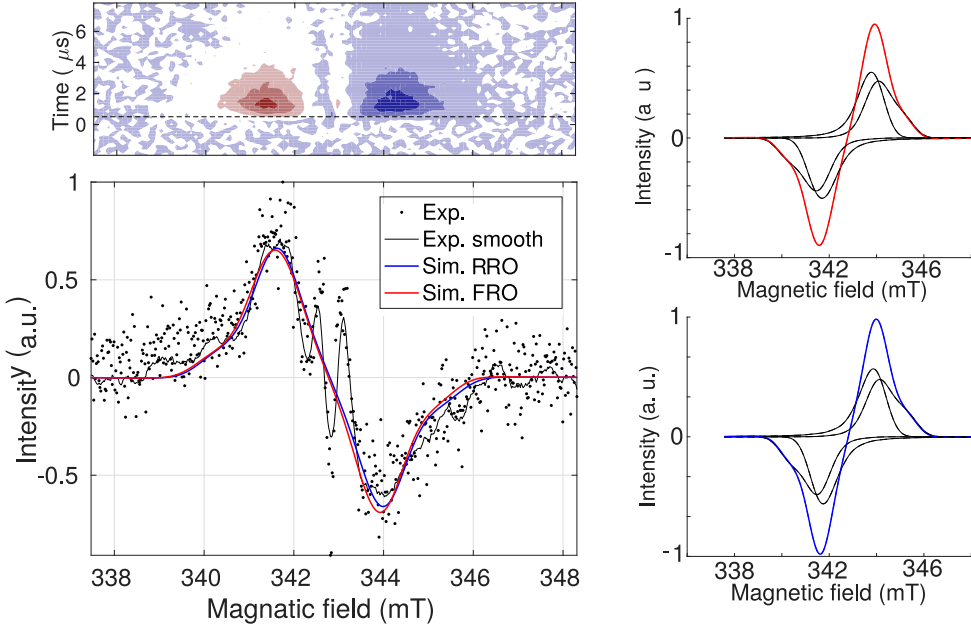


Figure 5.10: X-band trEPR spectra of PBTBT:PCBM. Measured at 25 dB. On the top left total trEPR spectrum is shown, the intensities are indicated by colors. Red corresponds to absorptive and blue - to emissive peaks. Time slice ($0.5 \mu\text{s}$) is simulated using two different models - random and fixed relative orientations (RRO and FRO, blue and red line respectively). The same couplings are used in both models $J = 20 \text{ MHz}$, $D = 100 \text{ MHz}$. Additional broadening is 0.9 mT . On the left, the black dots are the experimental data. On the right, the black line indicates the simulation of four separated transitions for each model for each band. Plots are normalized.

while a weaker CT is already there. Afterwards, it is hard to compare their intensities, because both signatures overlap. It seems that the weaker CT has the highest intensity at around $0.4 \mu\text{s}$. At around $0.7 \mu\text{s}$ both CT states have the same intensities. Afterwards, the stronger CT state is dominant and at around $1.8 \mu\text{s}$ it starts relaxing. It is interesting, that the spectrum becomes broader, thus bigger J is needed to get the right peak positions (at $1.4 \mu\text{s}$ $J = 27 \text{ MHz}$, while at $0.5 \mu\text{s}$ $J = 20 \text{ MHz}$ is used), after this time the width is not changing, only the intensity, until $5 \mu\text{s}$. Then it becomes narrower again, but the signal to noise ratio is very bad there, so it is hard to say anything. It seems that both CT states have similar life times.

PBTBT:PCBM and BTBT(2,3):PCBM

To continue an investigation of the local morphology, it was decided to consider the PBTBT, a well-ordered semi-crystalline polymer that is favorable for bulk heterojunction solar cells because of its high charge carrier mobility. PBTBT has a higher degree of crystallinity and order than the films of P3HT[37]. Zhang *et al.* [38], [39], [37] and others show that fullerene intercalation into PBTBT occurs when there is enough free volume between the side chains to accommodate the fullerene molecule. We can treat PCBM as a fullerene and we can use PBTBT polymer as well as its oligomers. Probably, PBTBT (or its oligomers) and PCBM have a fixed relative orientation in a blend (see Fig. 5.11), because when PCBM is rotated, its side chain will not let it to fit between two polymer

chains. Additionally to that, it was found out that BTET2:PCBM gives the highest efficiency as compared to other PBTET oligomers and the PBTET polymer in a blend with PCBM. This could be due to the 1D channels created by fullerene, as it is shown in Fig. 5.11b. [38]

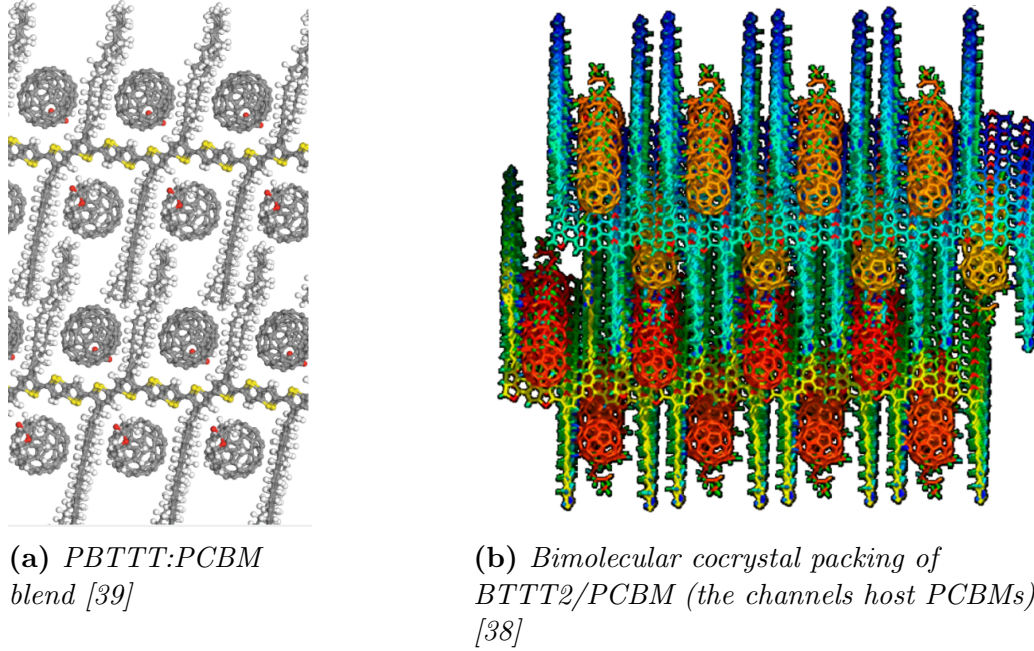
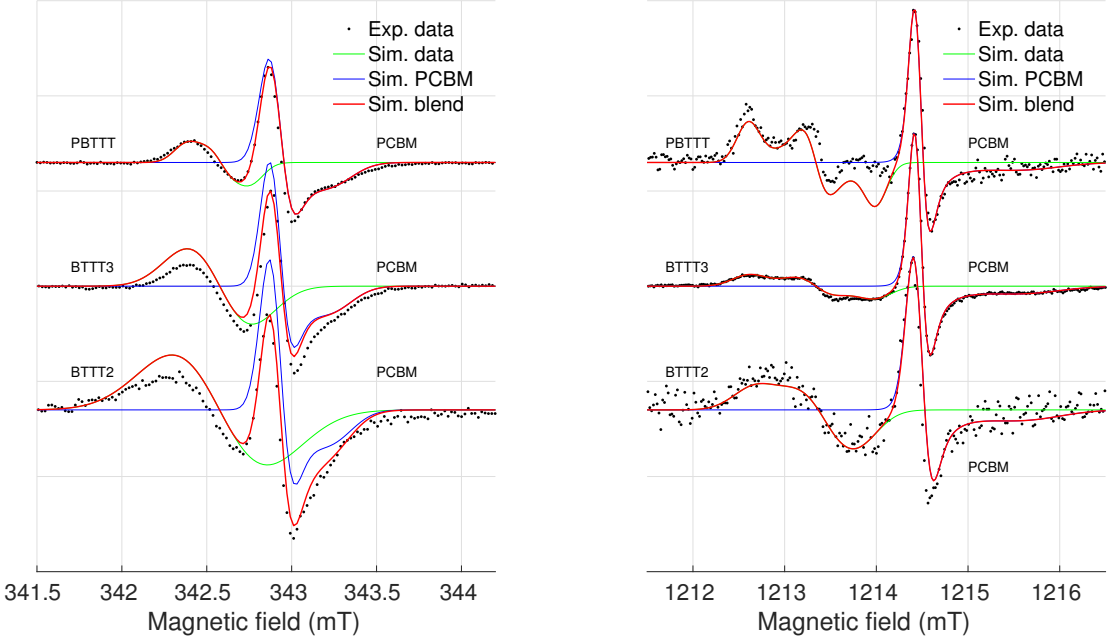


Figure 5.11: Intercalation of PCBM between side chains of the PBTET or oligomer BTET2.

In this thesis the most interesting points are, first, that there is a fixed orientation between PBTET (or its oligomers) and PCBM in a blend. Second, a positive polaron has different localization lengths on the polymer and on the oligomers [28]. These properties can affect the distance between the positive and the negative polaron and therefore, for different blends different interaction energies (D and J) result in different trEPR spectra. This was checked using the same samples (PBTET:PCBM, BTET3:PCBM and BTET2:PCBM) which were used in the [28] study. The sample preparation details can be checked in the article.

First of all, one needs to determine the g-tensor, the g-strain tensor and the line widths from cwEPR. Because a polymer cell in oligomers and in a polymer is the same, the environment of the positive polaron is the same on these materials. Thus the same g-values for PBTET, BTET3 and BTET2 should be used. Different line widths were used because the localization lengths are different and also some spectra contain a dark signal subtraction and others do not. There was no need to remeasure the dark signal for some samples, because all needed parameters can be extracted from the spectra without any dark subtraction.



(a) *X*-band. PBTTT:PCBM signal is a light induced signal, BTTT3:PCBM and BTTT2:PCBM - light signal

(b) *Q*-band. PBTTT:PCBM and BTTT2:PCBM signal is a light induced signal, BTTT3:PCBM - light signal

Figure 5.12: *CwEPR* spectra of PBTTT:PCBM, BTTT3:PCBM, BTTT2:PCBM blends measured in the *X*- and *Q*-band. The simulations are shown in red, as well as a simulation of separate components that is shown in green for a polymer (oligomer) and in blue for PCBM. For the donors, the same *g*-values are used. In all blends the same *g*-values and *g*-strain are used for PCBM. For more information about the parameters see Table 5.4.

	PBTTT	BTTT3	BTTT2	PCBM
$g_x(g\text{-strain}_x)$	2.00330(0)	2.00330(0)	2.00330(0)	2.00025(20)
$g_y(g\text{-strain}_y)$	2.00208(0)	2.00208(0)	2.00208(0)	2.00018(30)
$g_z(g\text{-strain}_z)$	2.00100(0)	2.00100(0)	2.00100(0)	1.99820(150)
lw X(Q) PBTTT:PCBM(mT)	0.17(0.29)			0.15(0.06)
lw X(Q) BTTT3:PCBM(mT)		0.36(0.42)		0.14(0.06)
lw X(Q) BTTT2:PCBM(mT)			0.61(0.54)	0.15(0.15)
weight X(Q) PBTTT:PCBM	0.40(1.64)			1.00(1.00)
weight X(Q) BTTT3:PCBM		1.24(0.64)		1.00(1.00)
weight X(Q) BTTT2:PCBM			3.15(1.44)	1.00(1.00)
Attenuation X-band (dB)	47	48	56	
Attenuation Q-band (dB)	35	32	49	

Table 5.4: Parameters that were used to get the best correspondence between the experimental spectrum and the simulations, that are shown in Fig. 5.12, for PBTTT and its oligomer blends with PCBM. As well as the used attenuations (att.). In brackets near *g*-values, *g*-strains are indicated. For the line widths (lw) and the weights, in brackets the values for the *Q*-band spectrum simulations are shown, when without brackets the values for the *X*-band are shown

		PBTM	BTM3	BTM2 Q	BTM2 X
RRO	J(MHz)	3	3	10	2
	D(MHz)	1	1	120	3
FRO	J(MHz)	5	4	10	3
	D(MHz)	1	1	120	-16
	TimeX(μs)	0.2	0.3	0.4	0.4
	TimeQ(μs)	0.2	0.2	0.1	0.1
	AddBrX(mT)	0.4	0.1	0.1	0.1
	AddBrQ(mT)	0.6	0.5	0.5	0.5

Table 5.5: Parameters that give the best fitting of the X- and Q-band trEPR spectra of PBTM:PCBM, BTM3:PCBM, BTM2:PCBM. Each spectrum was simulated with two different models - RRO and FRO. The time slice (TimeX and TimeQ for the X- and Q-band respectively) was chosen so that it gives the best signal to noise ratio and as early as possible in the same time. An additional broadening (AddBrX and AddBrQ for the X- and Q-band respectively) was added due to the Heisenberg principle, but was sometimes changed slightly in order to get a better fitting. Additionally, Euler angles were used for FRO model. They were the same for both components of all materials and were equal to [0.0 0.0 0.0], except for the BTM2:PCBM X-band trEPR spectrum. It was simulated using the Euler angles of PCBM equal to [0.0 0.5 0.0]. Usually a range of the couplings gives acceptable results, this determines the error that is around 10%. The smaller a coupling, the bigger becomes an error.

There are some oddities in the obtained values. The samples were prepared as 1:1 polymer to fullerene ratio. Thus the contribution of both components to the spectrum should be the same and the weights should be equal. But they differ a lot. We believe that this is due to the saturation effect, that is clearly present in the measured spectra since some of the spectra are asymmetric (an integral over the spectrum is not zero). It also can be due to inaccurate simulations and different T₂ times.

PCBM g-values differ from the values found in the P3HT:PCBM blend. This can be because of the penetration of a fullerene between the side chains of the polymer, that can lead to the distortion of the fullerene.

After cwEPR measurements, trEPR was performed and the obtained spectra were simulated, see Fig. 5.13 and for parameters see Table 5.5.

For PBTM:PCBM trEPR measurements another sample was used (not the same one as for cwEPR). Therefore different line widths were used: lw_{PBTM X-band}= 0.22 mT lw_{PBTM Q-band}= 0.29 mT lw_{PCBM X-band}= 0.15 mT lw_{PCBM Q-band}= 0.06 mT.

For the X-band trEPR PBTM:PCBM spectrum, there is some strange additional broad feature, this feature was assigned as a background and a corresponding correction was made. The simulations fit quite well. Both models with respect to the relative orientation give similar results.

In simulations using the FRO model, a change of Euler angles was not giving a big difference for BTM3:PCBM and for PBTM:PCBM. On the Fig. 3.3 it is shown that different orientations give almost no difference with a zero D coupling. This is the case here, the used D value is only 1 MHz and therefore it does not affect the spectrum.

The most interesting situation is for the BTM2:PCBM. The X-band and the Q-band spectra were simulated separately. For the X-band, it is strange, that a simulation for the FRO model is inverted (negative scaling was used). The Q-band was simulated using completely different coupling parameters, which are much bigger than one used for the

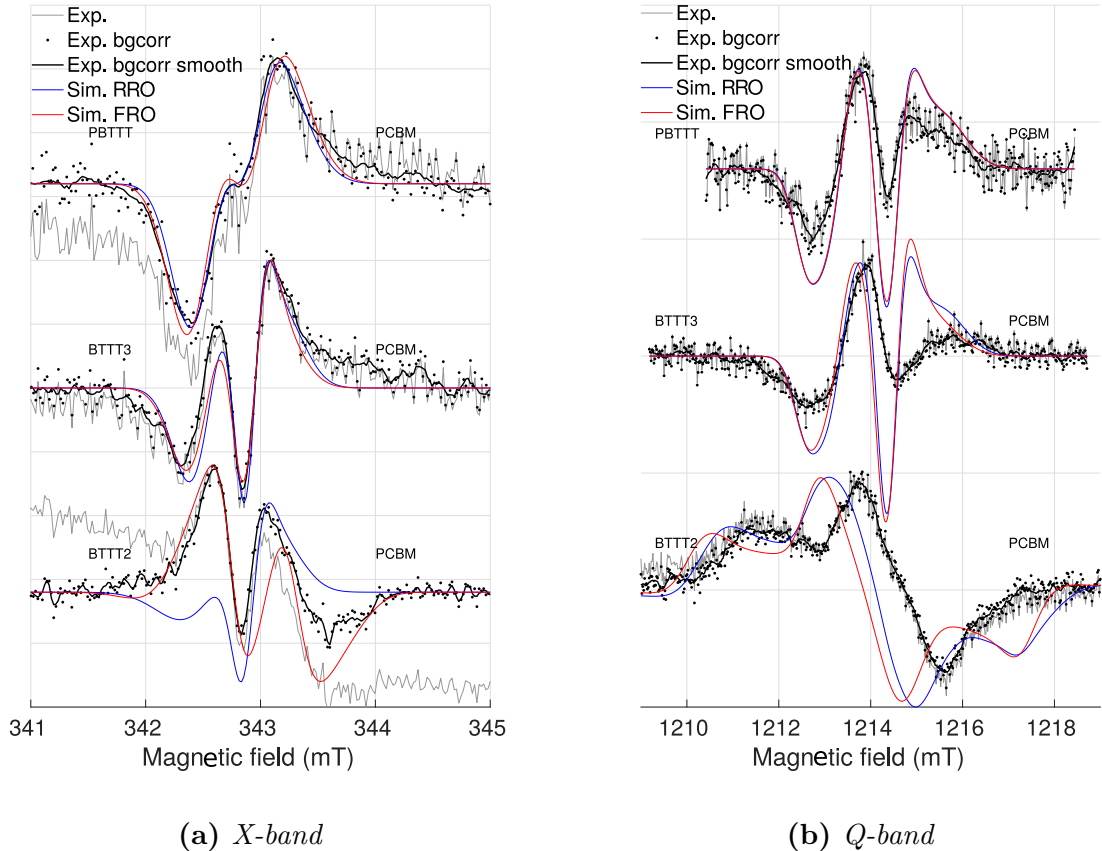


Figure 5.13: *TrEPR* spectra of CT states on PBT TT:PCBM, BTTT3:PCBM and BTTT2:PCBM blend interfaces and their simulations. For the *X*-band, attenuation of 35 dB was used, for the *Q*-band, 25 dB was used. In light-gray, initial (without corrections) spectra are shown, the dark dots is a background corrected spectrum, the black line is for a better visualization of the dots, that averages the dots a little bit. In blue - the simulations that correspond to the random relative orientations (RRO) model. In red - a fixed relative orientation (FRO) between a polymer (oligomer) and a fullerene is assumed. The parameters that were used for the simulations are indicated in Tables 5.4 and 5.5. The BTTT2:PCBM *Q*-band and *X*-band FRO spectra simulations are inverted (negative scaling was used for fitting). The used *D* parameter for BTTT2:PCBM *Q*-band is much bigger than for the other spectra, that suggests that it is not a singlet CT. For more details see the text.

X-band. So the recorded signal in the Q-band is coming not from the usual CT state. It can correspond to a stronger coupled CT state. Also an additional peak on the right part of the spectrum appears in the simulation. This can mean that several mechanisms overlap, that gives a shift and a missing peak in the experimental data. The shift with respect to the experimental spectrum can be explained as a wrong calibration, which is very improbable in this case, because the signal was recorded using a gauss-meter (the magnetic field was measured precisely) and a field calibration was made. Still, this shift could be due to some change during the measurements (for example, some external unexpected object near the magnets). To state something more defined, the experiment should be repeated once again. Also it is not good that the X-band and the Q-band give completely different signatures, it would be better to repeat the experiment using a fresh sample.

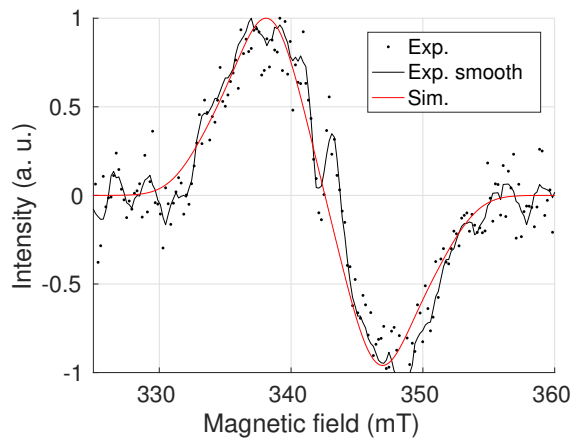


Figure 5.14: Simulated triplet for BT2T(2,3):PCBM, measured in the X-band. The used parameters are following: $D = 140$ MHz, $E = 130$ MHz, the line width 4.7 mT, temperature is $[1\ 1\ 0]$. The simulations are shown in red, the black dots is the experimental spectrum, the black solid line is numerically averaged (smoothed) experimental spectrum for a clearer view

There is one more feature on the spectrum - the background in the X-band measurement. It suggests that there is some additional signature. A wider scan was made and recorded spectrum was simulated, Fig. 5.14. The found couplings are $D = 140$ MHz and $E = 130$ MHz. The D coupling is close to the found D for the simulation of a stronger CT state in the Q-band ($D = 120$ MHz, $J = 10$ MHz). But non zero E makes the spectrum much broader. The attempt to simulate the Q-band signal using $E = 130$ MHz or similar was not successful. So in the Q-band it is probably not a signature coming from a triplet exciton.

It is also interesting, that there is no background in the Q-band. But if one looks at later times, there is a broad signature that arises. That should correspond to a signature of a triplet exciton.

This pushes the outcome that in BT2T(2,3):PCBM, there are three features visible: a CT state, a stronger coupled CT (or something else) and a triplet exciton. It is not clear why in the different bands these signatures arise differently. And it is suggested to redo the experiments with a fresh sample.

For BT2T(2,3):PCBM in the X-band, the FRO gives a better simulation as compared to the RRO model. This suggests, that the relative orientations are fixed and the model with

crystallization of BTBT2 and penetration of the fullerene seems to work.

The background of the PBTTT:PCBM also suggests some additional broad signal on top. Unfortunately, for that particular sample, a wider scan was not measured. But it was done for a new prepared PBTTT:PCBM sample. The results are shown in chapter about stronger coupled CT).

From extracted D values, the distances can be calculated using the equality 2.3.6, where an assumption of the point dipole approximation is made. The calculated distances are shown in Table 5.6.

	PBTTT	BTBT3	BTBT2 Q	BTBT2 X
RRO r(nm)	3.7	3.7	0.8	2.6
FRO r(nm)	3.7	3.7	0.8	1.5

Table 5.6: *Inter-spin distances calculated from extracted D couplings (from Table 5.5), under an assumption of the point dipole approximation.*

In the article [28] it was found that the localization of a hole on the polymer is over 10 thiophene rings long when the backbone is non-planar and up to 14 rings for a backbone forced to be completely planar. BTBT2 has 8 rings, BTBT3 - 12 rings and PBTTT a lot of rings. This means that the delocalization will be through the same length in PBTTT and in BTBT3. For BTBT2 the delocalization length should be $12/8 = 1.5$ times smaller.

Robert Steyrleuthner *et al.* [40] found that the hole is delocalized on PBTTT depending on its molar weight. The delocalization of a polaron on the PBTTT with $M_n = 15$ kDa (the same polymer that was used in this thesis) was found to be 4 nm. The found here inter-spin distances are 3.7 nm. For BTBT3 these values are the same, for BTBT2 both values are smaller.

Are these parameters (inter-spin distances and delocalization length) related to each other or is it a coincidence? This will be discussed in the "Inter-spin distances" section.

Small D couplings lead to the impossibility to say something about the relative orientations. But for BTBT2, a significant D was found. The FRO gave much better accordance between the simulations and the experiment than the RRO. From this, as well as from the previously mentioned studies, we can conclude, that the relative orientations are fixed between PBTTT (and oligomers) and PCBM. It was mentioned, that BTBT2:PCBM has higher efficiencies than the oligomers or the polymer. It is not clear, in which sense the small inter-spin distance influences the efficiency. More likely is that the main role is played by crystallinity and 1D channels of PCBM. A more detailed study should be done to understand the main cause. For example, different sample preparations and blend component ratios can be tried, as it should affect both 1D channels and crystallinity and should not affect couplings and inter-spin distances.

C-PCPDTBT:PCBM and F-PCPDTBT:PCBM

In [25] Kraffert et al. suggest that in C-PCPDTBT:PCBM blend triplet excitons are created through CT states via back electron transfer (Fig. 5.9) that is happening after singlet/triplet interconversion that results in the stronger coupled CT state (stronger coupled CT). It was decided to look in the PCPDTBT blends in order to find strongly coupled

CT states and try to simulate them. Actually, the initial purpose of the measurements was different, therefore broader scans for Q-band trEPR are missing.

C-PCPDTBT and F-PCPDTBT in blends with PCBM were used.

First of all, the cwEPR spectra were measured in the X- and Q-band. In Fig. 5.15 the dark, the light and the light-induced signals are shown. Unfortunately, the dark signal for F-PCPDTBT:PCBM in the Q-band was not recorded. The dark signals are very strong. Also it is interesting that the dark signals have additional feature at lower magnetic fields, that can correspond to some defects (for example, oxygen).

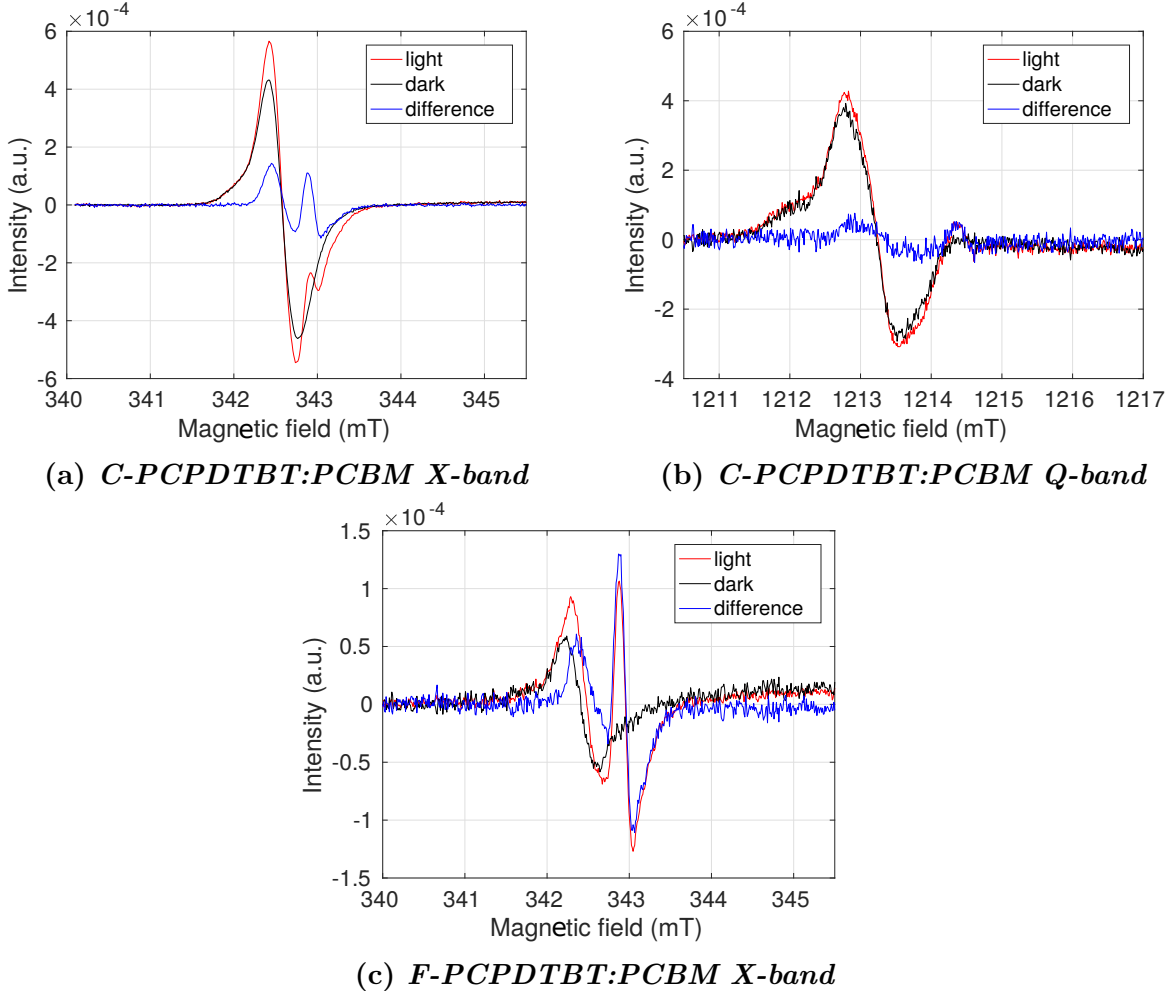


Figure 5.15: *CwEPR X-band spectra. The red line shows the light-induced signal, the black line is the dark (light off) signal and the blue line is the subtracted dark from the light signal. All measurements were done at $T = 80\text{ K}$, a field modulation frequency 10 kHz and a power attenuation of 53 dB (X-band) and 42 dB (Q-band)*

The obtained light-induced spectra were simulated, as well as the light signal for F-PCPDTBT:PCBM in the Q-band (Fig. 5.16). The dark signals were also simulated because they are differ from the polymer part of the light-induced spectrum (Fig. 5.17). The parameters used for the simulations are indicated in Table 5.7

It is interesting that the g-values used for the simulation of the dark signal are shifted compare to the values used for the light-induced signal simulation. All components g_x , g_y, g_z are shifted almost on the same value that is 0.0002 - 0.0003 for C-PCPDTBT and 0.0009 - 0.0010 for F-PCPDTBT. This can mean a change of the polaron environment

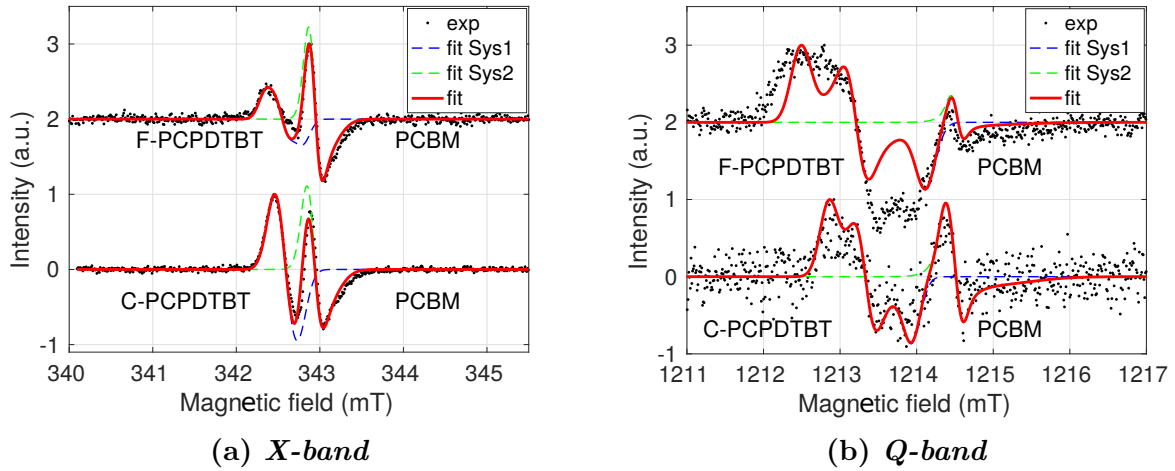


Figure 5.16: The background corrected light-induced cwEPR spectra (black dots) and the simulations (red solid lines) of the C-PCPDTBT:PCBM and F-PCPDTBT:PCBM samples. The dashed blue lines show the simulation of the donor polymer, the dashed green line - of the acceptor (PCBM). The light off signal was subtracted from the light signal for all cases except the F-PCPDTBT:PCBM Q-band spectrum, there the light-on signal spectrum is shown. All measurements were done at $T = 80\text{ K}$, a field modulation frequency 10 kHz and a power attenuation of 53 dB (X-band) and 42 dB (Q-band).

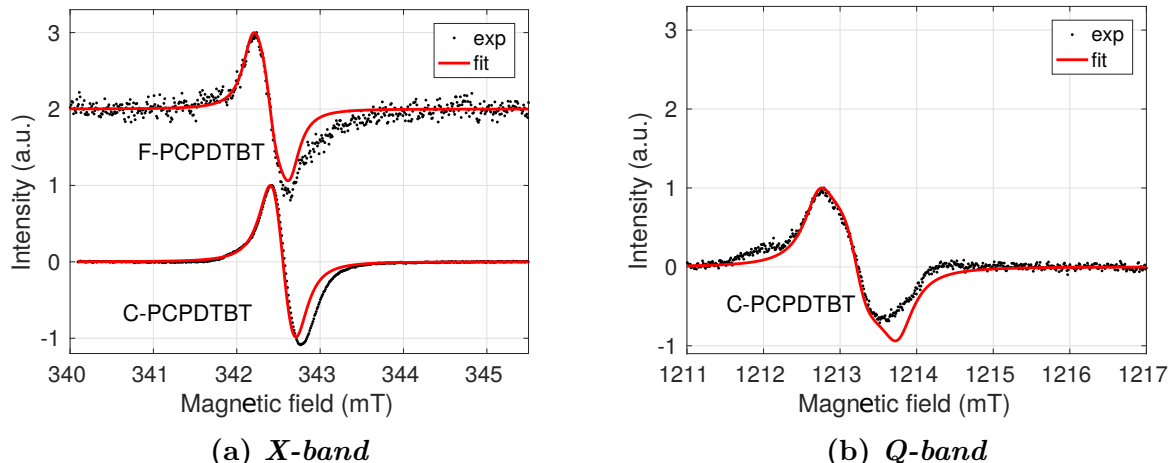


Figure 5.17: The background corrected dark cwEPR spectra (black dots) and the simulations (red solid lines) of the C-PCPDTBT:PCBM and F-PCPDTBT:PCBM samples. All measurements were done at $T = 80\text{ K}$, a field modulation frequency 10 kHz and a power attenuation of 53 dB (X-band) and 42 dB (Q-band).

and thus a blend structure under illumination.

The different PCBM g-values (g_x components) are used in the different blends. This can be due to the uncertainty due to the overlap of two components in the signal. Or the fullerene is somehow affected by the closeness of the polymer.

If stronger coupled CT states exist and are visible, then they can be seen in trEPR. The measured spectra are shown in the Fig. 5.18.

It seems that the right parts of the CT state spectrum are overlapping with some

	C-PCPDTBT		PCBM	F-PCPDTBT		PCBM
	dark	dif		dark	dif	
g_x	2.0031	2.0029	2.00035(10)	2.0044	2.0035	2.0002(1)
g_y	2.0023	2.0021	2.00010(1)	2.0032	2.0023	2.00010(1)
g_z	2.0014	2.0011	1.9989(18)	2.0018	2.0008	1.9989(18)
lwX	0.37 L	0.23	0.19	0.3 L	0.19	0.163
lwQ	0.5 L	0.27	0.16	-	0.3	0.143

Table 5.7: The parameters used for the simulations of C- and F-PCPDTBT:PCBM. In brackets the used g-strain is indicated. Gaussian broadenings are considered if other is not indicated. The line widths for the X-band and Q-band (lwX and lwQ) are in mT. 'L' means that the Lorentzian line shape was used.

	C-PCPDTBT (8 μ s)	F-PCPDTBT (0.6 μ s)	F-PCPDTBT(8 μ s)
g	2.0023	2.0023	2.0023
T	[1.0 0.1 0.1]	[0.0 0.3 1]	[1.0 0.1 0.1]
lw (mT)	1.3	1.7	1.3
D (MHz)	[980 143]	[980 143]	[980 143]

Table 5.8: Parameters used for the simulations of the triplet excitons for C-PCPDTBT and F-PCPDTBT at longer time after the laser flash (8 μ s) and for F-PCPDTBT at shorter times after the laser flash (0.6 μ s). For the simulations see Fig. 5.19

other signal, the right part of which should be negative. That coincides with a stronger coupled CT.

A wider scanned spectrum can give more insight. In the X-band the wider scans for both materials were measured. They show the presence of a triplet exciton state, that was simulated (Fig. 5.19).

It is interesting, that for later times ($t = 10 \mu\text{s}$) the triplet exciton signal spectrum for both materials can be simulated with the same parameters. But early times spectra ($t = 0.6 \mu\text{s}$) look differently. For C-PCPDTBT a triplet exciton signal is clearly visible, but it is not possible to simulate it at earlier times. This suggest that it overlaps with an additional signal, that is negative on the right side and positive on the left side, if the same triplet as for F-PCPDTBT earlier times assumed. It could be a stronger coupled CT state but the line width is to broad for it. So it may be signal from another triplet exciton.

For F-PCPDTBT, from a comparison of the triplet exciton spectrum simulations and the experiment at 0.6 μs , the existence of an additional signature is visible Fig. 5.19b. There is a CT state in the middle of the triplet, but there are also additional 'wings' around it. It is broader then usual a CT state. The attempt to simulate this signature was made. It was assumed that it is a stronger coupled CT state, and it was simulated in the X- and Q-band. The results are indicated on Fig. 5.20.

Two upper pictures show the simulation of the triplet exciton spectra (red dashed line), the stronger coupled CT state spectra (solid red line) and usual signal from triplet excitons (blue dashed line). It is hard too see all the simulations, thus a zoom was made (the right figure). It is clear that the sum of all simulations does not give the total experimental spectra. This is due to the very rough simulations of the signal from triplet

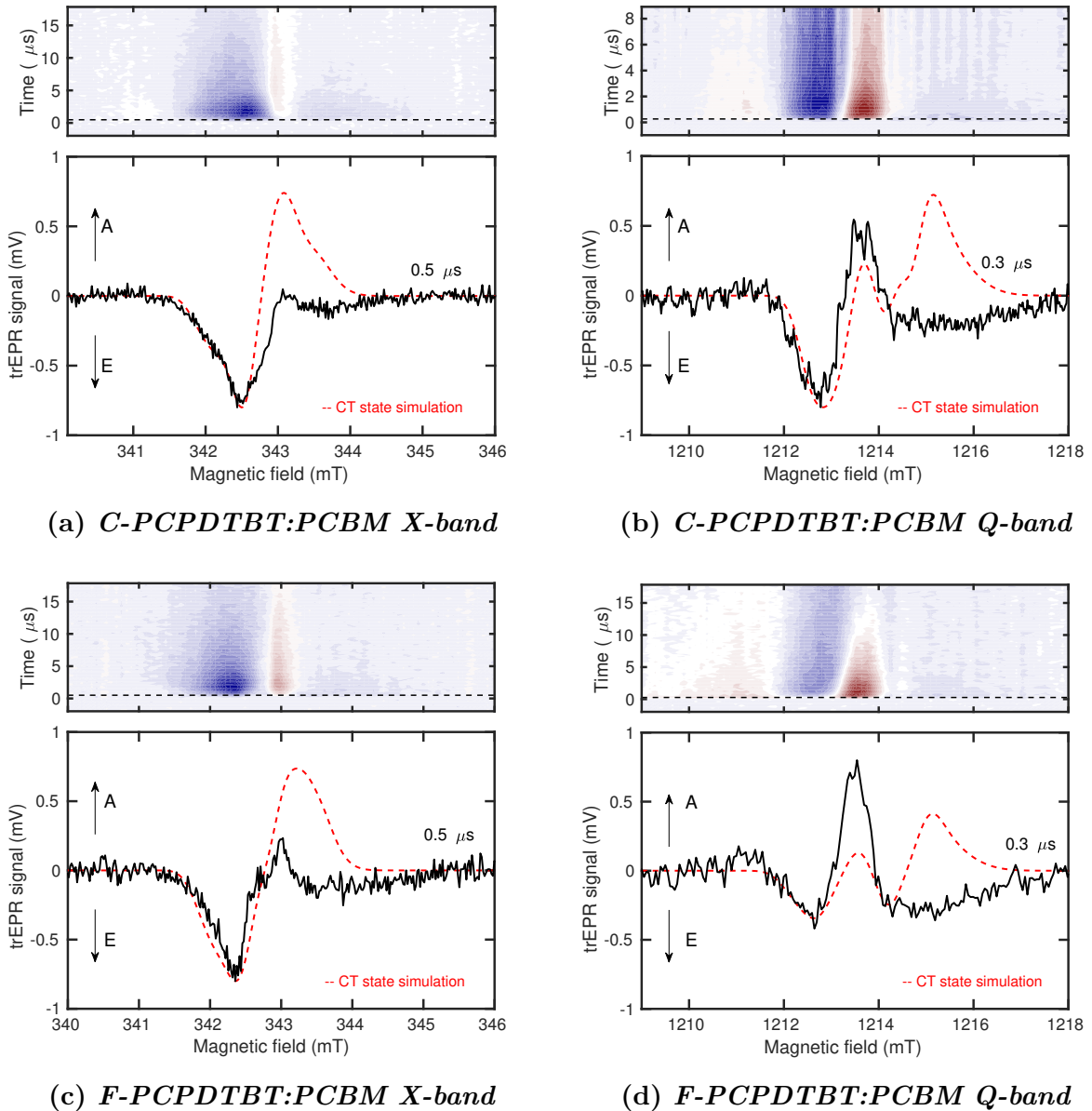


Figure 5.18: Background corrected trEPR spectra (black line) and the CT state simulations (red dashed lines) of the C-PCPDTBT:PCBM and F-PCPDTBT:PCBM samples. All measurements were done at $T = 80\text{ K}$, with a 532 nm light and a power attenuation of 35 dB (X-band) and 25 dB (Q-band). For the simulations, the extracted from the cwEPR spectra parameters are used. An additional broadening is considered due to Heisenberg uncertainty principle, for the X-band it is 0.2 mT and for the Q-band 0.4 mT . A powder spectrum with random relative orientations between the donor and the acceptor is assumed due to the disordered nature of the blend. The best fitting is obtained with the following coupling parameters: $J = 7\text{ MHz}$ and $D = -17\text{ MHz}$ for C-PCPDTBT:PCBM and $J = 9.6\text{ MHz}$, $D = -16\text{ MHz}$ for F-PCPDTBT:PCBM

excitons and big errors in the experimental data, since the broad scan was made with the large step (1 G). Also because of the three different components in the spectra, it is very difficult to find a total good simulation.

At the two bottom figure the simulation for the Q-band is shown. On the left pic-

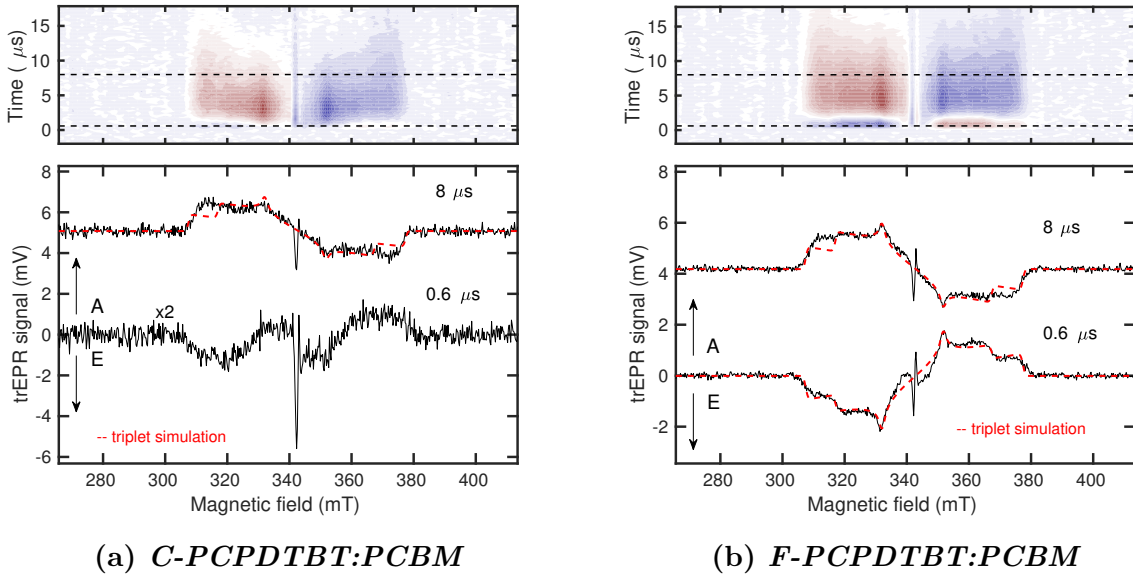


Figure 5.19: Background corrected and smoothed X-band trEPR spectra (black line) and the triplet exciton spectrum simulations (red dashed lines) of the C-PCPDTBT:PCBM and F-PCPDTBT:PCBM samples. All measurements were done at $T = 80\text{ K}$, with a 532 nm light with a power of 1 mJ and a power attenuation of 35 dB . For earlier times ($t = 0.6\text{ }\mu\text{s}$) for C-PCPDTBT:PCBM a good simulation could not be found, it could be that triplet exciton signatures are overlapping with a back electron transfer. All simulation parameters see in Table 5.8

ture the usual CT state simulation is shown (blue solid line), the black dotted line is the experimental data without corrections. The black solid line is a background corrected smoothed experimental data. On the right picture the black solid line is again the background corrected and smoothed spectrum, but as a background the strongly coupled CT state simulation is taken (red line). If one compares a correspondence between the usual CT state simulation and the experimental background corrected data, it is clear, that the right figure gives a better result. The fit is not perfect, this can be also due to the fact that the signal from triplet exciton background should be present, as it is present for the X-band.

In the Table 5.9 below the coupling parameters used for the simulations are indicated.

	Triplet	Stronger CT	CT
D (MHz)	980	120	-16.0
E (MHz)	143	30	0.0
J (MHz)	0	20	9.6
lw (mT)	1.7	0.9	0.2(0.4)
r (nm)	0.4	0.8	1.5

Table 5.9: Parameters used for the simulations of the signal from triplet exciton, stronger coupled CT and singlet CT states. As a line width for the CT states, additional broadening is meant. For the usual CT state, it is mentioned for the X-band and in brackets for the Q-band. From the found D coupling the inter-spin distances are calculated using equality 2.3.6, assuming the point dipole approximation.

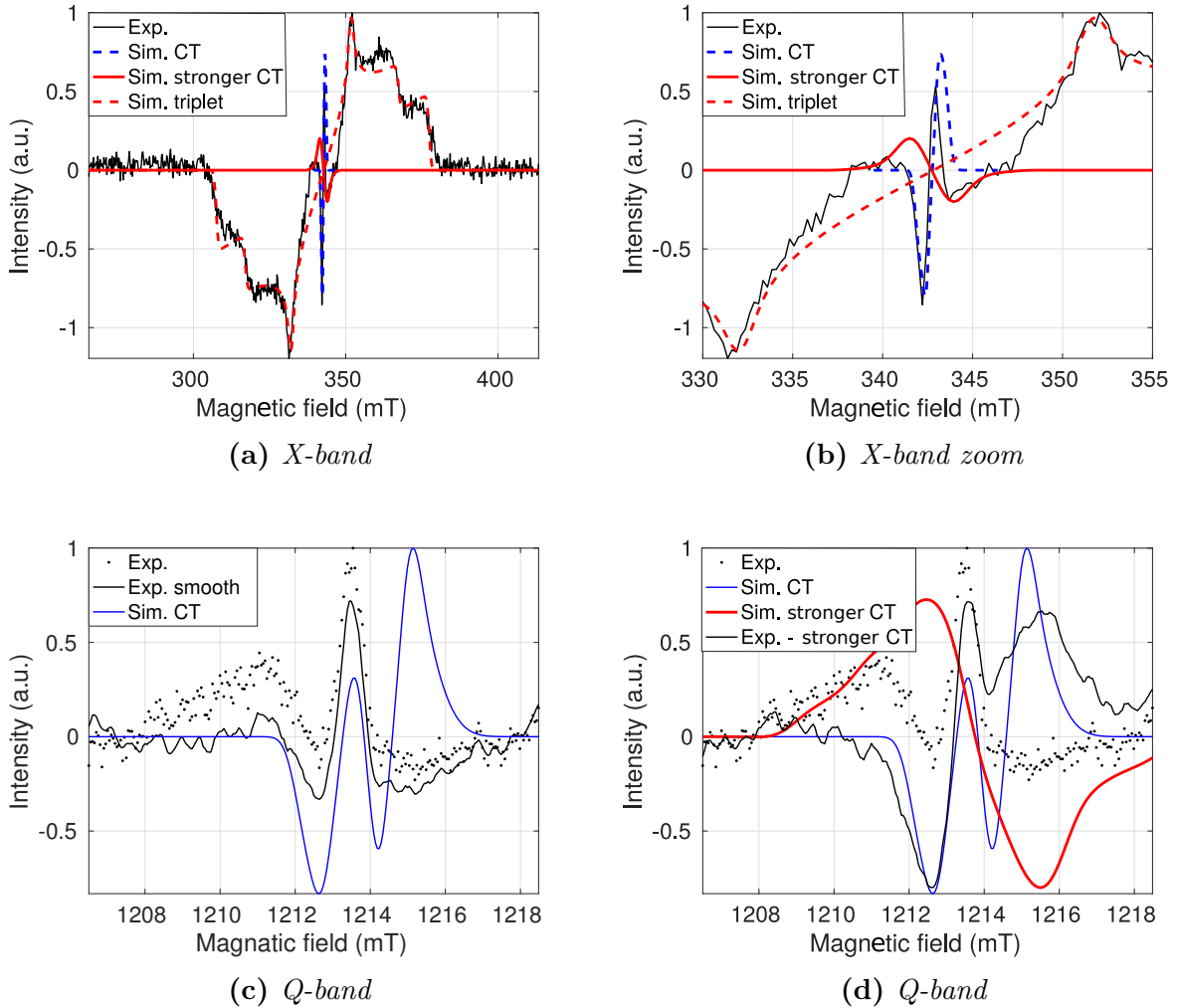


Figure 5.20: Triplet exciton (red dashed line), stronger coupled CT (solid red line) and singlet CT state (blue line) simulations for the experimental (black line) spectra measured at the trEPR X- and Q-bands. Two upper pictures show the X-band spectra. It is hard to see all the simulations, thus the zoom was made (the right figure). It is clear that the sum of all simulations does not give the total experimental spectra. This is due to the very rough triplet exciton spectrum simulations and big errors in the experimental data, since the broad scan was made with the large step (1 G). At the two bottom figures the simulation for the Q-band is shown. The black dotted line is the experimental data without corrections. The black solid line is the background corrected smoothed spectra. On the right picture as a background the stronger coupled CT simulation is used (red line).

Inter-spin distances

In this section we would like to discuss the obtained inter-spin distances. The found D and J couplings suggest that the assumed point dipole approximation is not valid anymore. The non zero J couplings indicate that there are some wave function overlaps. In general this should be taken into account. It is not clear how the corrections should be made, since the wave-functions as well as the other parameters are not known. There is another uncertainty. Positive and negative polarons are delocalized, thus the inter-spin distances are different. We assume that some average distances are found (Fig. 5.21).

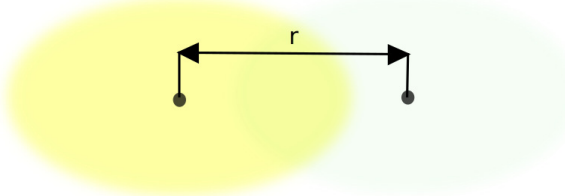


Figure 5.21: Delocalization of polarons is shown schematically, as well as the inter-spin distance, that corresponds to the extracted value from *treEPR*.

If we assume that wave function overlap is giving only a small error, do the found distances make sense?

Let us consider a P3HT:C₆₀ example. In this study it was found out that C₆₀ and P3HT more likely have the relatively fixed orientation and the inter-spin distances of around 2.2 nm. C₆₀ has a diameter of about 7 Å [41]. The delocalization of the positive polaron is around 4 nm (at least in a blend with PCBM [42, 43]). The schematics is shown in Fig. 5.22. It should look similar in case of C₆₀. If the most probable localization of the hole is in the middle of this range, this would mean that the vertical distance should be around 2.0 nm. That is quite a lot, at least one more fullerene can fit in between. On the other hand, the polymer has long side chains, that can keep the distance between the polymer and the fullerene. Or may be the polarons are sitting not on the neighboring atoms, that is also possible. But in this case, can we talk about a fixed relative orientation between a polymer and a fullerene?

Jahn-Teller distortion appears when an additional electron is jumping on the fullerene. In our case, an electron still interacts via Coulomb attraction with a hole that sits on the polymer, this can cause a distortion of the fullerene directional to the polymer. So it seems that the polymer and the distorted fullerene can have a fixed relative orientation even if the molecules are not neighboring.

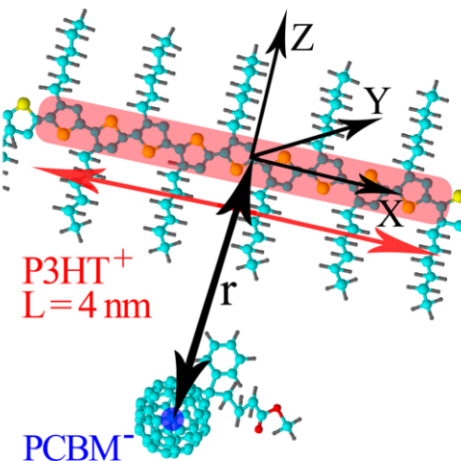


Figure 5.22: A model of a light-generated CT state at the P3HT-PCBM interface. The hole is assumed to be delocalized on the P3HT chain over $L = 4$ nm (approximately 10 thiophene monomers); the spin of the electron on PCBM is approximated as a point dipole. The principal axes of the dipolar interaction tensor are shown. [42]

This is just a hypothesis. And nothing confirms or refutes it, except for the very rough

estimated distances. Another experiments should be done, for example electron-nuclear double resonance (ENDOR), to check the delocalization of the electron on the distorted fullerene. If the electron is delocalized, then the distortion should have an arbitrary direction. And a relative orientation of the polymer and the distorted fullerene should be random.

There is an article [42], where the out-of-phase electron spin echo was performed on P3HT:PCBM. In order to get a better simulation, the assumption of the positive polaron delocalization was made. The assumed delocalization is 4 nm Fig. 5.22. This should lead to the inter-spin distance distribution, as it depends on the position of the positive polaron. The most probable inter-spin distance was determined, that is equal to 2-3 nm. In this thesis, and in the article [34], 4 nm distance was found. For this the point dipole approximation was made. The temperature, at which experiments were performed, is different. 4 nm distance was obtained at 80 K, when 2-3 nm distance at 65 K. For all three studies, a non zero J was not taken into account for calculations, that could have led to the wrong result, as the found J indicates the wave function overlap. Thus electrons can not be considered as points any more. So their delocalization should be taken into account. And equation 2.3.6 should be rewritten. Still the previous question stays open. It is not clear if the charges are sitting on the neighboring atoms or not. But in case of the random relative orientation it is not critical, as randomness will be conserved if the molecules are not neighboring.

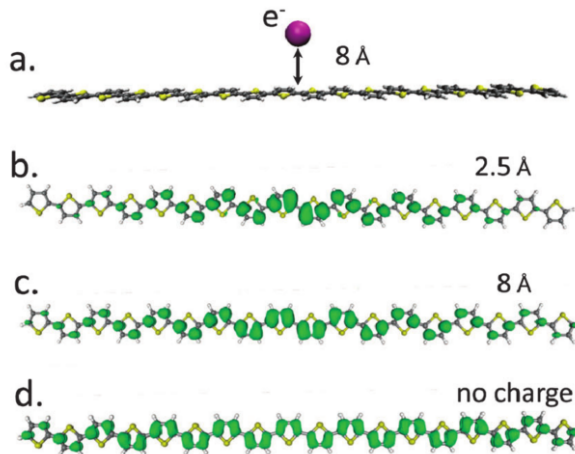


Figure 5.23: Geometry of the positively charged thiophene units P3HT 18-mer with one negative charge placed away from the center of the oligomer (a) and spin density isosurface plot of a P3HT 18-mer with negative charge at: (b) 2.5 Å, (c) 8 Å, (d) no negative charges in the vicinity. [43]

Now let us return to the PBT TT and its oligomers. The delocalization length for PBT TT is 4 nm (3.1 BTTTs). This means that the delocalization length on BTTT3 is almost the same (4 nm). BTTT2 is shorter, that leads to the delocalization length of 2.7 nm. The inter-spin distances were found to be the same for PBT TT and BTTT3 and smaller for BTTT2.

Niclas *et al.* [43] calculated using density functional theory (DFT) how the delocalization length of the hole is changed, when the negative charge is present nearby. The closer the negative charge, the more localized the hole (Fig. 5.23. But this should also holds in reverse. The more localized the hole, the stronger it interacts with an electron

and the smaller the inter-spin distance.

The found inter-spin distances are quite big, that is not corresponding to the model of intercalation of the fullerene between the side chains of the polymer. Or may be the polarons are sitting on the not neighboring molecules.

Chapter 6

Summary and Outlook

TrEPR spectroscopy was used for the investigations of CT states at the polymer-fullerene interface. By using different simulation models (fixed and random relative orientations in a powder), an attempt was made to find out the relative orientations between different polymer and fullerene molecules in a blend. The information about the relative orientations and the couplings was obtained by fitting an experimental trEPR spectrum with a simulation. It was shown, that without any preliminary information about the system, several sets of couplings and relative orientations can be extracted from the fitting. In this case, there is no exact information about the inter-spin distances and the local morphology. However, in some cases it is still possible to find both couplings and relative orientations, as it was done for a P3HT:C₆₀ sample. The preliminary information about the system can help to determine unknown parameters.

The inter-spin distances which are being calculated from the D-coupling usually contain an error due to the several factors:

- The relative orientations between donor and acceptor molecules are unknown that can lead to several sets of J and D couplings;
- The inter-spin distance can be distributed over some range;
- The extracted from cwEPR g-tensor and line widths can contain an error that leads to an error in the D-coupling;
- The relaxation processes can affect the spectrum shape and therefore the fitting parameters, including the D-coupling;
- Sometimes it is hard to say, which simulation fits an experimental spectrum better;
- A non zero J indicates that the wave functions of the electrons overlap, thus the point dipole approximation is not completely acceptable. If the overlapping part is small, then the error is also small;
- J and D couplings can influence the simulation in a similar way, therefore it is hard to determine the D coupling precisely;

Despite all these factors, an error of the inter-spin distance determination is not so critical. The considered CT state simulations show that the spectra for coupled polarons with 1 and 2 nm inter-spin distances are different. The smaller the distances, the bigger the D-coupling, the more precise the determination of the inter-spin distance. The distances

larger than 3-4 nm, give the same spectra and it is not possible to determine the inter-spin distances precisely.

This work has given a lot of ideas for further investigations that will allow to determine the couplings more precisely and it will give a better insight into the charge separation in organic solar cells. Some of them are mentioned below.

For some of the samples small D-values were obtained ($D \approx 1$ MHz, $r > 3$ nm). For such long distances (small couplings) the spectra look the same and it is hard to determine D and J precisely. The measurements at lower frequencies (S-band) can help, as Δg will play a smaller role and the couplings will prevail. But in this case, the line width can be a problem, as it is field-independent, it will stay the same and it will possibly intercept the spectral features.

The next problem is a precise determination of g-values, g-strains and line widths. The Q-band frequency is not high enough to completely resolve the mentioned parameters. This introduces an error that influences the J and D coupling determination. Some more precise values can be obtained in W- or V-band. It will reduce an error for the J and D couplings as a consequence.

There is one more uncertainty that is related to relaxation effects. The importance of these effects can be checked in different ways. First of all, the spectra can be measured at lower temperatures, where the relaxation should be slower and it will be possible to see if at early times a spectrum differs from the one observed at 80 K. If the difference is big, then the relaxation effects should be taken into account.

The other opportunity is to use a signal mixer to measure at earlier times in the Q-band.

There can be two relaxation processes - phase relaxation T_2 (spins compensate each other) and magnetization relaxation T_1 (recombination). Their influence on the magnetization is described by the Bloch equations [44]. The relaxations can be included in the simulations. However, this is going to give four additional parameters (both relaxation times for both materials). But on the other hand, one can consider some later time slices from the same trEPR spectrum which will give some additional data that will balance the unknown parameters.

Also pEPR spectroscopy can be applied to determine the relaxation times.

The non trivial charge separation steps in most materials make understanding of the full charge separation process almost impossible, since a lot of different energy states are involved. It is very hard to distinguish between some separated states with distinct couplings, because their signatures overlap in trEPR spectra. Despite, for a number of materials it is still possible to distinguish between the different energy states, whose signatures in trEPR then can be simulated. That allows to determine the inter-spin distances that show how far the charge carriers are. Studying different polymer:fullerene blends, it is possible then to determine, which combinations give larger distances between the charges. If the inter-spin distance is known from another experiment (for example DEER), then it is possible to determine the relative orientations between molecules. This knowledge then can be used to create a solar cell of a higher efficiency.

We believe that this work is a big help for further investigations because a helpful visualization tool was created and tested on several materials. This already gave some interesting results, including the stronger coupled CT states.

Bibliography

- [1] W. Shockley, H. J. Queisser, Detailed Balance Limit of Efficiency of p-n Junction Solar Cells, *Journal of Applied Physics* 32 (3) (1961) 510–519. doi:10.1063/1.1736034.
URL <http://aip.scitation.org/doi/10.1063/1.1736034>
- [2] Photovoltaic Research — NREL. Efficiency Chart, 30.10.2017. Accessed on 30.11.2017.
URL <https://www.nrel.gov/pv/assets/images/efficiency-chart.png>
- [3] A. Köhler, H. Bässler, Electronic Processes in Organic Semiconductors, Wiley-VCH Verlag GmbH & Co. KGaA, Weinheim, Germany, 2015. doi:10.1002/9783527685172.
URL <http://doi.wiley.com/10.1002/9783527685172>
- [4] J. Behrends, A. Sperlich, A. Schnegg, T. Biskup, C. Teutloff, K. Lips, V. Dyakonov, R. Bittl, Direct detection of photoinduced charge transfer complexes in polymer fullerene blends, *Physical Review B* 85 (12) (2012) 125206. doi:10.1103/PhysRevB.85.125206.
URL <https://journals.aps.org/prb/pdf/10.1103/PhysRevB.85.125206>
- [5] V. I. Krinichnyi, E. I. Yudanova, N. N. Denisov, Light-induced EPR study of charge transfer in poly(3-hexylthiophene)/fullerene bulk heterojunction, *The Journal of Chemical Physics* 131 (4) (2009) 044515. doi:10.1063/1.3193722.
URL <http://www.ncbi.nlm.nih.gov/pubmed/19655902>
<http://aip.scitation.org/doi/10.1063/1.3193722>
- [6] Y. Kobori, R. Noji, S. Tsuganezawa, Initial Molecular Photocurrent: Nanostructure and Motion of Weakly Bound Charge-Separated State in Organic Photovoltaic Interface, *J. Phys. Chem. C* 117 (4) (2013) 1589–1599. doi:10.1021/jp309421s.
URL <http://pubs.acs.org/doi/pdf/10.1021/jp309421s>
- [7] T. Miura, T. Tachikawa, Y. Kobori, Morphology Effect on Geometry of Photoinduced Charge-Separated State in P3HT:PCBM Blend Films as Studied by Time-Resolved EPR Spectroscopy, *Journal of Photopolymer Science and Technology* 29 (4) (2016) 561–564. doi:10.2494/photopolymer.29.561.
URL https://www.jstage.jst.go.jp/article/photopolymer/29/4/29_561_article
- [8] P. Beauchamp, Simple Molecular Orbitals -Sigma and Pi Bonds in Molecules. Accessed on 25.04.2017.
URL [http://www.cpp.edu/\\$\sim\\$psbeauchamp/pdf/314_supp_2_hybrid_MO.pdf](http://www.cpp.edu/\simpsbeauchamp/pdf/314_supp_2_hybrid_MO.pdf)

BIBLIOGRAPHY

- [9] Molecular Orbital Diagram For A Simple Pi Bond – Bonding And Antibonding — Master Organic Chemistry.
URL <http://www.masterorganicchemistry.com/2017/02/14/molecular-orbital-pi-bond/>
- [10] Organic Semiconductors — Optoelectronics. Cavendish Laboratory, Cambridge.
URL <http://www.oe.phy.cam.ac.uk/research/materials/osemiconductors>
- [11] R. A. Marcus, Electron Transfer Reactions in Chemistry: Theory and Experiment (Nobel Lecture), *Angewandte Chemie International Edition in English* 32 (8) (1993) 1111–1121. doi:10.1002/anie.199311113.
URL <http://doi.wiley.com/10.1002/anie.199311113>
- [12] T. Liu, A. Troisi, What Makes Fullerene Acceptors Special as Electron Acceptors in Organic Solar Cells and How to Replace Them, *Advanced Materials* 25 (7) (2013) 1038–1041. doi:10.1002/adma.201203486.
URL <http://doi.wiley.com/10.1002/adma.201203486>
- [13] H. Bässler, A. Köhler, “Hot or cold”: how do charge transfer states at the donor–acceptor interface of an organic solar cell dissociate?, *Physical Chemistry Chemical Physics* 17 (43) (2015) 28451–28462. doi:10.1039/C5CP04110D.
URL <http://xlink.rsc.org/?DOI=C5CP04110D>
- [14] D. Fazzi, M. Barbatti, W. Thiel, Hot and Cold Charge-Transfer Mechanisms in Organic Photovoltaics: Insights into the Excited States of Donor/Acceptor Interfaces, *The Journal of Physical Chemistry Letters* 8 (19) (2017) 4727–4734. doi:10.1021/acs.jpclett.7b02144.
URL <http://pubs.acs.org/doi/10.1021/acs.jpclett.7b02144>
- [15] L. J. A. Koster, S. E. Shaheen, J. C. Hummelen, Pathways to a New Efficiency Regime for Organic Solar Cells, *Advanced Energy Materials* 2 (10) (2012) 1246–1253. doi:10.1002/aenm.201200103.
URL <http://doi.wiley.com/10.1002/aenm.201200103>
- [16] J. Niklas, O. G. Poluektov, Charge Transfer Processes in OPV Materials as Revealed by EPR Spectroscopy, *Advanced Energy Materials* 7 (10) (2017) 1602226. doi:10.1002/aenm.201602226.
URL <http://doi.wiley.com/10.1002/aenm.201602226>
- [17] J. A. Weil, J. R. Bolton, *Electron Paramagnetic Resonance*, John Wiley & Sons, Inc., Hoboken, NJ, USA, 2006. doi:10.1002/0470084987.
URL <http://doi.wiley.com/10.1002/0470084987>
- [18] S. R. Eaton, G. R. Eaton, L. J. Berliner (Eds.), *Biomedical EPR, Part B: Methodology, Instrumentation, and Dynamics*, Vol. 24/B of *Biological Magnetic Resonance*, Kluwer Academic Publishers-Plenum Publishers, New York, 2005. doi:10.1007/b111471.
- [19] F. Kraffert, J. Behrends, Spin-correlated doublet pairs as intermediate states in charge separation processes, *Molecular Physics* 115 (19) (2017) 2373–2386. doi:10.1080/00268976.2016.1278479.
URL <http://dx.doi.org/10.1080/00268976.2016.1278479>

- [20] G. Zwanenburg, P. J. Hore, EPR of spin-correlated radical pairs. Analytical treatment of selective excitation including zero-quantum coherence, *Chem. Phys. Lett.* 203 (1) (1993) 65–74. doi:10.1016/0009-2614(93)89312-6.
URL <http://linkinghub.elsevier.com/retrieve/pii/0009261493893126>
- [21] R. Wenzel, Die lichtinduzierte Antwort des Photorezeptors in *Arabidopsis thaliana* Cryptochrom-1, Ph.D. thesis, Freie Universität Berlin (2011).
- [22] S. G. Zech, W. Hofbauer, A. Kamrowski, P. Fromme, D. Stehlik, W. Lubitz, R. Bittl, A Structural Model for the Charge Separated State in Photosystem I from the Orientation of the Magnetic Interaction Tensors, *The Journal of Physical Chemistry B* 104 (41) (2000) 9728–9739. doi:10.1021/jp002125w
URL <http://pubs.acs.org/doi/pdf/10.1021/jp002125w> <http://pubs.acs.org/doi/abs/10.1021/jp002125w>
- [23] S. Stoll, A. Schweiger, EasySpin, a comprehensive software package for spectral simulation and analysis in EPR, *Journal of Magnetic Resonance* 178 (1) (2006) 42–55. doi:10.1016/j.jmr.2005.08.013.
URL <http://www.ncbi.nlm.nih.gov/pubmed/16188474> <http://linkinghub.elsevier.com/retrieve/pii/S1090780705002892>
- [24] F. Kraffert, EPR investigations on low-bandgap polymer solar cells, Ph.D. thesis, FU (2013).
- [25] F. Kraffert, R. Steyrleuthner, S. Albrecht, D. Neher, M. C. Scharber, R. Bittl, J. Behrends, Charge Separation in PCPDTBT:PCBM Blends from an EPR Perspective, *The Journal of Physical Chemistry C* 118 (49) (2014) 28482–28493. doi:10.1021/jp509650v.
URL <http://pubs.acs.org/doi/10.1021/jp509650v>
- [26] F. Kraffert, R. Steyrleuthner, C. Meier, R. Bittl, J. Behrends, Transient electrically detected magnetic resonance spectroscopy applied to organic solar cells, *Applied Physics Letters* 107 (4) (2015) 043302. doi:10.1063/1.4927446.
URL <http://aip.scitation.org/doi/10.1063/1.4927446>
- [27] Fullerene-C60 99.5% — Sigma-Aldrich.
URL <http://www.sigmaproducts.com/catalog/product/aldrich/379646?lang=de®ion=DE>
- [28] Y. Zhang, R. Steyrleuthner, J.-L. Bredas, Charge Delocalization in Oligomers of Poly(2,5-bis(3-alkylthiophene-2-yl)thieno[3,2- b]thiophene) (PBTTT), *The Journal of Physical Chemistry C* 120 (18) (2016) 9671–9677. doi:10.1021/acs.jpcc.6b02378.
URL <http://pubs.acs.org/doi/10.1021/acs.jpcc.6b02378>
- [29] O. V. Mikhnenko, H. Azimi, M. Scharber, M. Morana, P. W. M. Blom, M. A. Loi, Exciton diffusion length in narrow bandgap polymers, *Energy & Environmental Science* 5 (5) (2012) 6960. doi:10.1039/c2ee03466b.
URL <http://xlink.rsc.org/?DOI=c2ee03466b>

- [30] C. Yang, J. G. Hu, A. J. Heeger, Molecular Structure and Dynamics at the Interfaces within Bulk Heterojunction Materials for Solar Cells, *Journal of the American Chemical Society* 128 (36) (2006) 12007–12013. doi:10.1021/ja063707f.
URL <http://pubs.acs.org/doi/pdf/10.1021/ja063707f>
<http://pubs.acs.org/doi/abs/10.1021/ja063707f>
- [31] J. Cazes (Ed.), *Analytical Instrumentation Handbook*, Second Edition, CRC Press, 2004. doi:10.1201/9780849390395.
URL <http://dx.doi.org/10.1201/9780849390395.ch13>
<http://www.crcnetbase.com/doi/book/10.1201/9780849390395>
- [32] P. M. Allemand, G. Srdanov, A. Koch, K. Khemani, F. Wudl, Y. Rubin, F. Diederich, M. M. Alvarez, S. J. Anz, R. L. Whetten, The unusual electron spin resonance of fullerene C₆₀ anion radical, *Journal of the American Chemical Society* 113 (7) (1991) 2780–2781. doi:10.1021/ja00007a078.
URL <http://pubs.acs.org/doi/abs/10.1021/ja00007a078>
- [33] A. J. Kupijai, K. M. Behringer, F. G. Schaeble, N. E. Galfe, M. Corazza, S. A. Gevorgyan, F. C. Krebs, M. Stutzmann, M. S. Brandt, Bipolar polaron pair recombination in polymer/fullerene solar cells, *Physical Review B* 92 (24) (2015) 245203. arXiv:1505.01411, doi:10.1103/PhysRevB.92.245203.
URL <https://link.aps.org/doi/10.1103/PhysRevB.92.245203>
- [34] M. N. Uvarov, A. G. Popov, E. A. Lukina, L. V. Kulik, Spin relaxation and structure of light-induced spin-correlated PCBM-/P3HT+ radical pairs, *Journal of Structural Chemistry* 55 (4) (2014) 644–650. doi:10.1134/S0022476614040088.
URL <http://link.springer.com/10.1134/S0022476614040088>
- [35] S. Shoaee, Charge photogeneration in donor/acceptor organic solar cells, *Journal of Photonics for Energy* 2 (1) (2012) 021001. doi:10.1117/1.JPE.2.021001.
URL <http://photronicsforenergy.spiedigitallibrary.org/article.aspx?doi=10.1117/1.JPE.2.021001>
- [36] J.-L. Brédas, J. E. Norton, J. Cornil, V. Coropceanu, Molecular Understanding of Organic Solar Cells: The Challenges, *Accounts of Chemical Research* 42 (11) (2009) 1691–1699. doi:10.1021/ar900099h.
URL <http://pubs.acs.org/doi/abs/10.1021/ar900099h>
- [37] A. C. Mayer, M. F. Toney, S. R. Scully, J. Rivnay, C. J. Brabec, M. Scharber, M. Koppe, M. Heeney, I. McCulloch, M. D. McGehee, Bimolecular Crystals of Fullerenes in Conjugated Polymers and the Implications of Molecular Mixing for Solar Cells, *Advanced Functional Materials* 19 (8) (2009) 1173–1179. doi:10.1002/adfm.200801684.
URL <http://doi.wiley.com/10.1002/adfm.200801684>
- [38] L. Zhang, F. Liu, Y. Diao, H. S. Marsh, N. S. Colella, A. Jayaraman, T. P. Russell, S. C. B. Mannsfeld, A. L. Briseno, The Good Host: Formation of Discrete One-Dimensional Fullerene “Channels” in Well-Ordered Poly(2,5-bis(3-alkylthiophen-2-yl)thieno[3,2- b]thiophene) Oligomers, *Journal of the American Chemical Society* 136 (52) (2014) 18120–18130. arXiv:1408.1149, doi:10.1021/ja510976n.
URL <http://pubs.acs.org/doi/abs/10.1021/ja510976n>
<http://arxiv.org/abs/1408.1149>
<http://pubs.acs.org/doi/10.1021/ja510976n>

- [39] A. C. Mayer, S. R. Scully, B. E. Hardin, M. W. Rowell, M. D. McGehee, Polymer-based solar cells, *Materials Today* 10 (11) (2007) 28–33. doi:10.1016/S1369-7021(07)70276-6.
URL <http://www.sciencedirect.com/science/article/pii/S1369702107702766> <http://linkinghub.elsevier.com/retrieve/pii/S1369702107702766>
- [40] R. Steyrleuthner, Y. Zhang, L. Zhang, F. Kraffert, B. P. Cherniawski, R. Bittl, A. L. Briseno, J.-L. Bredas, J. Behrends, Impact of morphology on polaron delocalization in a semicrystalline conjugated polymer, *Physical Chemistry Chemical Physics* 19 (5) (2017) 3627–3639. doi:10.1039/C6CP07485E.
URL <http://xlink.rsc.org/?DOI=C6CP07485E>
- [41] J. E. Fischer, P. A. Heiney, A. R. McGhie, W. J. Romanow, A. M. Denenstein, J. P. McCauley, J. Smith, A. B., Compressibility of Solid C₆₀, American Association for the Advancement of Science 252 (5010) (1991) 1288–1290.
URL <http://www.jstor.org/stable/2875961>
- [42] E. A. Lukina, A. A. Popov, M. N. Uvarov, L. V. Kulik, Out-of-Phase Electron Spin Echo Studies of Light-Induced Charge-Transfer States in P3HT/PCBM Composite, *The Journal of Physical Chemistry B* 119 (43) (2015) 13543–13548. doi:10.1021/acs.jpcb.5b02142.
URL <http://pubs.acs.org/doi/10.1021/acs.jpcb.5b02142>
- [43] J. Niklas, K. L. Mardis, B. P. Banks, G. M. Grooms, A. Sperlich, V. Dyakonov, S. Beaupré, M. Leclerc, T. Xu, L. Yu, O. G. Poluektov, Highly-Efficient Charge Separation and Polaron Delocalization in Polymer-Fullerene Bulk-Heterojunctions: A Comparative Multi-Frequency EPR & DFT Study, *Physical Chemistry Chemical Physics* 15 (24) (2013) 9562. arXiv:1305.6434, doi:10.1039/C3CP51477C.
URL <http://arxiv.org/abs/1305.6434%0A> <http://dx.doi.org/10.1039/C3CP51477C>
- [44] F. Bloch, Nuclear Induction, *Physical Review* 70 (7-8) (1946) 460–474. doi:10.1103/PhysRev.70.460.
URL <https://link.aps.org/doi/10.1103/PhysRev.70.460>

Appendix A

Visualization tool manual

On the Fig. 3.1a and 3.1b one can see how toolbox looks like. It has a lot of options and possibilities for more comfortable CT state simulations.

Here it is explained how one can use this tool. Please, pay attention, that we refer to D_{zz} as D for simplicity.

Running the tool

1. Run the program.
2. The dialog is automatically open: "Choose file for system data". If one runs the program for the first time or wants to create or change file with data about the system, then chose "Create/change file":
 - The new dialog is open.
 - Here one enters main information about the system (that is extracted from cwEPR spectrum). One can enter different line widths for X- and Q-band. This is useful if one does not distinguish between g-strains and line widths.
 - If such file already exists for the system and one wants to change it, press "Open" and chose corresponding file.
 - For saving the data press "Save" button. You can save it in the new file or replace existing one. If you do not save changes, they will be lost. If you rewrite file, previous data will be lost (saved simulations stay, but they will give another result with new system parameters).
 - After saving close the window.
 - If dialog "Choose file for system data" appears again, something wrong was done. Repeat previous steps.

If special file with information about the system (g-factors, line widths, ...) already exists, then chose "Open file". And chose the file.

3. The dialog is automatically open: "Select the MATLAB code file for X-band". One needs to select '*.mat' file that contains 1x1 'file' structure, where all needed information about experiment and spectra are stored: mw_freq_set (frequency of mw in GHz or Hz), B0 (magnetic field in mT), t (time in μ s), s_trcorr (spectra - recorded intensities).

4. The same for Q-band.
5. Additional window can appear. There you can chose saved simulations.
6. It can take several minutes for initial calculations. Afterwards the spectra are opened and the tool is ready for usage.

Background corrections and initial parameters

In visualization toolbox color plays a role: black - experimental spectrum, red - simulations for fixed relative orientation in powder model, blue - simulations for random relative orientations in powder model.

To better see the made changes, one can hide or show different spectra: simulations for fixed relative orientation in powder model ('FRO'), simulations for all relative orientation in powder model or full powder ('FP'), initial spectrum without any corrections ('Initial'), background corrections ('Backgr'), temporary saved spectra ('Saved'), experimental spectrum ('Experim'). Check-boxes are locates below Q-band plot.

Initial settings

1. Set the suitable **time slice** directly or by using a slider. Remember that for simulations relaxation effects are not taken into account and approximation, that only states $|2\rangle$ and $|3\rangle$ are occupied, is made. Hence, try to chose as early times as possible but not to early because of spectrometer time resolution and signal to noise ratio.
2. Next step is **background corrections**. Initially program is automatically in "Background corrections" regime. If not, press the button 'Background corrections'.
 - Choose ranges [minimum B0, B1] and [B2, maximum B0] by entering **B1** and **B2** for both X- and Q- band. This ranges are used for background fitting.
 - On the gray background (black color correspond to experimental spectrum) one can see parameters that can be changed: **fitting polynom power** and **smoothing power**. Below there is additional check-box, that allow to show/hide experimental spectrum with background corrections without smoothing. This is useful for finding appropriate smoothing power.

On the figures ranges (areas) that are used for background corrections are gray rectangles; polynomial background is shown as a gray curve (line); initial spectrum is dark-gray; background corrected experimental spectra without smoothing - light-gray; with smoothing - black.

3. When background corrections are done you can hide corresponding spectra and parameters by anticking the box 'Backgr corrections'.
4. Now one can start with simulations. First step is **number of points** that should be used for the model: an amount of different angles θ that should be considered. The total number of points is then recalculated automatically in Easyspin 'sphgrid' function (for more details see [23]). For changing number of points press 'Advanced settings' button.

-
- To easily see the difference between different amounts of points tick 'Saved spectrum' box. In the list below 'last' spectrum should be selected.
 - Check that the simulated spectrum of the chosen model(s) is on.
 - Now, when one changes the number of points there will be solid line for new amount of points and dashed line for previous one. If they are identical it does not matter which amount of points to use - current one or previous one. In order to have faster calculations it is better to chose as small amount of points N as possible but such that for N+1 points result is the same.
 - ***Attention!*** Calculation takes time, be patient. If you press the same amount of points twice (if after entering the number of points, 'Enter' button was pressed twice), then previous and current spectra are the same! This can lead to the selection of the wrong N. It is important to remember, that different line widths, coupling and other parameters can require different amount of points. It is useful to check if the right number of points is used, when parameters are changed.
5. There is '**Additional broadening**'. The line widths are taken from cwEPR spectrum. In trEPR line widths are slightly different, because of Heisenberg uncertainty principle and probably different delocalization, hence different HFI. It was calculated from Heisenberg uncertainty principle that for X-band it is about $0.2 \mu\text{s}$ and for Q-band is about 0.4 mT for early times.

Simulations

The spectra are chosen, background corrections are made and optimal number of points is found. The simulations can be started. Here we describe which parameters can be changed.

Random relative orientations or full powder (FP) model (blue)

1. **Couplings J and D.** They can be changed by entering a number or by using a slider. It is also possible to enter E (the second field near D). But then calculations will take more time, as then more points should be considered.
2. Additionally **strains of J and D** can be chosen. $J \propto \exp(-R)$ and $D \propto \frac{1}{R^3}$. They are recalculated from the fact that distances R between radicals can be various. Approximation is made that R have Gaussian distributions around some average value. Because proportional coefficients between $J(D)$ and R are usually not known by user, one enters the average value and a range in terms of $J(D)$.

As average entered J_0 value is taken. In '**Width of range R**' the $2\Delta J = 2 \cdot (|J|_{max} - J_0)$ should be put in. Then this values are recalculated to distance Gaussian distribution and back in order to find second limit of J. The resulting $J(D)$ range is written in the '**Range**' field. Also one needs to enter total **number of points for the range** - number of different J-values from range that should be considered. It should be odd. If it is even it is automatically changed to bigger odd number.

The calculating time for J(D) strains is very long. So calculation does not start automatically. One should press 'Start simulation button'. Appeared dialog after parameter change reminds about this.

After calculations additional window is appearing. It shows distribution of the considered J and D values.

3. There is additional possibility that allows automatically find J- and D-couplings (without strains). It can be ran by pressing '**fit D and J**' button. After fitting the old results are open in new window. It is not clear why, but it finds opposite result almost all the time. Even if it finds some fitting, one should keep in mind that found minimum can be just local one and it can be possible to find a better fitting.

Fixed relative orientation (FRO) in a powder model (red)

1. **Couplings J and D.** They can be changed by entering a number or by using a slider. It is also possible to enter E (the second field near D).
2. **Euler angles.** There are three Euler angles for fist system and three for the second one. They can have values from 0 to π .
3. In oder to visualize relative orientation of radicals, press '**Draw**' button.

Temporaly saving

If one finds parameters or the simulations one want to remember for some time, one can temporary save this data. Data is saved only while program is working. For temporary saving press 'Save temporary' button. In opened window one can enter desired name of saving. After 'Ok' pressing, new line appears in the list box below with the entered name. By selecting saved data in the list one can:

- **Plot saved result.** For this 'Saved spectrum' check-box should be ticked. Saved spectra will be plotted as a dashed line.
- **Load saved parameters** by pressing 'Load selected parameters' button.
- **Delete saved parameters** by pressing 'Delete selected parameters' button.

Additional possibilities

1. One can change **normalizations** of simulations separately. This can be done by entering the values or by using sliders. See on the left side of the plots. Red one correspond to the fixed relative orientation and gray one to the all relative orientation model.

-
2. **Coefficient of determination** R^2 is calculated. There are four of them (below plots). **R $\hat{2}$ FRO** is for fixed relative orientation model calculated for X- and Q-band simultaneous. **R $\hat{2}$ FP** is for random relative orientations model (full powder) calculated together for both bands. **R $\hat{2}$ X** is one for X-band and **R $\hat{2}$ Q** is one for Q-band, which calculated for the current model. If both models are considered, then the R^2 parameters show the result for FRO model.
 3. In the lower left corner data about system are written. If one presses '**Change system parameters' button**', they can be changed. Here one can open another file with system data or change parameters manually. One can see changes in spectra without saving by pressing 'Update without saving'. If one wants to save changes, one should press 'Save'. If saving was done, then one needs to reopen file with system data (see next point).
 4. In the lower right corner there are three buttons. 1st one with opened X-band spectrum path and file name, 2nd one with system data file path and 3rd one for Q-band. This **files can be changed** by pressing corresponding data.

Saving the result

After right parameters are found and a good fitting occurs, one can save the result by pressing **yellow 'Save' button** in different ways. The different variants are indicated in new dialog:

1. **'System data file'**. It is useful to save parameters that were used for simulations in the file with system data. When this visualization tool will be run again there will be opportunity to open saved parameters and continue simulations. Only in this type of saving it is possible to resume fitting from saved parameters (all temporary saved data will be lost).
2. **'mat-file'**. It saves the parameters in a file with extension '.mat'. This type of file is used in the Matlab. There the simulated spectra as well as experimental spectrum are saved for both X- and Q-band. All the used parameters are saved in the parameter 'info'. This is useful if one wants to replot simulations.
3. **'Picture'**. It is nice feature if one wants to save plots only like a picture. The plots can be saved in two formats: '.bmp' and '.eps'. There will be two plots and below them all parameters that were used for simulations.
4. **'ASCII'**. Needed if one wants to save result external. In the beginning of the file all parameters that were used for simulations are stored. Afterwards there are columns of data:
 - Magnetic fields for X- and Q-band: 'XbandB0 (mT)' and 'QbandB0 (mT)'
 - Initial spectra for X- and Q-band without any changes: 'initialX' and 'initialQ'
 - Background corrected spectrum without smoothing: 'bgcorrX' and 'bgcorrQ'
 - Background corrected spectrum with smoothing: 'bgcorrsmoothX' and 'bgcorrsmoothQ'

- All relative orientation in powder (full powder) model simulations and separated four peaks: 'FullPowderSimX< _,1,2,3,4>' and 'FullPowderSimQ< _,1,2,3,4>'
- Fixed relative orientation in powder model simulations and separated four peaks: 'FixedOrSimX< _,1,2,3,4>' and 'FixedOrSimQ< _,1,2,3,4>'

Acknowledgments

I would like to thank everyone who helped me with studying in the Master program and with performing my research phase.

First of all, I am very thankful to Prof. Dr. Jan Behrends for the given opportunity to work on the very interesting topic that includes a lot of physics in such a friendly atmosphere, for his highly responsive leadership, for the thoughtful suggestions, relevant recommendations and the corrections he made, for a friendly and wise response to the all appeared questions.

Many thanks to Felix Kraffert, who was a rock solid reliable support for me every day. He also supervised me a lot, giving brilliant explanations and ideas during our discussions. Special thanks to him for correcting my work.

I also want to thank Dr. Robert Steyrleutner, who taught me to work in a glovebox and showed me how to prepare the samples, for his great help and response. And I want to thank all the members of AG Behrends and AG Bittl for the seminar discussions, suggestions and a friendly support. I had a really nice time and it was a great pleasure to work with you all!

Special thanks to Kelvin Yao for the extracurricular activities and to Ilia Kulikov who was always by my side in the hard times and whose support and motivation is inestimable during the whole Master education. I give many thanks to all my friends and family for all the fun. I am very thankful to my parents, without whom my education would not be possible, for their kindness, patience, support and advices.

Declaration of Authorship

I, Daria Dymnikova, declare that this thesis titled, "Influence of local donor/acceptor geometry on charge separation in organic solar cells" and the work presented in it are my own. I hereby confirm that I have written the thesis personally and independently and I have used no aids other than the sources and aids listed.

Signed: _____

Date: _____